

Multi-axle Vehicle Modeling and Stability Control: A Reconfigurable Approach

by

Yubiao Zhang

A thesis
presented to the University of Waterloo
in fulfillment of the
thesis requirement for the degree of
Doctor of Philosophy
in
Mechanical Engineering

Waterloo, Ontario, Canada, 2019

© Yubiao Zhang 2019

Examining Committee Membership

The following served on the Examining Committee for this thesis. The decision of the Examining Committee is by majority vote.

External Examiner	Name: Yuping He Title: Professor, Automotive, Mechanical and Manufacturing Engineering, University of Ontario Institute of Technology
Supervisor	Name: Amir Khajepour Title: Professor, Mechanical and Mechatronics Engineering
Internal Member	Name: William Melek Title: Professor, Mechanical and Mechatronics Engineering
Internal Member	Name: Behrad Khamesee Title: Professor, Mechanical and Mechatronics Engineering
Internal-external Member	Name: Nasser Lashgarian Azad Title: Associate Professor, System Design Engineering

I hereby declare that I am the sole author of this thesis. This is a true copy of the thesis, including any required final revisions, as accepted by my examiners.

I understand that my thesis may be made electronically available to the public.

Yubiao Zhang
August 18, 2019

Abstract

Multi-axle vehicles, such as trucks and buses, have been playing a vital role in trucking industry, public transportation system, and long-distance transport services. However, at the same time, statistics suggest more than one million lives are lost in road accidents each year over the world. The high adoption and utilization of multi-axle vehicles hold a significant portion of road accidents and death.

To improve the active safety of vehicles, active systems have been developed and commercialized over the last decades to augment the driver's actions. However, unlike two-axle vehicles (e.g., passenger cars), multi-axle vehicles come in a rich diversity and variety to meet with many different transportation needs. Specifically, vehicle configurations are seen in different numbers of axles, numbers of articulations, powertrain modes, and active actuation systems. In addition, multi-axle vehicles are usually articulated, which makes the dynamics and control more complex and challenging as more instability modes appear, such as, trailer sway and jackknife.

This research is hence motivated by an essential question: **how can a universal and reconfigurable control system be developed for any multi-axle/articulated vehicle with any configuration?** Leveraging the matrix approach and optimization-based techniques, this thesis developed a reconfigurable and universal modeling and control framework to this aim. Specifically, a general dynamics modeling that unifies any multi-axle and articulated vehicles in one formulation is developed in an intuitive manner. It defines the 'Boolean Matrices' to determine any configuration of the articulation, the number of axles, and the active actuation systems. In this way, the corresponding dynamics model can be easily and quickly formulated when axles, articulations or actuators are added or removed.

The general modeling serves to achieve the universality and reconfigurability in controller design. Therefore, a hierarchical, i.e., two-layer, control system is proposed. In the high layer, the optimization process of a model predictive control (MPC) calculates corrective Center of Gravity (CG) forces/moments, which are universal to any vehicle. The lower-level controller is achieved by a Control Allocation (CA) algorithm. It aims to realize the MPC commands by regulating the steering or torque (driving or braking) at each wheel

optimally. In addition, the optimization takes into account real-time constraints, such as actuator limits, tire capacity, wheel slips, and actuators failure.

Simulations are conducted on different vehicle configurations to evaluate control performance, reconfigurability, and robustness of the system. Additionally, to evaluate the real-time performance of the developed controller, experimental validation is carried out on an articulated vehicle with multiple configurations of differential braking systems. It is observed that the controller is very effective in dynamics control and has a promising reconfigurability when moving from one configuration to another.

Acknowledgment

In writing the Ph.D. thesis of indisputable logic and rigor, here is the only room I can pour some sentiments out from my heart and I will not leave them behind. Interestingly, the writing process gives me a unique chance to look back from the very beginning of this journey. What flows to my mind is not just the research I've accomplished, but also the people I worked with, the discussion we heated and friendship built in daily.

I keenly feel how important of others' help and support to one's achievement. Believe me, I can tell the difference of this research with and without these people behind is like but more than the difference of a car using and un-using active controls.

First and foremost, I would like to thank my supervisor, Dr. Amir Khajepour. I was lucky to have him as my advisor over the past years, including my masters' program. He taught me lots of valued insights from vehicle controls, conducting research, demonstrating ideas, to life in general. Time and again, he inspired me to stand higher, see further, and go deeper when I was narrow-minded. Leading a very large research group, he also motivates and cares for every individual with genuine patience. Personally, the example he is setting goes beyond academia and his impact on me will last.

The research would not be going so smooth without many friends around. My special thanks to Dr. Yanjun Huang, who firstly helped my wife and me settling down in Canada in 2016. He is so nice and knowledgeable yet humble. Continuously and generously, he shared what he knew to me so I could stand on the shoulders. In addition, I would like to thank my dear friends, Wang Hong, Qin Yechen, Qi Ronghuai, Ehsan Hashemi, Mansour Ataei, Mehdi Abroshan, and my office friends, Bruce Huang, Fernando Barrios, for their support and assistance to my research and GM projects. It has been a wonderful memory to have them over the years. Same thanks to the MVS lab technicians, Jeff Graansma and Jeremy Reddekopp, who make the vehicle tests possible.

Special thanks to Bakhtiar Litkouhi and Alireza Kasaeizadeh from GM R&D in Warren during the summer internship in 2018. Although not a part of my thesis, I learned a lot from industry perspectives and them. I also appreciate my committee members, for their time and insights in reviewing my thesis.

The most unsung people are usually family members, but I know I have never traveled so far without them. I am so grateful for my parents, Zhang Jinchong and Ouyang Baifeng, who are educated limitedly but push their son to achieve a Ph.D. with so much love, trust and toil. This thesis is also dedicated to my wife, Yang Min, who came to Canada with boldness and faith, and then stayed with me by countless love and patience. How many times she encouraged me to just rely on God and rest on HIS hands patiently when I am frustrated, I can not remember, honestly.

Gary Zhang
Waterloo, Canada
August, 2019

Dedication

To my parents and my wife, Min Yang.

Table of Contents

List of Tables	xiii
List of Figures	xiv
1 Introduction	1
1.1 Motivation and Objectives	1
1.2 Contributions	4
1.3 Thesis Outline	5
2 Literature Review and Background	8
2.1 Configuration Diversity	8
2.1.1 Axle/Articulation Configurations	9
2.1.2 Powertrain/Driveline Configurations	10
2.2 Vehicle Instability	11
2.2.1 Yaw-plane Instability	12
2.2.2 Roll-plane Instability	14
2.3 Active Actuation Systems	15
2.4 Integrated, Reconfigurable and Universal VDC	17

2.5	MPC and CA Techniques	18
2.6	Summary and Discussion	21
3	Dynamics and Modeling of Multi-axle Vehicles	22
3.1	Coordinate Systems and Methodology	23
3.2	Non-articulated Vehicles	24
3.2.1	Corner Forces	24
3.2.2	CG Forces/Moment	26
3.2.3	Body Dynamics	29
3.2.4	Tire Model and Load Transfers	30
3.3	Model Linearization	33
3.3.1	Linearized Tire Model	33
3.3.2	Linearized Body Dynamics	37
3.3.3	State Space Formulation	37
3.4	Articulated Vehicles	38
3.4.1	Detached Tractor/Trailer	38
3.4.2	Articulation Constraints	41
3.4.3	Reconfigurable Formulation	42
3.4.4	Extension to Any Vehicles	43
3.5	Model Evaluation	44
3.6	Summary and Discussion	50
4	Reconfigurable Controller Development	52
4.1	Control Overview	53
4.2	Stability and References	55

4.2.1	Longitudinal Control	55
4.2.2	Lateral Stability	56
4.2.3	Steady State Handling	57
4.2.4	Trailer Yaw Behavior	60
4.2.5	Rollover Stability	62
4.3	High-level: Reconfigurable MPC	64
4.3.1	A General Prediction Model	64
4.3.2	Quadratic Programming Problem	66
4.3.3	Feasibility and Stability	70
4.4	Lower-level: Control Allocation	73
4.5	Real-time Constraints	74
4.6	Controller Parameters Tuning	78
4.7	Summary and Discussion	84
5	Applications and Simulations	86
5.1	Matrix Size Reduction	86
5.2	Three-axled Bus with TVC&DBS	89
5.3	Articulated Bus with ATS/DBS	91
5.4	Articulated Truck with DBS	96
5.5	Actuator Failure and Robustness	99
5.6	Summary and Discussion	101
6	Experimental Study	103
6.1	Experimental Facilities	103
6.2	Cornering Stiffness Identification	107

6.3	Experimental Results	109
6.3.1	Tractor Differential Braking	111
6.3.2	Trailer Differential Braking	115
6.3.3	Integrated Differential Braking	117
6.4	Summary and Discussion	119
7	Conclusions and Future Work	121
7.1	Conclusions	121
7.2	Future Work	123
	References	125
	APPENDICES	137
A	State-space Matrices	138
A.1	State-space Formulation (3.31) (Single Unit)	138
A.2	State-space Formulation (3.34) (Tractor Unit)	139
A.3	State-space Formulation (3.36) (Trailer Unit)	140
B	Footage of Vehicle Tests	141

List of Tables

2.1	Different powertrain/driveline/steer mode configurations	11
3.1	The rule of articulated vehicles model	43
3.2	Evaluation errors of an articulated four-unit truck	50
4.1	Tractor-trailer steady state behavior	61
4.2	Possible application and its boundaries	75
4.3	Rise time of tractor-trailer responses	79
5.1	Applications description	87
5.2	Performance of different controller of App. III	96
6.1	Dynamics parameters of tractor trailer	105
6.2	Parameters of reconfigurable controller	107

List of Figures

1.1	Footage of a truck rollover due to excessive speed in a turn	2
1.2	The basic framework of the research	4
2.1	13-category vehicle classifications by FHWA	9
2.2	Different axle/articulation configuration of buses and coaches	10
2.3	Unstable modes of articulated vehicles in yaw-plane	13
2.4	Active chassis control systems	16
3.1	From a single unit to articulated multi-unit vehicle	24
3.2	Corner forces on an arbitrary wheel i	25
3.3	A multi-axle vehicle with active differential braking and front steering	26
3.4	Corner forces in a global view and CG forces/moment	27
3.5	Longitudinal, lateral, yaw and roll dynamics	29
3.6	Brush tire model V.S. experimental data at different normal loads	32
3.7	Tire load transfers at combined condition	34
3.8	Affine approximation of brush tire model	35
3.9	Yaw and roll dynamics of the tractor and trailer	39
3.10	An articulated vehicle with any units	44

3.11	A two-axled SUV	45
3.12	A three-axled bus	46
3.13	A articulated bus	48
3.14	An articulated four-unit truck	49
4.1	Control structure	54
4.2	Steady-state handling model for a articulated vehicle (two-units)	58
4.3	Tractor weight distribution affected by the trailer	58
4.4	Tractor understeer gradient V.S. trailer CG location	59
4.5	Five cases of tractor-trailer steady state behavior	62
4.6	A friction ellipse model of tire i	76
4.7	Tractor-trailer open loop responses	80
4.8	Predicted outputs over different control horizon-1	82
4.9	Predicted outputs over different control horizon-2	83
5.1	Controller algorithm flowchart	88
5.2	A three-axled bus with rear torque vectoring	89
5.3	Results of longitudinal (cruise control) and yaw control in App. I	90
5.4	Results of yaw and rollover control in App. I	92
5.5	An articulated bus with active trailer steering	92
5.6	Results of yaw and sway control of App. II	93
5.7	An articulated bus with differential braking system	94
5.8	Results of yaw and sway control of App. III	95
5.9	An articulated truck with differential braking system	97
5.10	Results of rollover prevention of App. IV	98

5.11	Results of jackknife prevention of App. IV	99
5.12	Fault-tolerance control of fishhook maneuver in App. I while a brake actuator failed	100
5.13	Robustness performance of fishhook maneuver in App. I to tires and vehicle parameters variations	101
6.1	Test tractor (Equinox) and customized trailer, and main hardwares	104
6.2	The estimation scheme for computing \hat{Y}_{sim}	108
6.3	Fitting results using optimized C_{α}^i	109
6.4	Tractor-trailer responses for Control OFF and Controller A in sine steer	110
6.5	Corrective torques by Controller A in sine steer	111
6.6	Tractor-trailer responses for Control OFF and Controller A in DLC	112
6.7	Corrective torques by Controller A in DLC	113
6.8	Tractor-trailer responses for Control OFF and Controller B in sine steer	114
6.9	Corrective torques by Controller B in sine steer	115
6.10	Tractor-trailer responses for Control OFF and Controller B in DLC	116
6.11	Corrective torques by Controller B in DLC	117
6.12	Tractor-trailer responses for Control OFF and Controller C in DLC	118
6.13	Corrective torques by Controller C in DLC	119
B.1	Footage for Control OFF and Controller A in sine steer	142
B.2	Footage for Control OFF and Controller A in DLC	143

Chapter 1

Introduction

Multi-axle vehicles come in a rich diversity and variety of configurations, i.e., articulations, number of axles, powertrains, drive mode, and active actuators. For the purpose of active dynamics control, there are considerable challenges in designing a controller that is equally diverse. This thesis hence aims to develop a universal and reconfigurable control framework for dynamics and stability control of any vehicle configurations by leveraging matrix approaches and optimization-based techniques. This chapter is organized as follows. Section 1.1 describes the needs and challenges for multi-axle vehicle stability control and then suggests the objectives. Section 1.2 outlines the proposed framework and contributions of this research. Section 1.3 provides the outline and structure of the thesis.

1.1 Motivation and Objectives

In order to transport a larger volume of freights or passengers via a relatively fixed infrastructure, one way to increase transportation efficiency is to employ longer vehicles with more axles or multiple articulated units [1, 2]. These multiple axle vehicles are used most often in trucks, tractor-trailers, buses, and less frequently on passenger cars. Trucks are the main transportation means of goods in the world, more than trains, ships or planes [3]. In 2015, nearly 72% of over 875 million tons of goods in Canada was carried by trucks.

In 2016, about 10.9 million two-way trucking movements were recorded at Canada/U.S. border points, the value of trucking traffic between Canada and the U.S. reached \$418 billion [4]. In the public transportation system and long-distance transport services, coaches are often the only means of moving people comfortably across long distances for most of the world's population. Thanks to its availability and economic benefits, buses account for 55% of public transport in Europe. In the U.S. alone, over 751 million passengers' trips are made annually. Over distances of between 500 to 1,000 kilometers, buses and coaches have the lowest cost per passenger of any kind of transport, according to IRU, a world's road transport organization. In addition, American Public Transportation Association (APTA) [5] suggests that public transportation system contributes environmental protection as it saves the U.S. an equivalent of 4.2 billion gallons of gasoline annually or more than 11 million gallons of gasoline per day.

The appeal to multi-axle vehicles, such as trucks and buses, is obvious. Nevertheless, the popularity of such vehicles garnered increased public attention to safety problems. Annually, approximately 500,000 accidents involving trucks or buses occur in U.S.. Of the approximately 415,000 crashes involving large trucks in 2016, there were 4440 fatal crashes and estimated 119,000 injury crashes [7, 8]. Multi-axle vehicles are usually characterized by a high wheelbase to track ratio, a high center of gravity (CG), and uneven weight distributions between axles, prone to instability or even rollover, see a truck rollover example illustrated in Figure 1.1. In addition, the majority of accidents with heavy trucks involve passenger cars, where the severity is much worse for the passenger car due to its vulnerability. Moreover, only a minority of these commercial vehicles, nowadays, are equipped with stability control systems.



Figure 1.1: Footage of a truck rollover due to excessive speed in a turn [6]

On the other side, multi-axle vehicles differ from the passenger car quite a lot and it makes a big challenge for dynamics controls. One of such challenges is to design a controller that applies to diverse configurations of these vehicles as mentioned. Another challenge comes from the complex dynamics characteristics of these vehicles that result in more instability modes. Compared to passenger cars, more control objectives should be further considered, for instance, trailer sway and trailer jackknife. Control objectives have to be prioritized considering the vehicle characteristics and application context. Thus, an ideal controller should be inclusive yet reconfigurable and selective to these stability objectives.

In the decades, a great deal of theoretical and experimental work is done for vehicle system dynamics control among researchers and automobile manufacturers. Implemented solutions such as anti-lock braking system (ABS), electronic stability program (ESP) and automatic traction control systems (TCS) have saved many lives today. Such active safety systems are mainly for passenger cars and single unit vehicles and less work has been done in active safety of articulated vehicles. What's more, due to diversity and variety from vehicles to vehicles, there are increased challenges for control system design in terms of design costs, transplant and tuning efforts.

Therefore, the objective of this research is motivated by an essential question: how can we develop a universal and reconfigurable control system for any multi-axle vehicle with any number of axles, articulation joints, and control actuation system? The framework illustrated in Figure 1.2 summarizes the goal of work in brief. To this aim, first and foremost, given any multi-axle vehicles, a reconfigurable and general dynamics model is needed. The model serves to describe longitudinal, yaw and roll dynamics behavior of any articulated/multi-axle vehicle, as well as analyze the vehicle stability characteristics. Secondly, as the core of this research, the proposed model is utilized in the model-based controller design. To achieve its universality and reconfigurability, the controller is expected to be reconfigurable to any given vehicles and capable of integrating multiple active actuators, such as active steering control, and differential braking. An integrated manner provides a compact and coupled formulation between multi-inputs and multi-outputs and avoids any conflict in the actuation responses. While different vehicles have different stability objectives, last but not least, the controller should be inclusive yet selective to various stability objectives. Many different objectives, such as longitudinal control, lateral

stability, slip control, rollover prevention, trailer sway and jackknife control in articulated vehicles, should be easily and quickly selected and configured when a specific vehicle is given. Furthermore, the controller is able to provide optimal, effective and relatively robust control performance when applying to different vehicles.

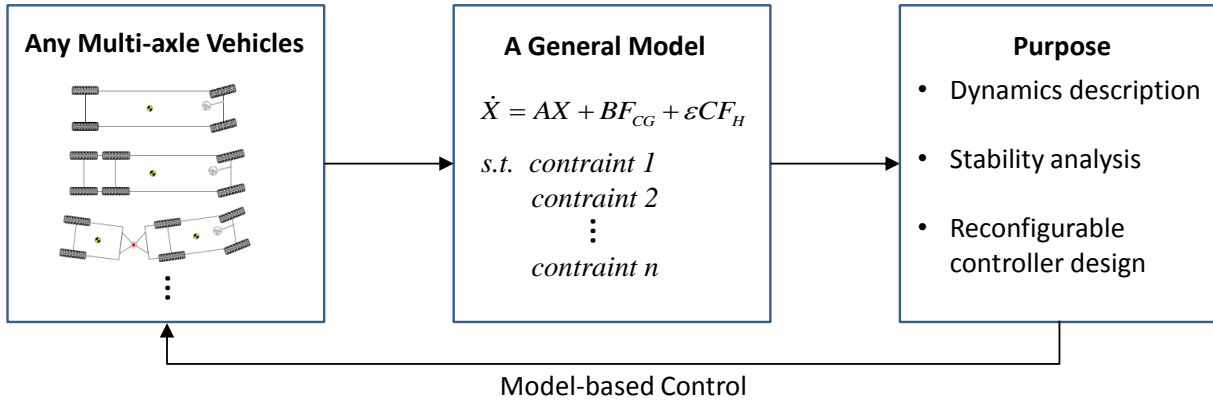


Figure 1.2: The basic framework of the research

1.2 Contributions

Aiming to address challenges of configuration diversity, multiple control objectives, and actuation redundancy, the contributions of this work in modeling and dynamics control of multi-axle and articulated vehicles could be summarized as:

- A novel dynamics modeling methodology that unifies any multi-axle and articulated vehicles in one formulation is developed. When any axle, articulation joints, and/or active actuator is added or removed, it can easily and quickly formulate the corresponding dynamics model. Furthermore, a liner time varying model derived at tires' operating point is achieved for control purposes. It results in a less computation load yet the model accuracy and reliability are reversed .
- A hierarchical (two-layer) control system using optimization-based control techniques is proposed, where the high-level MPC controller represents universality while the

lower-level CA controller, reconfigurability. Using this scheme, there is no need to reformulate the control problem when a new vehicle with new configuration is given. Moreover, the controller provides optimal control actions by solving the optimization problem in real time.

- Fault tolerance control that considers actuators failure is investigated. In the the lower-level control allocation, the constraints of actuator limits, tire capacity, wheel slips, and actuators failure are defined and updated in real time. Once a fault is detected, CA will systematically set the boundaries of faulty actuators to the failure values and use the rest of actuators to achieve fault tolerance control.
- Simulation and experimental studies are conducted to validate the proposed control system. In particular, an optimization-based identification method of the trailer cornering stiffness is proposed using nonlinear least squares algorithm and experimental data. The identified result is then used in tractor trailer modeling, where the dynamics responses show a very comparative performance with these of the experimental tractor trailer.

It is hoped that this methodology will provide a new perspective on articulated vehicle dynamics control and aid researchers and engineers in implementing many different active systems. This research assumes vehicle states, including motion states and road condition, are available from sensor or estimation modules as the research focus is on modeling and controller design.

1.3 Thesis Outline

The remaining chapters are organized as follows:

Chapter 2 Literature Review and Background

This chapter presents a review on the background of the multi-axle configurations and control. It starts with a general survey of major configurations of multi-axle vehicles and

proceeds with a discussion on the instability phenomenon of multi-axle vehicles. In the last portion, the literature of vehicle stability control systems and techniques is reviewed with emphasis on the model predictive control technique. In summary, it infers the significance and novelty of the proposed work.

Chapter 3 Dynamics and Modeling of Multi-axle Vehicles

This chapter presents a detailed work on how multi-axle vehicles are modeled using a reconfigurable concept and matrix approach. A general model that describes the longitudinal, lateral, yaw and roll dynamics for multi-axle non-articulated vehicles is firstly formulated. Following that, articulated vehicle modeling with any number of units is also tackled. Lastly, simulations on vehicles of different axle/articulation configurations are presented to evaluate the model reconfigurability and accuracy.

Chapter 4 Reconfigurable Controller Development

In this chapter, an optimization-based reconfigurable control framework is developed that can be used for any multi-axle vehicles. First, the stability objectives of yaw and roll planes are studied, especially focusing on steady-state of tractor yaw rate and articulation angle. Second, in the high-level, multi unit vehicles are unified into a general prediction model and a general MPC controller is developed to calculate corrective CG control forces. The feasibility and stability of the LTV-MPC are discussed. Third, a lower-level controller is developed as control allocation problem with different real-time constraints to distribute high-level calculations into actuators optimally. Last, a comprehensive work in MPC tuning with a specific vehicle example is presented.

Chapter 5 Applications and Simulations

This chapter presents a simulation work on three representative vehicles with different active actuation systems and different objectives. To reduce the computational burden, the model formulation is simplified and customized for each case before any online computation. Next, by setting the ‘Boolean Matrices’ and gains properly, the controller problem for each application is quickly formulated. Furthermore, the results of each application demonstrate

the effectiveness of the controller in stabilizing the vehicles from undesired conditions, including situations of actuator failures, and vehicle and road uncertainties.

Chapter 6 Experimental Study

This chapter presents an experimental study to validate the reconfigurability and performance of the proposed controller. First, test facilities and platform, such as the vehicle, sensors, and hardware are introduced and the cornering stiffness of the trailer is identified by solving an optimization problem. Since both tractor and trailer are equipped with differential braking systems, it validated and compared three potential braking strategies and the results are presented and compared with control OFF cases. It is shown that the controllers work properly and effectively to maintain the stability of the tractor and the trailer and are robust with respect to the road conditions.

Chapter 7 Conclusions and Future Work

This chapter concludes the work presented in the previous chapters and directs potential future work and directions.

Chapter 2

Literature Review and Background

This chapter establishes a review on multi-axle vehicles configurations, stability and control. The intent is to provide the necessary background to understand the challenges on multi-axle vehicles and the attempts have been made. The configuration diversity is firstly introduced in Section 2.1. Then, Section 2.2 discusses the main instability behaviors of multi-axle (articulated) vehicles in yaw and roll planes, such as trailer sway, tractor/trailer jackknife, and rollover phenomena. In Sections 2.3 and 2.4, potential active actuation systems and the concept of integrated, reconfigurable and universal control are reviewed and compared. Follow on this, common control methods are presented and the focus turns to MPC and Control Allocation (CA) techniques on vehicle stability control. A concept of universal and reconfigurable control is thus unfolded. Finally, Section 2.6 summarizes the chapter and reveals the work in next chapters.

2.1 Configuration Diversity

The following presents the multi-axle vehicle configurations in terms of axle/articulation and powertrain modes. Despite a wide range of multi-axle vehicles, it focuses on trucks and buses as multi-axle/articulated vehicles for demonstration.

2.1.1 Axle/Articulation Configurations

The great majority of articulated vehicles are commercial heavy vehicles whose purpose is to transport goods and materials in a logistically efficient and cost-effective manner as much as possible [1]. In the concept of ‘bigger is better’, the bigger the vehicle within a practical limitation, the more payload that can be transported with just one driver. To meet many different transportation purposes, a wide range of truck combinations exists. A 13-category of vehicles is classified by the Federal Highway Administration (FHWA) in Figure 2.1. It is seen that there are large varieties in truck combinations, axle configurations, number of articulations, load variations, and auxiliaries. Additionally, when more than two units are articulated, a dolly is usually used between units, see category 11-13.

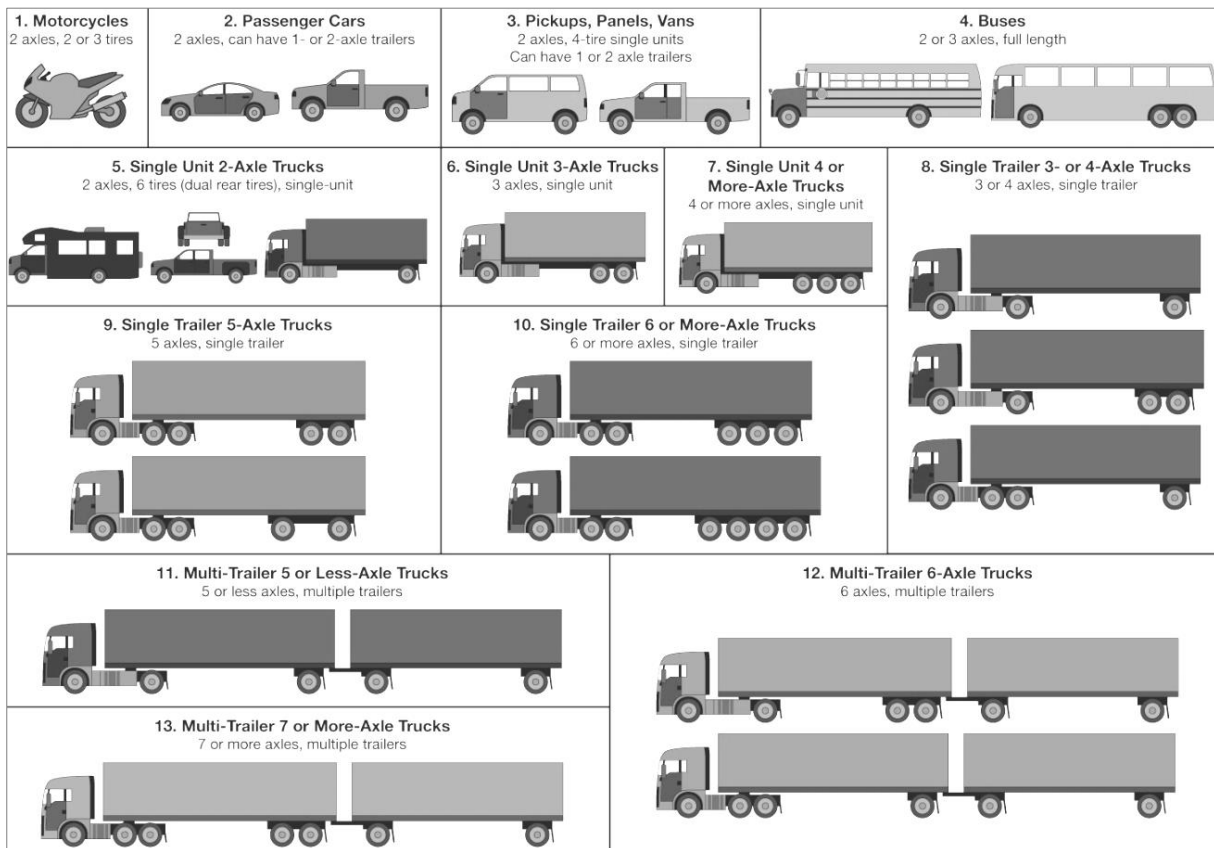


Figure 2.1: 13-category vehicle classifications by FHWA [9]

In additions, multi-axle buses often have different forms and configurations for the purpose of transporting a different volume of passengers on a relatively fixed infrastructure. Modified from the bus-category in [9], Figure 2.2 demonstrates six possible axle/articulation configurations of current buses or coaches in market. Extra axles are usually added due to legal weight restriction. Multi-axle buses with more than two axles usually three are known as tri-axle buses shown as type-b and type-c , or more rarely, four are known as quad-axle buses shown as type-d [10]. Furthermore, to accommodate different vehicle designs, the bus might be articulated with articulation joints to implement trailer buses of multiple units, see type-e and type-f in Figure 2.2.







			
a. Two axles (1-front, 1-rear)	b. Three axles (2-front, 1-rear)	c. Three axles (1-front, 2-rear)	d. Four axles (2-front, 2-rear)
			
e. Articulated bus (2 units)		f. Articulated bus (3 units)	

Figure 2.2: Different axle/articulation configuration of buses and coaches [9]

2.1.2 Powertrain/Driveline Configurations

The powertrain of a vehicle includes main components that serve to generate the drive power and deliver it to the driving wheels. The driveline or drivetrain of a motor vehicle describes the parts of a powertrain excluding the engine and transmission, which may be configured with various deliver modes. Multi-axle vehicles also have different propulsion systems and driving mode. It could be a conventional internal combustion engine, electric

motor, or hybrid electric power [11, 12]. Among driving modes, it is the actuator delivering the power to specific wheels. A multi-axle vehicle may be front-wheel drive, rear-wheel drive, all-wheel drive or any combination of wheels drive. In addition, although front-wheel steering system is the most common mode, there could be other steer modes depending on the needs, see in [13]. Table 2.1 outlines all possible powertrain, drive modes and steer modes configurations.

Table 2.1: Different powertrain/driveline/steer mode configurations

Propulsion Systems	Drive Mode	Steer Mode
Combustion engine	All-wheel drive	Front-wheel steer
Electric motor	Front-wheel drive	All-wheel steer
Hybrid power	Rear- wheel drive	
	Any combination wheels drive	

2.2 Vehicle Instability

Fundamentally speaking, the dynamics of multi-axle vehicles is similar to that of passenger cars. There are, however, differences due to different designs and applications. First, multi-axle vehicles are usually articulated with one or several articulation joints with multiple axles. This certainly makes the dynamics much more complex, for example, the oscillatory modes that are excited in various maneuvers [14]. Another major difference is that multi-axle vehicles are usually prone to rollover due to a high wheelbase to track ratio, a high CG and an uneven or varied weight distribution between axles. It points out that the truck may exhibit unstable behavior at a lateral acceleration of 0.3 g to 0.4 g (m/s^2), during tasks of steering and braking [15]. Passenger cars normally do not roll over, except for tripped rollover, because the tires will saturate and start to slide long before reaching a sufficiently high lateral acceleration. A third important difference is that passenger car chassis is fairly stiff with respect to torsion and bending, but multi-axle vehicles are normally not. This may have a great influence on the truck dynamic behavior in various areas. To summarize, major instabilities of the yaw plane and roll plane are presented.

2.2.1 Yaw-plane Instability

Yaw-plane instability indicates an unstable behavior of the vehicle lateral or yaw motion when it is during a sudden lane change or excessive entry-speed in a curve or driving in a straight line. As shown in Figure 2.3, articulated vehicles may experience three types of instability in the yaw-plane, which have been identified in [16–20].

- **Trailer Snaking/Sway:** This type behaves a trailer yaw oscillation (periodic instability), which is dynamic in nature and may lead to oscillatory response with increasing amplitude known as fish tailing, snaking or sway, shown in Figure 2.3(a). Trailer sway is usually associated with high speed and external disturbance, for instance, by gusts of wind, or the passing of big vehicles. In addition, internal factors, such as a sharp steer and an unstable trailer configuration, such as high payload and poor CG location, could also trigger sway [21]. This phenomena can be seen in the experimental study.
- **Trailer Jackknife:** Jackknife means the units of an articulated vehicle try to fold, where two units form a ‘V’ shape instead of driving in a proper line. Figure 2.3(b) shows a ‘trailer jackknife’, and it is a divergent instability in which the tractor is stable on the road, but the trailer turns around the articulation joint in a highly unstable manner. The trailer jackknife may occur when the trailer axle wheels are locked during braking and the road is slippery, for example, a braking and steering operation conditions.
- **Tractor Jackknife:** Similar to trailer jackknife, in tractor jackknife, the trailer is stable on the road, but the tractor slips to the side, shown in Figure 2.3(c). This occurs most commonly when the tractor is under excessive braking, e.g. rear wheels lock-up or acceleration e.g. rear wheels spinning on a road low road friction coefficient, and in particular the rear wheels of the tractor loose grip or traction [19].

Both sway and jackknife are very dangerous unstable motion modes of articulated vehicles and jackknife becomes one of the main causes for fatal accidents. In addition, the trailer off-tracking phenomenon is different from instability issues but might bring risks.

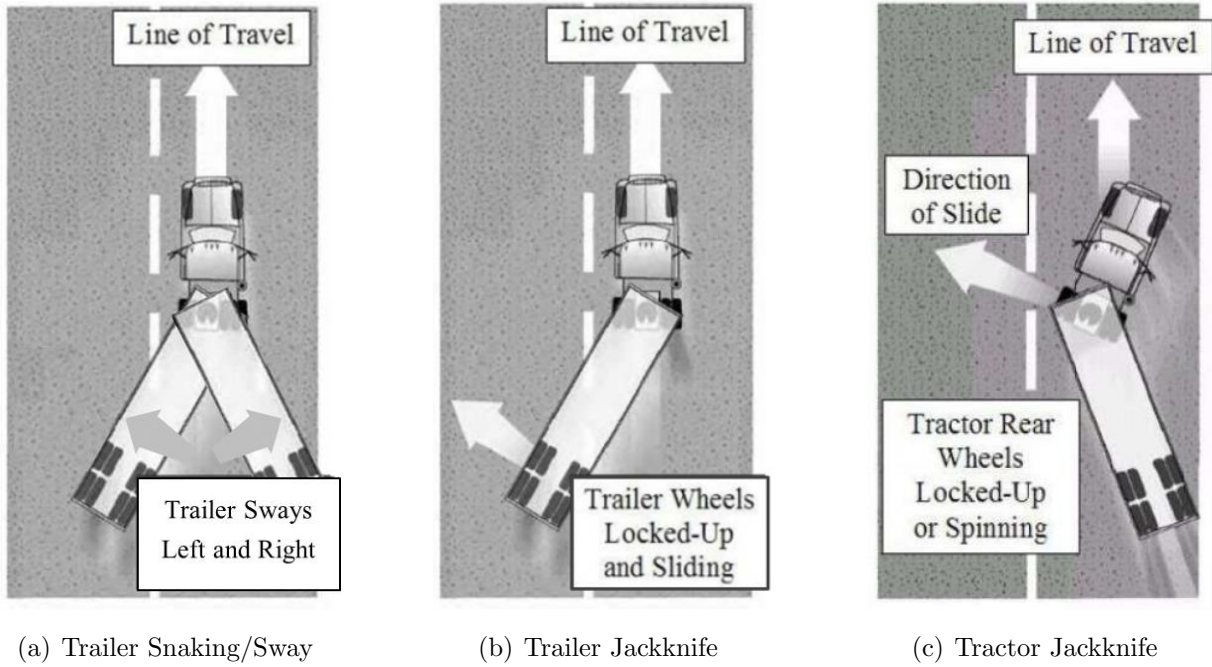


Figure 2.3: Unstable modes of articulated vehicles in yaw-plane [22]

Suppose a truck is making a low speed turn at 90° , off-tracking is defined as the deviation of the semi-trailers' axles or the articulation hitch from the path of the steering axle of the lead tractor during a turn [23]. In a non-articulated vehicle, the front and rear wheels take different paths when cornering but it is not obvious. However, in the case of the articulated vehicles, such as tractor-(semi)trailer combination (see the configuration in Figure 2.3), the trailer does not follow the path of the lead tractor during a turn for a lane change or a turn. Such a deviation is potentially very dangerous because it is possible for the semi-trailer to violate the lane outer boundary or crash with an adjacent car during a lane change, even though both the tractor-(semi)trailer and the car are within safe speed limits. Thus the driver or active control has to compensate for this off-tracking to ensure the safety and stability.

2.2.2 Roll-plane Instability

Multi-axle vehicles rollover is another significant portion of accidents. According to NHTSA /NCSA statistics, it is suggested that half of heavy truck crash fatalities in the US involve vehicle rollover, and comparable results were shown by examinations made in Europe [24]. Roll instability is related to the possibility that the vehicle will roll over. An example of a truck rollover has been shown in Figure 1.1. Factors of the vehicle type (such as the height of the CG and track width of the vehicle), driver behavior and the environmental conditions (such as road condition) play a significant role in the rollover phenomenon [25]. What's more, it is also influenced by other factors such as the suspension compliance and lash and the distribution of roll stiffness between the axles [14]. Rollover of a vehicle occurs in two ways, known as tripped and untripped rollovers.

A tripped rollover commonly occurs at two situations: the vehicle tires skidded and digged into soft soil; the vehicles hits a tripping mechanism (e.g., a curb) with a large lateral velocity [26]. Static rollover indicators used to indicate tripped rollover of a vehicle are the Tilt Table Ratio, Critical Sliding Velocity, Static Stability Factor and the Track Width Ratio [27]. These indicators determine the static rollover only by using the vehicle parameters. Apart from tripped rollover instability, which is not discussed in this thesis, the untripped rollover is induced by caused by three critical driving situations: sudden course deviation, often in combination with braking, from high initial speed; excessive speed while curving; and load shift. The rollover of a tractor semi-trailer combination usually starts at the semi-trailer. To detect wheel lift-off conditions when a vehicle is moving, the lateral Load Transfer Ratio (LTR), or rollover indicator (RI) in this thesis, is used to indicate the rollover risk and calculated by [28, 29]:

$$RI = \frac{F_{zr} - F_{zl}}{F_{zr} + F_{zl}} \quad (2.1)$$

where F_{zr} and F_{zl} are the total vertical loads of the right-side and left-side wheels of the vehicle, respectively. When wheels lift off the road, and the RI takes on the limit value, which is -1 or 1 . For straight driving on a horizontal road, the lateral RI holds zero. Since the lateral acceleration and roll angle/rate are closely related to the lateral load transfer condition, they are usually chosen as the control objective of articulated vehicles

for roll stability improvement. For instance, in [30], Hyun and Langari proposed a practical LTR approximation only using the unsprung mass roll angle (ϕ_{um}) and the equivalent axle stiffness (K_{um}). RI is hence calculated as $RI = K_{um}\phi_{um}$. Cheng and Cebon [31] chose lateral acceleration and roll angle for deduction as to improve roll stability of heavy vehicles.

2.3 Active Actuation Systems

Actuation systems are the key to implement any vehicle dynamics control (VDC) strategy. Among them, steering and driving/braking actuators are the basic parts of the vehicle chassis. This makes active control of yaw/roll stability possible through these active actuators. It includes direct yaw-moment control (DYC) or active steering control (ASC) or the combination of both (integrated). In addition, active/semi-active suspension systems are also implemented for dynamics control, especially for rollover prevention. Figure 2.4 classified the major types of active chassis control systems.

First, direct yaw moment control generates a compensated yaw moment by redistributing tire longitudinal forces to improve the yaw and roll stability, for instance, common systems are active torque vectoring or differential braking. Due to its high cost-effective, DYC is one of the prominent approaches and numerous research works with different active systems and control algorithms can be found, see [26] and [32–35]. It is proved that DYC could enhance the vehicle stability for critical driving conditions, but it may be less effective under a split road condition. DYC could also decrease the yaw rate and increase a burden to the driver while driving at a high-speed steady state cornering [35].

Second, active steering control combines the steering angle from the driver and designed controller input. Depending on needs, the controller steering correction may be added to or subtracted to modify the steering command and then affect tire lateral forces. Possible control strategies are active front steering (AFS) or active rear steering (ARS) or all-wheel active steering control for implementation. Research works of vehicle dynamics control using ASC have been continuously conducted, some representatives can be seen in [36–40]. For instance, Zhu and He investigated the active steering system for articulated heavy vehicles to improve directional performance with the evaluation of different controllers.

Active steering is especially effective under steady driving conditions or when the tire lateral force is operating in small slip angles, namely linear area, but it becomes less effective while tires enter into nonlinear characteristics that usually happens in critical situations.

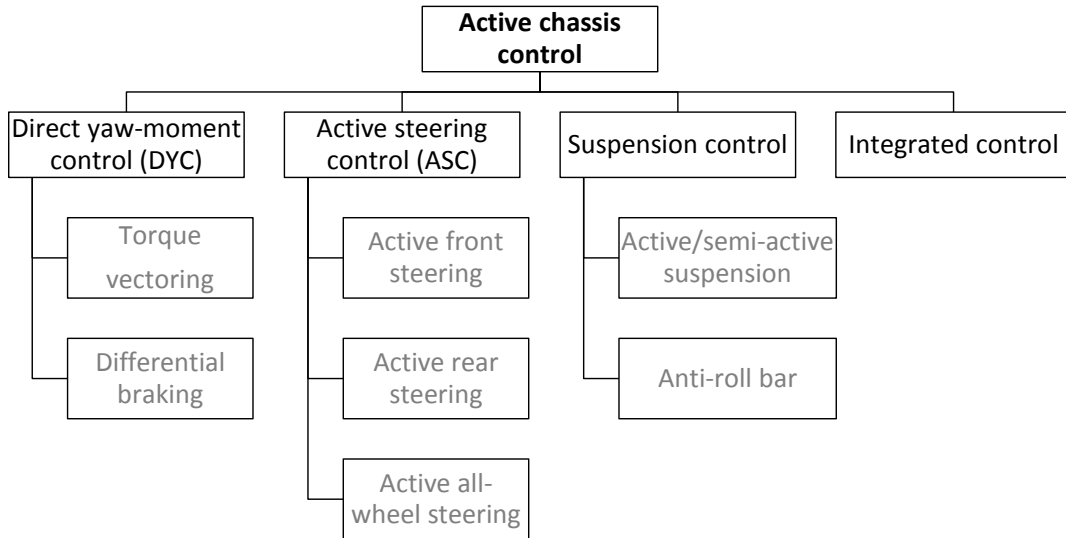


Figure 2.4: Active chassis control systems

Last, active/semi-active suspension and anti-roll bar systems are well-known to improve ride comfort, but also they could enhance vehicle stability and rollover mitigation via coordinating the vertical forces of each corner. Papers [29] and [41–43] showed how active suspensions/anti-roll bar, i.e. roll moment distribution and yaw rate control, effectively improved the handling performance and reduced rollover risk. In addition, any combination of above systems is also possible. Integrated systems of differential braking, active steering, and active suspension or active stabilizer are implemented in [40, 44–46]. It suggested that the integrated active chassis control is appealing since it covers all the shortages while using only one active control system. However, these active actuators configurations vary from vehicle to vehicle, considering attributes such as physical complexity and cost.

As autonomous driving and advanced driver assistant system (ADAS) are actively studied and popularized, it is anticipated that the current systems will increase the effectiveness of active safety interventions beyond what is previously available [37]. This is facilitated

not only by active actuator types, such as active steering or active differentials but also by additional sensor information, such as the onboard cameras, radars and GPS/IMU system. It will be great news for active dynamics control. In this context, the active system is ‘more active and smart’ as the vehicles would be able to identify road condition, avoid obstacles or dangers, and assist the driver by keeping the right lane, see examples in [47–50].

2.4 Integrated, Reconfigurable and Universal VDC

To address the various actuator configurations, control objectives, and over-actuated system, it is worth mentioning that, recently, integrated chassis control [40, 51–53], reconfigurable control and control allocation have gained much attention [54–57]. Integrated control makes the most use of all actuation systems and prevents conflicts of different objectives and subsystems. In [58], it well reviewed Integrated Vehicle Dynamics Control (IVDC) architectures, that are differentiated as centralized, supervisory, hierarchical, and coordinated control. For instance, in [57], Jalali proposed a model predictive control by coordinating active steering and differential brakes for vehicle stability. Unlike separate controllers, the integration of control objectives, (i.e., yaw control and wheel slip control) and available actuators (i.e., differential braking and active steering) avoids the potential conflict between the outputs of individual control modules, while providing optimal control actions. An example of integrating stability and energy management for an electric car is introduced in [52]; the novel algorithm optimizes wheel torque outputs, body stability, wheels traction control, power management, and actuator limits.

Reconfigurable control provides much freedom for controller design to fit different configurations of vehicle. It means moving from one configuration to another does not need to start over the controller design where the reconfigurable scheme has the universality to include all configurations. In [54], a coordinated reconfigurable vehicle dynamics control system is proposed by high-level sliding mode control, and distributed to the slip and slip angle of each tire by lower-level control allocation (CA), where an accelerated fixed-point algorithm is used to enhance the convergence properties of the allocation method. Reconfigurable control usually uses multi-layered structure control systems that provide

good flexibility and reduces complexity by decoupling the problem. For instance, [51] presented a unified chassis control (UCC) strategy with three layers: a supervisor, a control algorithm, and a coordinator, where each layer serves designate purposes. In [56], a modular-based reconfigurable and integrated longitudinal and lateral vehicle stability control using optimal control techniques was proposed for electric vehicles and validated experimentally. Similarly, Ataei [59] presented a reconfigurable modeling work particularly for four-wheeled and three-wheeled vehicles by using the reconfiguration matrices and then developed a reconfigurable vehicle stability control that applied to an SUV with different actuation combinations [60].

Although, in most of the aforementioned studies, controllers might be integrated and reconfigurable, they were designed to control a particular vehicle and most focus on two-axle passenger cars. Research on multi-axle vehicles dynamics control is, however, scarce. In addition, to cope with the diversity of vehicle configurations, a feasible yet universal control scheme is expected.

2.5 MPC and CA Techniques

Common Control Methods

Numerous control theories/methods have been explored for vehicle stability control. Generally, there are model-free control and model-based control, including the linear and the nonlinear. From the classical PI/PID controllers found in [61, 62], such as Marino [61] designed and combined with a decentralized proportional controller for active front steering and a proportional-integral controller for active rear steering based on the error of yaw rate tracking without lateral speed measurements and car model. However, model-free control requires high tuning efforts and provides not optimal solution and is sensitive to the derivative term. Studies show that most of the reported research use the model-based controller. Typical methods are linear quadratic regulator (LQR) [63–65], sliding mode control (SMC) [15, 66], H infinity control [26, 36] and other methods and variants [32, 67, 68].

Each control method has its own pros and cons depending on different features and

applicability. For example, generally, LQR highly depends on model accuracy. Moreover, it gives globally optimal control calculation but does not consider control input and output constraints. H infinity control has a complex formulation and is not optimal. SMC is easy to tune and reasonably robust but has excessive switching and chattering phenomena (actuator damage) and noise sensitivity issues. Very often, these methods are used for an unconstrained system and a mandatory saturation is added to restrict the control input, and the output constraints are even more challenge to limit. Since that no control method is perfect and there is a compromise among many sides, e.g. performance, cost, implementability, optimality and etc, one has to choose the method that fits the problem formulation most.

Model Predictive Control

In the past decade, Model Predictive Control (MPC) technique for vehicle control and applications has attracted extensive attention from the researchers [69]. MPC has the unique capability of considering the inputs and output constraints explicitly. Besides that the constraints are formulated and satisfied in real time, the control action is an optimal (locally) solution. In an MPC scheme [70, 71], a model of the plant is used to predict the future evolution of the system. Based on this prediction, at each time step, an open-loop optimal control problem with a certain performance index (or cost function) and operating constraints is solved over a finite horizon. Thus, the control action sequence is achieved by repeatedly solving finite time optimal control problems in a receding horizon fashion. The control action only applies the first of the computed optimal sequence to the plant at current time step. At the next time step, a new optimal control problem based on new measurements of the state is reformulated and solved over a shifted, where the slip history is considered as an external input to the model.

Taken in the context of the vehicle stability control problem, the objective of longitudinal, yaw and roll control is to track some desired states or reduce to certain threshold values. The outputs are usually bounded for safety concern and actuators have physical limitations or capacity due to tires. The problem setting is well-matched to the MPC formulation. The finite time optimal control law is the solution to an optimization problem online, providing a method for incorporating both an objective as well as constraints.

Comprehensive introduction on MPC and its applications to vehicle stability control can be found from many literature and books. For instance, Falcone [37] used an MPC-based approach to control yaw and lateral dynamics through integrated active front steering and braking. It used a full tenth-order vehicle model and a simplified bicycle model, respectively. Results showed the latter one is not able to stabilize the vehicle at high entry speeds and the first one has good tracking performance at both low and high entry speed but with high computational burden. Unlike tracking or regulation problems, Beal [72] presented a model predictive envelope controller that enforces the boundaries of the safe handling envelopes in real time. In his approach, the controller is only activated to stabilize the vehicle when the vehicle is leaving or out of the stable envelope. Jalaliyazdi [53] designed an integrated MPC system to address vehicle stability, traction control, and power distribution objectives at the same time in one controller. The proposed controller is reconfigurable to work with various driveline configurations and various(braking) actuator configurations.

Control Allocation

Vehicles are usually over-actuated mechanical systems, e.g. four or more than four-wheel providing driving/brake torques, or even steering. To coordinate the control actions on a constrained over-actuated system properly is a key problem to address. Control allocation (CA) offers the advantage of over-actuated systems to allocate the desired generalized controls (typically virtual) among all active actuators optimally. CA is usually used in conjunction with high-level feedback control laws [54], wherein this research is an MPC as the high-level controller. The high-level motion control algorithm can be designed without detailed knowledge about actuators, so universality is achieved for any vehicles. Important issues such as input saturation and rate constraints, actuator and fault tolerance, and minimal control energy are handled within the control allocation algorithm [73].

Wang [54] developed a coordinated and reconfigurable VDC system in which high-level control of generalized forces/moment are virtual controls allocated to tire slip values. A lower-level combined tire slip and slip angle tracking controller manipulates each wheel's driving/braking/steering torque to achieve a desired tire slip/slip angle by using a control allocation (CA). Kasinathan [74] proposed a novel holistic cornering control (HCC) of torque vectoring strategy using control allocation techniques. HCC calculates the wheel

torque distribution or command steer angle adjustments in real-time to minimize CG forces and moment errors, amplitudes of the control adjustments and maximize tire reserves for stabilizing the vehicle. Similarly, Nahidi [56] extended the HCC and used a control allocation to distribute the required longitudinal force and yaw moment adjustments from the high-level controller. The framework allows modularity and optimality in control design and its performance is validated by experimental tests.

2.6 Summary and Discussion

In this chapter, the literature on multi-axle vehicle modeling and control was reviewed, with special focus on multi-axle trucks and buses. Many different configurations were presented to demonstrate the variety and complexity of multi-axle vehicles. Common vehicle instability behaviors, such as, trailer snaking/sway, the jackknife, off-tracking, and the rollover instability were explained. The analysis of vehicle instability provides essential evidence on dynamics control. Utilizing steering and torque/braking, and suspension actuators, different active vehicle chassis techniques were presented. Following that, the strategy of integrated, reconfigurable and universal vehicle dynamics control was reviewed and discussed. Special attention was given to model predictive control and control allocation along with several applications in the literature.

Although the aforementioned active control systems and controller design could be applied to the articulated multi-axle vehicle, there is a paucity research on articulated multi-axle vehicle control found in the literature. In most stability control systems, it requires significant efforts in ‘re-designing’ and ‘re-tuning’ of the controller to obtain a similar performance while transferring the controller from one vehicle to another with a different configuration. This is even more evident in multi-axle vehicles due to the variety and complexity of their configurations.

This research is intended to bridge the gap by developing a reconfigurable model for any multi-axle vehicle, and upon which, to design a reconfigurable vehicle dynamics control system. That means the stability control performance does not change and major re-tuning can be avoided while transplanting from one configuration to another.

Chapter 3

Dynamics and Modeling of Multi-axle Vehicles

Vehicle and tire models are widely studied and utilized for stability control, which will not be repeated here, but what this chapter presented is a framework of the reconfigurable modeling process. It finalizes a general and reconfigurable formulation that unites any multi-axle vehicles, no matter how many axles are configured and it is articulated or not. The majority of this chapter was published in the Journal of Vehicle System Dynamics in 2018 [75].

The chapter is organized as follows. Section 3.1 begins with a necessary introduction on coordinate systems and notations used in the modeling and methodology description. Starting with non-articulated vehicles, a reconfigurable modeling process is developed in Section 3.2 and a linearization is presented in Section 3.3 for controller design purposes. Since an articulated vehicle is a combination of two or more vehicle units, the modeling process is extended to any articulated vehicle in Section 3.4. In Section 3.5, the proposed models are evaluated and compared using CarSim/TruckSim with a variety of different vehicles and configurations. Section 3.6 summarizes the chapter.

3.1 Coordinate Systems and Methodology

Vehicle dynamics equations are usually expressed in a set of vehicle coordinate system ($C - xyz$) attached to the CG point. As shown in Figure 3.5 and Figure 3.9, in where, the body dynamics are developed in a right-handed coordinate system according to a standard ISO 8855 [76]. The positive x is a longitudinal axis passing through hand directed forward. The positive y goes laterally to the left from the driver's viewpoint. The positive z goes upwards, opposite to the gravitational direction.

The global coordinate system ($O - XYZ$) is fixed to the ground. The position and orientation of the vehicle coordinate system ($C - xyz$) are measured with respect to a global coordinate frame. Following to the right-hand rule, the positive yaw angle is the angle from global axis- X to vehicle axis x about axis- Z ; the positive roll angle is the angle from global axis- Y to vehicle axis y about axis- X ; the positive pitch angle is the angle from global axis- Z to vehicle axis z about axis- Y . These conventions are very important while dealing with the tractor-trailer or even articulated multi-unit vehicle dynamics modeling.

In consideration of a holonomic rigid multi-body system (MBS), the dynamics of a vehicle system can be described by ordinary differential equations using the Newtonian or Lagrangian method. In our modeling process, the vehicle dynamics is firstly derived from the tire forces or corner forces. Next, all the forces of the tires are equalized to the CG of the vehicle, which will result in CG forces/moment. At last, treating the body as a point mass, the desired dynamics equations are formulated. It defines the '*Actuator Boolean Matrix*' to determine the availability (or configuration) of the active actuation and '*Axle Boolean Matrix*', the availability (or configuration) of axles, namely, the number of axles. How are articulated multi-unit vehicles then modeled? The benefits of reconfigurable modeling process of a single vehicle unit are taken. In Figure 3.1, the vehicle is articulated with two arbitrary units by a physical articulation joint. Following this intuition, the model can be formulated as a two vehicle units dynamics modeling developed, along with corresponding dynamics/kinematic constraints at articulation point. The '*Articulation Boolean Matrix*' is defined to judge the availability of the articulation, namely, the vehicle is articulated or not.

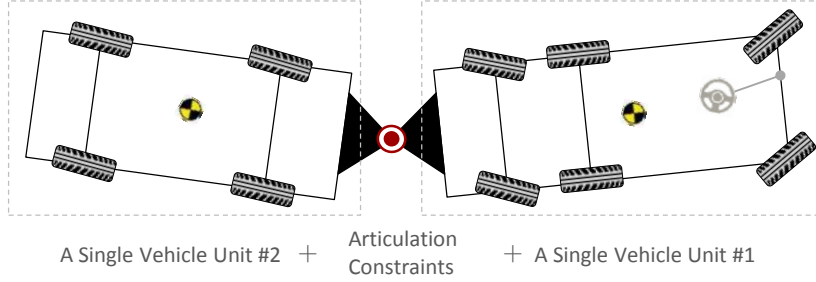


Figure 3.1: From a single unit to articulated multi-unit vehicle

3.2 Non-articulated Vehicles

3.2.1 Corner Forces

Generally, it is assumed that the vehicle is equipped with two different actuators at each corner including torque/braking and steering while the effect of the camber angle is neglected [2]. As shown in Figure 3.2, local forces (or tire forces) are depicted in the axles attached to the tire and comprise the longitudinal forces from torque/brake and the lateral forces from steering. This research assumes that the tire longitudinal force and tire lateral force are decoupled, and calculated separately. One could note that each tire force includes a term from the driver command and an augmenting term applied by active control systems, such as Active Steering Control, Torque Vectoring or Differential Braking System. Therefore, the so-called corner forces (differentiating from tire cornering force or lateral force) are defined as a 2-dimension vector forces from the resultant of all tire forces with respect to x and y axis.

The equation of corner forces for an arbitrary wheel i can be derived as:

$$F_{xi} = (f_{xi} + t_{xi}\Delta f_{xi}) \cos \delta_i - (f_{yi} + t_{yi}\Delta f_{yi}) \sin \delta_i \quad (3.1a)$$

$$F_{yi} = (f_{xi} + t_{xi}\Delta f_{xi}) \sin \delta_i + (f_{yi} + t_{yi}\Delta f_{yi}) \cos \delta_i \quad (3.1b)$$

where δ_i , f_{xi} and f_{yi} denote the local steering angle, longitudinal and steering (lateral) forces for wheel number i , respectively. Δf_{xi} and Δf_{yi} suggest the augmenting forces on

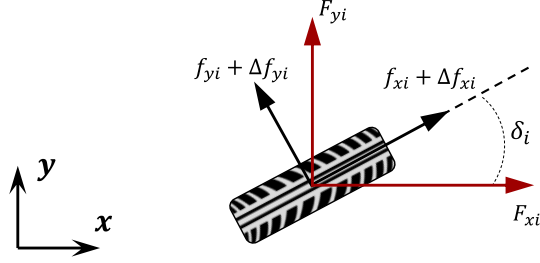


Figure 3.2: Corner forces on an arbitrary wheel i

the tire forces applied by the active controller. The symbol t_{xi} and t_{yi} are defined as ‘Actuator Boolean Parameters’ to determine the availability of longitudinal and steering actuators. These parameters can only be 1 or 0, where the basic rule is that 1 activates the corresponding actuator and 0 deactivates.

For simplicity and convenience of reconfigurable vehicle model formulation, the relationship of corner forces and tire forces along with the actuator configuration is written in matrix form:

$$F_{ci} = L_{wi}(f_i + T_{wi}\Delta f_i), F_{ci} \in \mathbb{R}^{2 \times 1} \quad (3.2)$$

where the tire forces, $f_i = \begin{bmatrix} f_{xi} & f_{yi} \end{bmatrix}^T$, the local actuator configuration matrix, $T_{wi} = \text{diag}(t_{xi}, t_{yi})^1$, the augmenting term applied by the controller, $\Delta f_i = \begin{bmatrix} \Delta f_{xi} & \Delta f_{yi} \end{bmatrix}^T$, L_{wi} is the mapping matrix from local tire forces to corners force.

For demonstration’s sake, assuming that the generalized model for the multi-axle vehicle has the maximum axle of 4 and a minimum of 2, the equations will extend to eight wheels in matrix form. The vector including all wheels is defined as:

$$f = \begin{bmatrix} f_1^T & f_2^T & \cdots & f_8^T \end{bmatrix}^T, f \in \mathbb{R}^{16 \times 1} \quad (3.3)$$

Finally, to include the local and corner forces of all wheels along with the actuator configurations in matrix form, it is written as:

$$F_c = L_w(f + T_w\Delta f), f \in \mathbb{R}^{16 \times 1} \quad (3.4)$$

¹D = diag(v) denotes a square diagonal matrix with the elements of vector v on the main diagonal.

where $F_c = \begin{bmatrix} F_{c1}^T & F_{c2}^T & \dots & F_{c8}^T \end{bmatrix}^T$, and F_{ci} refers to (3.2). T_w is defined as the ‘*Actuator Boolean Matrix*’, where configures the active actuators to determine the specific actuator configuration in a active control system.

To have a general idea of how it works, an active control case is introduced and demonstrated. A three-axled vehicle with one front axle and two rear axles is assumed. The vehicle is capable of active differential braking of rear axles and active front steering, shown in Figure 3.3. Given such configuration of the active system, the ‘*Actuator Boolean Matrix*’ will be modified as:

$$T_w = \text{diag}[(0, 1), (0, 1), (0, 0), (0, 0), (1, 0), (1, 0), (1, 0), (1, 0)] \quad (3.5)$$

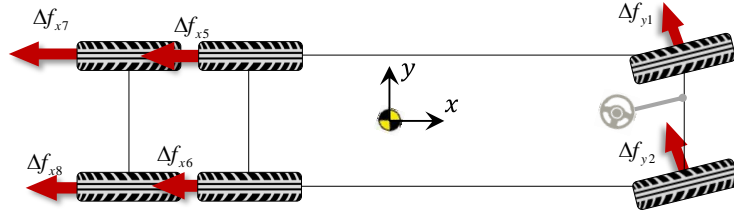


Figure 3.3: A multi-axle vehicle with active differential braking and front steering

3.2.2 CG Forces/Moment

Finishing analyzing a single wheel and extending to eight wheels, this section aims to map all the corner forces to CG forces/moments in a matrix formulation. Figure 3.4 depicts a four-axle, eight wheel vehicle and the forces in a global view. The wheel numbers are indicated next to each wheel. The front left wheels are wheel number 1 and 3, and the front right wheels are number 2 and 4. Moving to the rear on the left side, it counts the wheels numbered 5 and 7, and then the right side wheels are numbered 6 and 8. By summing each wheel's corner forces, the total longitudinal force, total lateral force and total CG moment

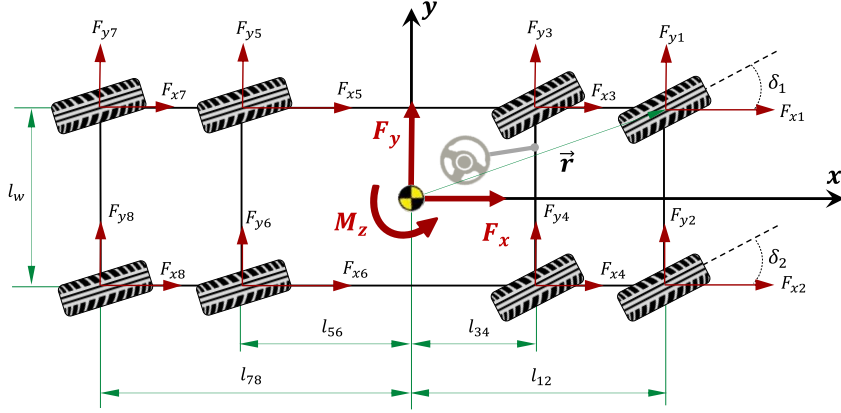


Figure 3.4: Corner forces in a global view and CG forces/moment

of the vehicle can be expressed as:

$$F_x = \sum_{i=1}^8 t_{cxi} F_{xi} \quad (3.6)$$

$$F_y = \sum_{i=1}^8 t_{cyi} F_{yi} \quad (3.7)$$

$$M_z = \sum_{i=1}^8 \vec{r}_i \times (T_{ci} F_{ci}) \quad (3.8)$$

where \vec{r}_i is defined as the displacement vector from CG position to the hinge joint point of wheel number i . The symbol t_{cxi} and t_{cyi} are defined as ‘Axle Boolean Parameters’ to determine the availability of longitudinal force and lateral force and T_{ci} is a matrix that $T_{ci} = \text{diag}(t_{cxi}, t_{cyi})$. The ‘Axle Boolean Matrix’ of the whole vehicle is defined as:

$$T_c = \text{blockdiag}(T_{c1}, T_{c2}, T_{c3}, T_{c4}, T_{c5}, T_{c6}, T_{c7}, T_{c8}), \in \mathbb{R}^{16 \times 16}. \quad (3.9)$$

In order to apply the proposed model to the different types of multi-axle vehicles, these parameters could easily meet the end by giving 1 or 0. Since the transformation is based on axle(s) removal from the four-axle vehicle, one could easily understand that the forces

of removed wheels will be set zero. For example, the vehicle in Figure 3.3, given the configuration of three axles, the 'Axle Boolean Matrix' will be modified as:

$$T_{ci} = \begin{bmatrix} 0 & 0 \\ 0 & 0 \end{bmatrix}, i = 3, 4; T_{ci} = \begin{bmatrix} 1 & 0 \\ 0 & 1 \end{bmatrix}, i = \text{rests.}$$

Utilizing the vehicle's geometric parameters shown in Figure 3.4, total CG moment in (3.8) is expanded as:

$$M_z = \sum_{i=2,4,6,8} \frac{l_w}{2} t_{cxi} F_{xi} - \sum_{i=1,3,5,7} \frac{l_w}{2} t_{cxi} F_{xi} + \sum_{i=1,2} l_{12} t_{c yi} F_{yi} + \sum_{i=3,4} l_{34} t_{c yi} F_{yi} - \sum_{i=5,6} l_{56} t_{c yi} F_{yi} - \sum_{i=7,8} l_{78} t_{c yi} F_{yi} \quad (3.10)$$

where l_w is the vehicle track and a unified vehicle track is used for all axles. $l_{12}/l_{34}/l_{56}/l_{78}$ are the distances from the first/second/third/fourth axle to CG position in the X-Y plane, respectively, shown in Figure 3.4. Writing all forces/moments in matrix form, F_{CG} is defined as the force vector on CG:

$$F_{CG} = \begin{bmatrix} F_x & F_y & M_z \end{bmatrix}^T, F_{CG} \in \mathbb{R}^{3 \times 1} \quad (3.11)$$

And defining the mapping matrix from corners to CG force by:

$$L_c = \begin{bmatrix} 1 & 0 & 1 & 0 & 1 & 0 & 1 & 0 & 1 & 0 & 1 & 0 & 1 & 0 & 1 & 0 \\ 0 & 1 & 0 & 1 & 0 & 1 & 0 & 1 & 0 & 1 & 0 & 1 & 0 & 1 & 0 & 1 \\ -\frac{l_w}{2} & l_{12} & \frac{l_w}{2} & l_{12} & -\frac{l_w}{2} & l_{34} & \frac{l_w}{2} & l_{34} & -\frac{l_w}{2} & -l_{56} & \frac{l_w}{2} & -l_{56} & \frac{l_w}{2} & -l_{78} & \frac{l_w}{2} & -l_{78} \end{bmatrix} \quad (3.12)$$

Hence, the force vector F_{CG} at CG is succinctly expressed as:

$$F_{CG} = L_c T_c F_c \quad (3.13)$$

To have more idea of how the generalized model fits different types of vehicles, another multi-axle vehicle with two front axles and one rear axle is applied. The 'Axle Boolean Matrix' will be configured as:

$$T_{ci} = \begin{bmatrix} 0 & 0 \\ 0 & 0 \end{bmatrix}, i = 5, 6; T_{ci} = \begin{bmatrix} 1 & 0 \\ 0 & 1 \end{bmatrix}, i = \text{rests.}$$

where if one substitutes the above configuration to (3.9), and then to (3.13), the CG forces will be only calculated from available axle and wheels.

3.2.3 Body Dynamics

As the CG forces have been formulated in terms of wheels forces, a dynamic model for the multi-axle vehicle is developed in this section. The vehicle dynamics includes longitudinal motion, lateral motion, yaw motion, and roll motion, where the vertical movement and pitch motion are not considered. Figure 3.5 depicts the coupling yaw and roll dynamics of the vehicle.

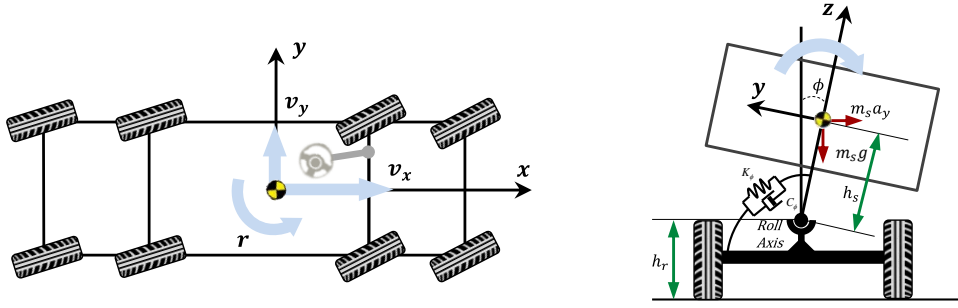


Figure 3.5: Longitudinal, lateral, yaw and roll dynamics

Angular orientation and angular velocity are expressed by two angles: yaw and roll, and their rates: yaw rate and roll rate. The roll angle is assumed small and the roll axis is parallel to the horizontal plane. One can refer to [77, 78], and then the Newton-Euler equations of motion are established by:

$$m(\dot{v}_x - rv_y) - m_s h_s (\phi \dot{r} + 2r \dot{\phi}) + 0.5 C_d A_f \rho_a v_x^2 = F_x \quad (3.14a)$$

$$m(\dot{v}_y + rv_x) + m_s h_s (\ddot{\phi} - r^2 \ddot{\phi}) = F_y \quad (3.14b)$$

$$I_{zz} \dot{r} - I_{xz} \ddot{\phi} - m_s h_s (\dot{v}_x - rv_y) \phi = M_z \quad (3.14c)$$

$$(I_{xx} + m_s h_s^2) \ddot{\phi} - m_s h_s (\dot{v}_y + rv_x) - I_{xz} \dot{r} - (m_s h_s^2 + I_{yy} - I_{zz}) r^2 \phi = M_x \quad (3.14d)$$

Given that the CG force vector is formulated in (3.11), here the external rolling moment can be derived by:

$$M_x = -K_\phi \phi - C_\phi \dot{\phi} + m_s g \cdot h_s \phi \quad (3.15)$$

where the vehicle's inherent parameters: the vehicle's total mass m , the sprung mass m_s , the distance of the sprung mass CG location from the roll axis h_s , the moments of inertia about roll axis I_{xx} , pitch axis I_{yy} , and yaw axis I_{zz} , the roll stiffness coefficient K_ϕ , the roll damping coefficient C_ϕ ; and the vehicle's the longitudinal velocity v_x and lateral velocity v_y . In addition, $0.5C_dA_f\rho_a v_x^2$ is the term of aerodynamic drag force, wherein, C_d is the aerodynamic drag coefficient, ρ_a is the mass density of air, A_f is the frontal area of the vehicle.

The derived equations are obviously all nonlinear. By defining the vehicle state, $x = [v_x \ v_y \ r \ \phi \ \dot{\phi}]^T$, it can be expressed as a matrix form:

$$\dot{x} = f(\dot{x}, x) + B_F F_{CG} \quad (3.16)$$

where,

$$f(\dot{x}, x) = \begin{bmatrix} v_y r + (2m_s h_s (\phi \dot{r} + r \dot{\phi}) - C_d A_f \rho_a v_x^2) / 2m \\ -r v_x - m_s h_s (\ddot{\phi} - r^2 \phi) / m \\ I_{xz} \ddot{\phi} + m_s h_s (\dot{v}_x - r v_y) \phi / I_{zz} \\ \dot{\phi} \\ \frac{-(m_s h_s (\dot{v}_y + r v_x) - I_{xz} \dot{r} - (m_s h_s^2 + I_{yy} - I_{zz}) r^2 \phi + (K_\phi - m_s g h_s) \phi + C_\phi \dot{\phi})}{(I_{xx} + m_s h_s^2)} \end{bmatrix}, B_F = \begin{bmatrix} 1/m & 0 & 0 \\ 0 & 1/m & 0 \\ 0 & 0 & 1/I_{zz} \\ 0 & 0 & 0 \\ 0 & 0 & 0 \end{bmatrix}.$$

By far three layers of vehicle modeling process have been presented, from corner forces to CG forces, and to body dynamics. Now that these three layers of the formulations are given in (3.4), (3.13) and (3.16), the final generalized vehicle model including the corner forces matrix and actuator forces matrix is then achieved by:

$$\dot{x} = f(\dot{x}, x) + B_F L_c T_c L_w (f + T_w \Delta f) \quad (3.17)$$

This compact equation describes the full vehicle dynamics. There are two sources of nonlinearities which make it nonlinear and complicated. One is the differential equations at CG dynamics, and the other is the nonlinear tire forces generation.

3.2.4 Tire Model and Load Transfers

Tires play an essential role in vehicle dynamics as the forces and moments come from the road acting on each tire. Without consideration of moments, tires may be considered as

a force generator that creates two outputs: the longitudinal force and lateral force. The input of the force generator is the tire load f_{zi} , sideslip angle α_i , longitudinal slip s_i and the camber angle γ_i :

$$f_{xi} = f(f_{zi}, \alpha_i, s_i, \gamma_i) \quad (3.18a)$$

$$f_{yi} = g(f_{zi}, \alpha_i, s_i, \gamma_i) \quad (3.18b)$$

where the right-hand side of the equation, f and g represents the function of f_{zi} , α_i , s_i and γ_i of wheel number i ($i = 1$ to 8). A variety of tire models attempts to capture describe the tire's nonlinearity and complexity. They are usually derived from its physical mechanism [79, 80] or empirical formulation or the combined [78, 81] and additionally, some construct many details of the tire through finite element method [82, 83]. The nonlinear brush tire model [80] provides a very good description on tire forces yet with its simple formulation, which is examined by Beal and Gerdes in [84].

Hence, brush tire model is used to represent the tire lateral force in this research. It has much similarities with the well-known 'Magic Formula' tire model but with only two calibration parameters. The relationship between the slip angle and the tire force is expressed by:

$$f_{yi} = \begin{cases} -C_{\alpha i} \tan \alpha_i + \frac{C_{\alpha i}^2}{3\eta_i \mu f_{zi}} |\tan \alpha_i| \tan \alpha_i - \frac{C_{\alpha i}^3}{27\eta_i \mu f_{zi}} \tan^3 \alpha_i & |\alpha_i| < \alpha_i^{sat} \\ \eta_i \mu f_{zi} \text{ sign} \alpha_i & \text{otherwise} \end{cases} \quad (3.19)$$

where $C_{\alpha i}$ and μ are tire cornering stiffness and tire-road friction coefficient, respectively, that can be identified experimentally. The saturated slip angle is defined at the point, where greater slip angles generate no more additional lateral force:

$$\alpha_i^{sat} = \tan^{-1} \left(\frac{3\eta_i \mu f_{zi}}{C_{\alpha i}} \right) \quad (3.20)$$

Figure 3.6 provides an example of the brush tire model proposed and experimental data at different normal loads in a pure-slip condition when $C_{\alpha i}$ and μ are estimated. The brush model has a relatively accurate performance that covers a wide range of the tire slip angle. To take account for the longitudinal force, the derating factor (η_i) is added in (3.19) to capture the reduced lateral based on a presumed f_{xi} . The expression of η_i is derived from the tire friction circle', see more detail in [85]. However, in this research, η is assumed to

be 1. Considering the single-track model, small angle assumptions allow the slip angle of tire number i to be written as:

$$\alpha_i = \frac{v_y + r l_i}{v_x} - \delta_i, \quad (i = 1, \dots, 8) \quad (3.21)$$

where the sign of l_i depends on the location of the axle with respect to the CG. This thesis considers the axle configuration in Figure 3.4, which gives that: $l_1 = l_2 = l_{12}, l_3 = l_4 = l_{34}, l_5 = l_6 = -l_{56}, l_7 = l_8 = -l_{78}$.

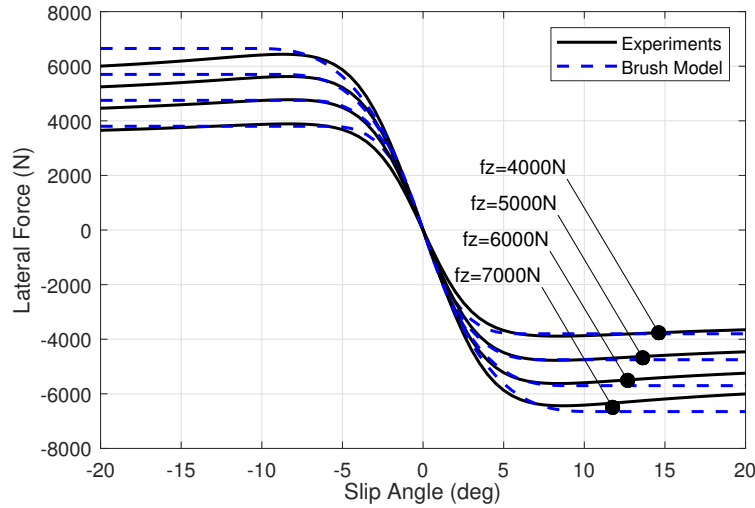


Figure 3.6: Brush tire model V.S. experimental data at different normal loads

Another nonlinearity of importance is the relationship between cornering stiffness and the vertical tire force. Due to load transfer among wheels, the nonlinearity causes a reduction of the total axle cornering stiffness and it is even more pronounced when the load transfer is large, that is, for high lateral accelerations. To calculate both longitudinal and lateral forces of tires, the tires' vertical loads are needed at first. An equivalent displacement approach [86] is introduced to calculate the tires' dynamic vertical load transfers:

$$f_z = K_s L_z^T (L_z K_s L_z^T + P_0)^{-1} S_0 \quad (3.22)$$

where f_z is the vector of vertical tire force, K_s is the equivalent stiffness matrix including each wheel of the suspension system, L_z is the geometrical mapping matrix recording position of

the each tire, and are matrixes including the information of the vehicle parameters and system states. These matrices are given as ,

$$f_z = \begin{bmatrix} f_{z1} & f_{z2} & \cdots & f_{z8} \end{bmatrix}^T, f_z \in \mathbb{R}^{8 \times 1},$$

$$K_s = \text{diag}(k_{s1} \quad k_{s2} \quad \cdots \quad k_{s8}), K_s \in \mathbb{R}^{8 \times 8},$$

$$L_z = \begin{bmatrix} 1 & 1 & 1 & 1 & 1 & 1 & 1 & 1 \\ l_w/2 & -l_w/2 & l_w/2 & -l_w/2 & l_w/2 & -l_w/2 & l_w/2 & -l_w/2 \\ -l_1 & -l_2 & -l_3 & -l_4 & -l_5 & -l_6 & -l_7 & -l_8 \end{bmatrix}, L_z \in \mathbb{R}^{3 \times 8}$$

$$P_0 = \begin{bmatrix} 0 & 0 & 0 \\ 0 & -m_s g(h_s - h_p) & 0 \\ 0 & 0 & -m_s g(h_s - h_q) \end{bmatrix}, P_0 \in \mathbb{R}^{3 \times 3},$$

$$S_0 = \begin{bmatrix} mg & -ma_y h & ma_x h \end{bmatrix}^T, S_0 \in \mathbb{R}^{3 \times 1}.$$

Among the matrices, where f_{zi} ($i = 1, \dots, 8$) represents the vertical force of tire number i , k_{si} is the equivalent suspension stiffness at the wheel number i , generally, its value on the left wheel and right wheel of each axle is identical, h_p is the height of rolling center and h_q is the height of the pitching center.

In this load transfer scheme, the vertical forces distribution can be obtained by using the longitudinal and lateral accelerations, which can be acquired from approachable sensors, e.g. IMU. Figure 3.7 gives an example of a three-axled bus and the actual vertical forces and calculated ones are compared. A combined acceleration/deceleration and steer maneuver is performed. It is shown that the load transfers consideration has a fair accurate performance applying to multi-axle vehicles.

3.3 Model Linearization

3.3.1 Linearized Tire Model

Plenty of experimental results have shown that the longitudinal tire force is proportional to the slip ratio at small slip ratio. And with the torque of wheel number Q_i and the tire effective radius R_{eff} , the longitudinal force is calculated with the assumption of constant

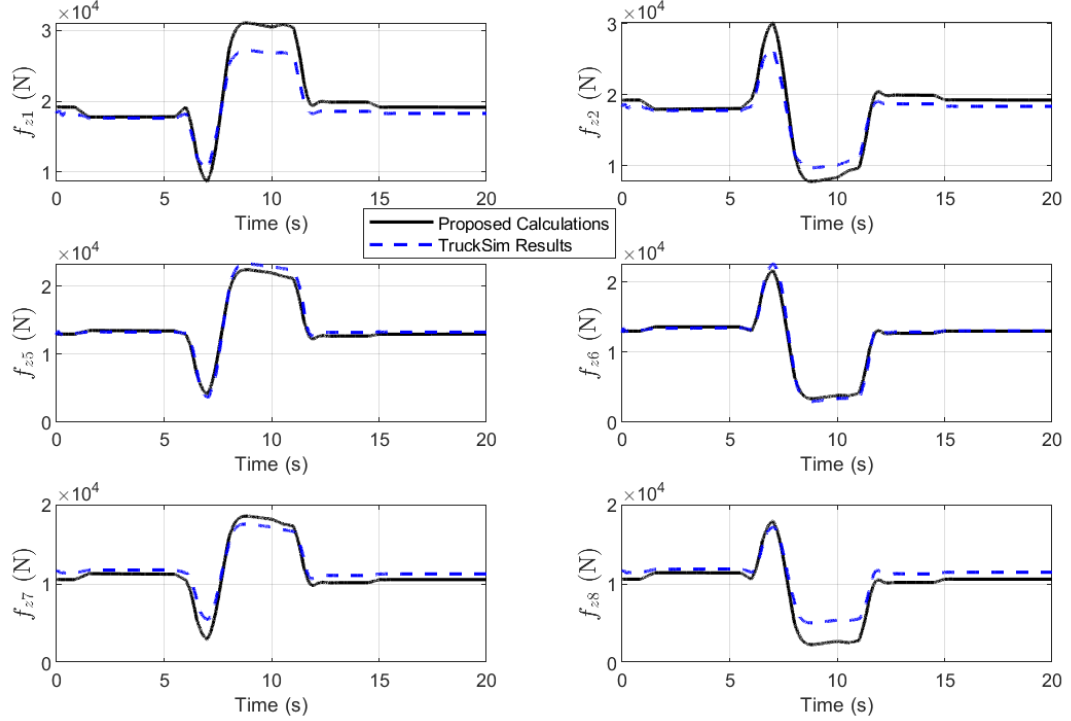


Figure 3.7: Tire load transfers at combined condition

rotation:

$$f_{xi} = \frac{Q_i}{R_{eff}}, \quad (i = 1, \dots, 8) \quad (3.23)$$

Generally, the effective radius R_{eff} depends on many factors, such as the type of tire, stiffness, inflation pressure, and wheel speed [77]. However, the effective radius of radial tires is very close to its unloaded radius.

To establish the vehicle motion equations with tire forces, the nonlinear brush tire model may provide a very good description and result in an accurate vehicle dynamics behavior. However, the computational cost grows significantly with increased model complexity. In an MPC control algorithm, the issue becomes considerable while calculating control actions in real time at 100Hz by automotive-grade hardware.

Therefore, the underlying model for the controller is simplified. To represent the link between the vehicle motion and the tire forces, the brush tire model is linearized at the slip angle operating point, shown in Figure 3.8. Given a nonlinear explicit tire model, its linearization is found by taking the differentiation of the operation point [72] and an affine model is formulated:

$$-\bar{C}_{\alpha i} = \frac{f_{yi} - \bar{f}_{yi}}{\alpha_i - \bar{\alpha}_i} \Rightarrow f_{yi} = \bar{f}_{yi} - \bar{C}_{\alpha i}(\alpha_i - \bar{\alpha}_i), \quad (i = 1, \dots, 8) \quad (3.24)$$

where at the operating point ($\bar{\alpha}_i$), the tire force (\bar{f}_{yi}), and the equivalent cornering stiffness ($\bar{C}_{\alpha i}$), can be found through the brush model formed in look-up tables. The brush model combining longitudinal slips fits into the vehicle experimental data. The linearizing technique connects the vehicle state and tire force, which results in a Linear Time-Variant (LTV) model and allows the further MPC controller to formulate the predictions near the operating point as well as considering tire saturation area. Furthermore, in the active steering strategy, the equivalent cornering stiffness $\bar{C}_{\alpha i}$ is assumed to be constant for the purpose of calculating lateral tire forces in a small corrective (active) angle. Figure 3.8 illustrates the approximation at an arbitrary operating point.

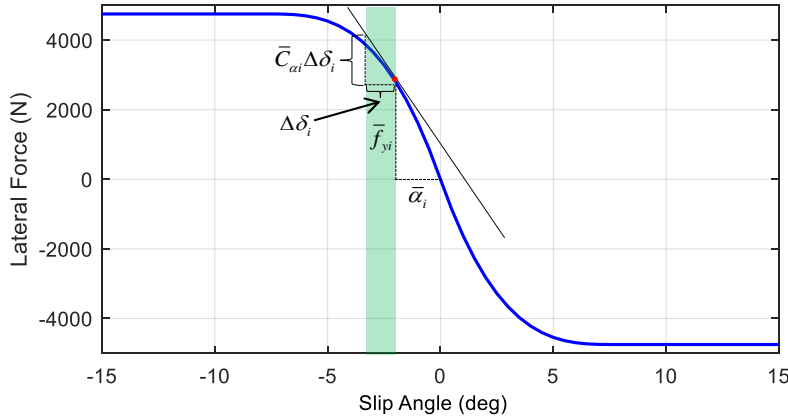


Figure 3.8: Affine approximation of brush tire model

With the ignorance of air drag force and road grade angle, the linearized tire forces of

tire number i can be written in matrix form:

$$\begin{bmatrix} f_{xi} \\ f_{yi} \end{bmatrix} = \underbrace{\begin{bmatrix} 0 & 0 & 0 & 0 & 0 \\ 0 & -\bar{C}_{\alpha i}/v_x & -l_i\bar{C}_{\alpha i}/v_x & 0 & 0 \end{bmatrix}}_{A_{ti}} x + \underbrace{\begin{bmatrix} 1/R_w & 0 \\ 0 & \bar{C}_{\alpha i} \end{bmatrix}}_{B_{ti}} \begin{bmatrix} Q_i \\ \delta_i \end{bmatrix} + \underbrace{\begin{bmatrix} -f_{ri} \\ f_{yi} + \bar{C}_{\alpha i}\bar{\alpha}_i \end{bmatrix}}_{d_{ti}} \quad (3.25)$$

where vector $w_i = [Q_i \ \delta_i]^T$ is the driver's command mapped to on wheel i , wherein, Q_i represents the torque from drive or brake while δ_i represents the steering angle. f_{ri} is the rolling resistance of wheel i , and it is known that $\sum_{i=1}^8 f_{ri} = mg\mu_r$ (μ_r is the resistance coefficient). Combining all the wheels in one matrix equation, it is achieved that:

$$f = A_t x + B_t w + d_t \quad (3.26)$$

where, matrix A_t , B_t , w and d_t are naturally structured as,

$$\begin{aligned} A_t &= \begin{bmatrix} A_{t1}^T & A_{t2}^T & A_{t3}^T & A_{t4}^T & A_{t5}^T & A_{t6}^T & A_{t7}^T & A_{t8}^T \end{bmatrix}^T, \in \mathbb{R}^{16 \times 5} \\ B_t &= \text{blockdiag}(B_{t1}, B_{t2}, B_{t3}, B_{t4}, B_{t5}, B_{t6}, B_{t7}, B_{t8}), \in \mathbb{R}^{16 \times 16} \\ w &= \begin{bmatrix} w_1^T & w_2^T & w_3^T & w_4^T & w_5^T & w_6^T & w_7^T & w_8^T \end{bmatrix}^T, \in \mathbb{R}^{16 \times 1} \\ d_t &= \begin{bmatrix} d_{t1}^T & d_{t2}^T & d_{t3}^T & d_{t4}^T & d_{t5}^T & d_{t6}^T & d_{t7}^T & d_{t8}^T \end{bmatrix}^T, \in \mathbb{R}^{16 \times 1}. \end{aligned}$$

Using the same linearization process, the forces generated from the active controller is given by:

$$\begin{bmatrix} \Delta f_{xi} \\ \Delta f_{yi} \end{bmatrix} = \begin{bmatrix} 1/R_w & 0 \\ 0 & \bar{C}_{\alpha i} \end{bmatrix} \begin{bmatrix} \Delta Q_i \\ \Delta \delta_i \end{bmatrix}, (i = 1, \dots, 8) \quad (3.27)$$

where $u_i = [\Delta Q_i \ \Delta \delta_i]^T$ is defined as the controller's command on wheel i , wherein, ΔQ_i represents the correction torque while $\Delta \delta_i$ represents the correction steering angle. It should be noted that the equivalent cornering stiffness $\bar{C}_{\alpha i}$ at current tire slip angle is used to calculate the active lateral forces, shown in Figure 3.8.

Combining all the wheels' correction forces in one matrix equation, it is written as:

$$\Delta f = B_1 u \quad (3.28)$$

where, $u = [u_1^T \ u_2^T \ u_3^T \ u_4^T \ u_5^T \ u_6^T \ u_7^T \ u_8^T]^T, \in \mathbb{R}^{16 \times 1}$.

Finally, combining equation (3.26) and (3.28) along with the ‘Actuator Boolean Matrix’, the approximatively linearized tire forces is stated as:

$$f + T_w \Delta f \approx A_t x + B_t w + T_w B_t u + d_t \quad (3.29)$$

3.3.2 Linearized Body Dynamics

The compromise between modeling complexity and computing efficiency for the advanced controller is handled by linearizing the vehicle model. The linear body dynamics of the longitudinal motion, lateral motion, yaw motion, and roll motion can be described as:

$$m\dot{v}_x - mg\mu_r = F_x \quad (3.30a)$$

$$m(\dot{v}_y + rv_x) - m_s h_s \ddot{\phi} = F_y \quad (3.30b)$$

$$I_{zz} \dot{r} = M_z \quad (3.30c)$$

$$I_{xx} \ddot{\phi} - m_s h_s (\dot{v}_y + rv_x) = -K_\phi \phi - C_\phi \dot{\phi} + m_s g \cdot h_s \phi \quad (3.30d)$$

The linearized equations can be rearranged to obtain the continuous time state space form of the system and written as:

$$\dot{x} = Ax + BF_{CG} \quad (3.31)$$

where $x = [v_x \ v_y \ r \ \phi \ \dot{\phi}]^T$ is defined as the vehicle states. Matrix A and B are provided in the Appendix A.1.

3.3.3 State Space Formulation

Using the derived formulation of tires forces (3.29) and vehicle dynamics (3.31) and CG forces (3.13), the whole linear vehicle model yields the following expressions:

$$\begin{aligned} \dot{x} &= Ax + BL_c T_c L_w (A_t x + B_t w + T_w B_t u + d_t) \\ &\Rightarrow \dot{x} = A_v x + G_v w + B_v u + d_v \end{aligned} \quad (3.32)$$

where, we define this state space formulation as ‘reconfigurable model’ for any multi-axle vehicle. Based on the features of these matrices, it is defined that,

vehicle matrix: $A_v = A + BL_c T_c L_w A_t$;
driver matrix: $G_v = BL_c T_c L_w B_t$;
controller matrix: $B_v = BL_c T_c L_w T_w B_t$;
remainder vector: $d_v = BL_c T_c L_w B_t d_t$.

3.4 Articulated Vehicles

Articulated vehicles dynamics is complex due to the coupled constraints at articulation point. Many tried to model it directly through differential equations and complex transformations and items elimination. The idea in this thesis is simple and straightforward. Intuitively, the dynamics of articulated vehicles (one articulation) is ‘dynamics of two separate units + constraints at articulation point’. Following the idea, now the modeling is moving from a single vehicle unit to articulated vehicle. Taking the tractor-trailer in Figure 3.9 as an example, the articulated vehicle has 6 DoFs, where the tractor unit has the freedom to go forward, side-slip, yaw, and roll, while the trailer has the freedom to yaw relative to the tractor and to roll.

3.4.1 Detached Tractor/Trailer

Following the same method of linearization on multi-axle vehicle dynamics formulation, the forces/moments at a detached tractor or trailer are added shown in Figure 3.9(a). The linear dynamics equations of the tractor unit for longitudinal, lateral, yaw, and roll motions can be described as [31]:

$$m^t \dot{v}_x^t = F_x^t + F_{x,h}^t \quad (3.33a)$$

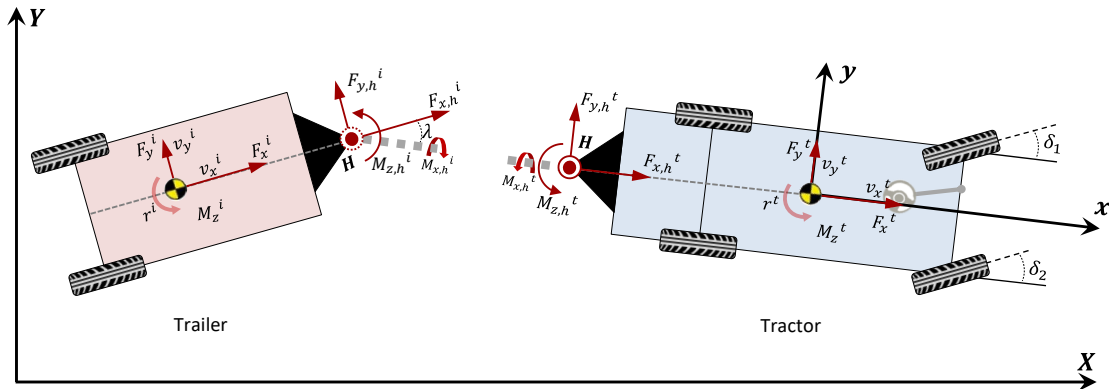
$$m^t (\dot{v}_y^t + r^t v_x^t) - m_s^t h_s^t \ddot{\phi}^t = F_y^t + F_{y,h}^t \quad (3.33b)$$

$$I_{zz}^t \dot{r}^t = M_z^t - l_h^t F_{y,h}^t + M_{z,h}^t \quad (3.33c)$$

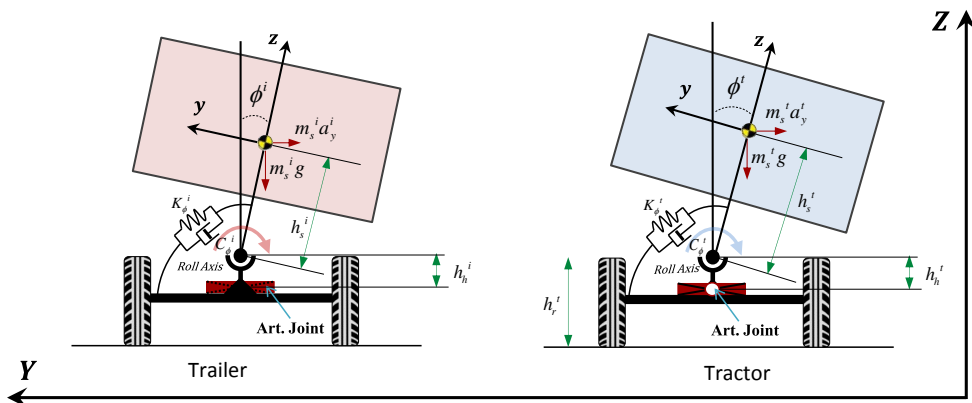
$$I_{xx}^t \ddot{\phi}^t - m_s^t h_s^t (\dot{v}_y^t + r^t v_x^t) = -K_{\phi}^t \phi^t - C_{\phi}^t \dot{\phi}^t + m_s^t g h_s^t \phi^t + M_{x,h}^t + h_h^t F_{y,h}^t \quad (3.33d)$$

wherein, the yaw moment at the articulation point due to the articulation characteristics:

$$M_{z,h}^t = K_{\lambda,h}^{t,i} \lambda + C_{\lambda,h}^{t,i} \dot{\lambda} + \Delta T_h$$



(a) Yaw dynamics(top view)



(b) Roll dynamics(rear view)

Figure 3.9: Yaw and roll dynamics of the tractor and trailer

and the roll moment at the articulation point due to the articulation characteristics,

$$M_{x,h}^t = K_{\phi,h}^{t,i}(\phi^i - \phi^t)$$

where all the superscripts of the parameters indicates the tractor', $F_{x,h}^t$ and $F_{y,h}^t$ are the longitudinal and lateral forces acting at the articulation point in term of the tractor unit, $M_{z,h}^t$ is the yaw moment generated at the articulation point, which comes from two parts: $K_{\lambda,h}^{t,i}\lambda + C_{\lambda,h}^{t,i}\dot{\lambda}$, (for instance, a damping system of articulated buses) and ΔT_h (could be from a active articulation control system). $K_{\lambda,h}^{t,i}$ and $C_{\lambda,h}^{t,i}$ are the articulation angle stiffness coefficient and damping coefficient, ΔT_h is the input torque from the controller at the articulation point. l_h^t is the distance between the articulation point and the CG of the tractor, h_h^t is the height of articulation point, measured upwards from roll center of sprung mass (illustrated in Figure 3.9(b)). $K_{\phi,h}^{t,i}$ is the roll stiffness of articulation point (front/rear), where $M_{x,h}^t = K_{\phi,h}^{t,i}(\phi^i - \phi^t)$ corresponding to Figure 3.9. The remainder parameters are explained by referring to subsection 3.2.3.

Referring to the body dynamics formulation in terms of CG forces in equation (3.31), the state-space form of the detached tractor unit is expressed in terms of CG forces and articulation forces:

$$\dot{x}^t = A^t x^t + B^t F_{CG}^t + C^t F_H^t \quad (3.34)$$

where $x^t = [v_x^t \ v_y^t \ r^t \ \phi^t \ \dot{\phi}^t]^T$ is defined as the tractor unit state. The tractor CG forces, $F_{CG}^t = [F_x^t \ F_y^t \ M_z^t]^T$, the tractor articulation forces, $F_H^t = [F_{x,h}^t \ F_{y,h}^t \ M_{z,h}^t \ M_{x,h}^t]^T$. Their corresponding matrices A^t , B^t and C^t can be easily derived from equation group in (3.33), provided in Appendix A.2.

Similarly, the linear dynamics equations of the trailer unit:

$$m^i \dot{v}_x^i = F_x^i + F_{x,h}^i \quad (3.35a)$$

$$m^i (\dot{v}_y^i + r^i v_x^i) - m_s^i h_s^i \ddot{\phi}^i = F_y^i + F_{y,h}^i \quad (3.35b)$$

$$I_{zz}^i \dot{r}^i = M_z^i + l_h^i F_{y,h}^i + M_{z,h}^i \quad (3.35c)$$

$$I_{xx}^i \ddot{\phi}^i - m_s^i h_s^i (\dot{v}_y^i + r^i v_x^i) = -K_{\phi}^i \phi^i - C_{\phi}^i \dot{\phi}^i + m_s^i g h_s^i \phi^i + M_{x,h}^i + h_h^i F_{y,h}^i \quad (3.35d)$$

where all the superscripts of the parameters represent the ‘trailer’, $F_{x,h}^i$ and $F_{y,h}^i$ are the longitudinal force and lateral force at the articulation point in term of the trailer unit, $M_{z,h}^i$ and $M_{x,h}^i$ is the reactive yaw and roll moment at articulation point, l_h^i is the distance between the articulation point and the CG of the trailer, h_h^i is the height of articulation point, measured upwards from roll center of sprung mass. The remainder parameters are explained by referring to section 3.2.3.

The state-space form of the detached trailer unit is expressed in terms of CG forces and articulation forces:

$$\dot{x}^i = A^i x^i + B^i F_{CG}^i + C^i F_H^i \quad (3.36)$$

where $x^i = [v_x^i \ v_y^i \ r^i \ \phi^i \ \dot{\phi}^i]^T$ is defined as the trailer unit state. The trailer CG forces, $F_{CG}^i = [F_x^i \ F_y^i \ M_z^i]^T$, the trailer articulation forces, $F_H^i = [F_{x,h}^i \ F_{y,h}^i \ M_{z,h}^i \ M_{x,h}^i]^T$. Their responding matrices A^i , B^i and C^i can be easily derived from equation group in (3.35) provided in Appendix A.3.

3.4.2 Articulation Constraints

Two groups of constraints are suggested at the articulation point. First, the kinematic constraint, namely, the velocities and accelerations at the CG of the trailer can be written with respect to the velocities and accelerations at the CG of the tractor:

$$v_x^i = v_{x,h}^i = v_x^t \cos \lambda + (v_y^t - l_h^t r^t) \sin \lambda \quad (3.37a)$$

$$v_y^i = v_{y,h}^i - l_h^i r^i = -v_x^t \sin \lambda + (v_y^t - l_h^t r^t) \cos \lambda - l_h^i r^i \quad (3.37b)$$

$$\dot{v}_x^i = \dot{v}_x^t \cos \lambda - v_x^t \dot{\lambda} \sin \lambda + (\dot{v}_y^t - l_h^t \dot{r}^t) \sin \lambda + (v_y^t - l_h^t r^t) \dot{\lambda} \cos \lambda \quad (3.38a)$$

$$\dot{v}_y^i = -\dot{v}_x^t \sin \lambda - v_x^t \dot{\lambda} \cos \lambda + (\dot{v}_y^t - l_h^t \dot{r}^t) \cos \lambda - (v_y^t - l_h^t r^t) \dot{\lambda} \sin \lambda - l_h^i \dot{r}^i \quad (3.38b)$$

where λ is the articulation angle, indicating the angle difference between the yaw angles of the tractor and trailer. According to the coordinate system used, the angle rate yields,

$$\dot{\lambda} = r^i - r^t$$

Second, the dynamics constraint, namely, the relationship of the longitudinal and lateral force between the tractor and trailer at the articulation are written as:

$$F_{x,h}^t = -F_{x,h}^i \cos \lambda - F_{y,h}^i \sin \lambda \quad (3.39a)$$

$$F_{y,h}^t = F_{x,h}^i \sin \lambda - F_{y,h}^i \cos \lambda \quad (3.39b)$$

And the interaction yaw and roll moment at articulation yield:

$$M_{z,h}^t = -M_{z,h}^i = K_{\lambda,h}^{t,i} \lambda + C_{\lambda,h}^{t,i} \dot{\lambda} \quad (3.40a)$$

$$M_{x,h}^t = -M_{x,h}^i = K_{\phi,h}^{t,i} (\phi^t - \phi^i) \quad (3.40b)$$

3.4.3 Reconfigurable Formulation

The constraints of the moment at articulation point and kinematic relationships are as demonstrated from (3.37) to (3.40). By summarizing these equations, the matrix form with the equality constraints of the articulated vehicle is written as:

$$\text{state space form.} \quad \dot{x} = Ax + BF_{CG} + T_\varepsilon(CF_H) \quad (3.41)$$

2 units

$$F_H^t = L_{t-i} F_H^i$$

$$\text{s.t.} \quad \begin{aligned} v_x^i &= v_x^t \cos \lambda + (v_y^t - l_h^t r^t) \sin \lambda \\ v_y^i &= -v_x^t \sin \lambda + (v_y^t - l_h^t r^t) \cos \lambda - l_h^i r^i \\ \dot{\lambda} &= r^i - r^t \end{aligned}$$

where,

$$\begin{aligned} x &= \begin{bmatrix} x^t \\ x^i \end{bmatrix}, \quad A = \begin{bmatrix} A^t & 0_{(5 \times 5)} \\ 0_{(5 \times 5)} & A^i \end{bmatrix}, \quad B = \begin{bmatrix} B^t & 0_{(5 \times 5)} \\ 0_{(5 \times 5)} & B^i \end{bmatrix}, \\ F_{CG} &= \begin{bmatrix} F_{CG}^t \\ F_{CG}^i \end{bmatrix}, \quad C = \begin{bmatrix} C^t & 0_{(5 \times 3)} \\ 0_{(5 \times 3)} & C^i \end{bmatrix}, \quad F_H = \begin{bmatrix} F_H^t \\ F_H^i \end{bmatrix}, \\ L_{t,i} &= \begin{bmatrix} -\cos \lambda & -\sin \lambda & 0 & 0 \\ \sin \lambda & -\cos \lambda & 0 & 0 \\ 0 & 0 & -1 & 0 \\ 0 & 0 & 0 & -1 \end{bmatrix} \end{aligned}$$

T_ε is defined as 'Articulation Boolean Matrix' in Table 3.1 to determine the availability of the articulation. Note that, by following the modeling approach, one could readily extend the one-articulation vehicle to any number of articulations vehicles. Each unit of the vehicle is allowed to allocate any axles and each axle is allowed to steer or drive/brake independently.

Table 3.1: The rule of articulated vehicles model

T_ε	Rule Description
$I_{(10 \times 10)}$	Articulated vehicle, articulation constraints should be included
$0_{(10 \times 10)}$	No articulation exists, considered as separated units

3.4.4 Extension to Any Vehicles

Figure 3.10 shows an articulated vehicle with 'n' units. Each unit of the vehicle is allowed to allocate any axles with the numbers from one to four. Each axle is allowed to steer or drive independently. Following the similar modeling approach, we extend the one-articulation vehicle to any number of articulations vehicles in this section. The unified form of the model is:

$$\text{state space form.} \quad \dot{x} = Ax + BF_{CG} + T_\varepsilon(CF_H) \quad (3.42)$$

n units

$$\begin{aligned} & F_H^{j-1} = L_{(j-1),(j)} F_H^j, j = 2, 3, \dots, n \\ \text{s.t.} \quad & v_x^j = v_x^{j-1} \cos \lambda^{j-1} + (v_y^{j-1} - l_h^{j-1} r^{j-1}) \sin \lambda^{j-1}, j = 2, 3, \dots, n \\ & v_y^j = -v_x^{j-1} \sin \lambda^{j-1} + (v_y^{j-1} - l_h^{j-1} r^{j-1}) \cos \lambda^{j-1} - l_h^j r^j, j = 2, 3, \dots, n \\ & \dot{\lambda}^{j-1} = r^j - r^{j-1}, j = 2, 3, \dots, n \end{aligned}$$

where j represents the j th unit of the vehicle, and the articulation numbers starts with $j - 1$, which applies to the articulation angle with symbol λ^{j-1} . Each unit has its own state vector x^j and system matrices A^j , B^j and C^j . Assembling every unit together in a unified form, it is obtained,

$$A = \text{blockdiag}(A^1, A^2, \dots, A^n); B = \text{blockdiag}(B^1, B^2, \dots, B^n);$$

$$C = \text{blockdiag}(C^1, C^2, \dots, C^n);$$

$$x = \begin{bmatrix} x^1 \\ x^2 \\ \vdots \\ x^n \end{bmatrix}; F_{CG} = \begin{bmatrix} F_{CG}^1 \\ F_{CG}^2 \\ \vdots \\ F_{CG}^n \end{bmatrix}; F_H = \begin{bmatrix} F_H^1 \\ F_H^2 \\ \vdots \\ F_H^n \end{bmatrix}.$$

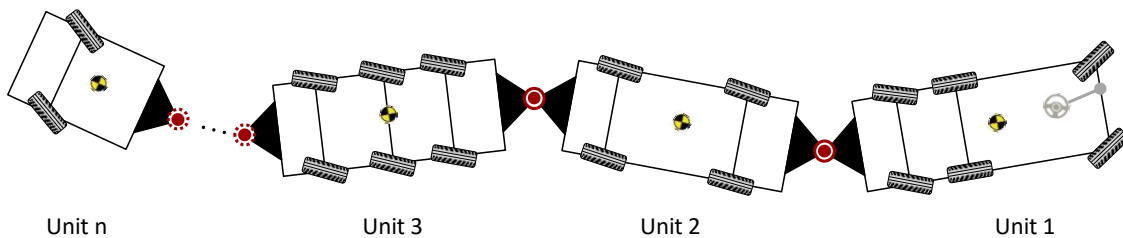


Figure 3.10: An articulated vehicle with any units

3.5 Model Evaluation

Model evaluation is performed to validate the reconfigurable modeling approach. To prove its general characteristics in different cases, the evaluation cases are not limited to one specific vehicle but applied to different types of multi-axle vehicles. There are two key aspects verified in this section: one is whether the approach is applicable and reconfigurable to any multi-axle or articulated vehicles. The other is whether the simulation results show a good match to high-fidelity models.

High-fidelity CarSim/TruckSim model received from the manufacturer of the test vehicles, is used to represent the vehicle dynamics for comparison. CarSim is for simulating the performance of passenger vehicles, light-duty trucks, and car-trailers while TruckSim is for multi-axle commercial and military vehicles. The accuracy of CarSim/TruckSim models has been previously validated by automotive engineers and found to be comparable to the real-world vehicle responses [87]. For the sake of model-based controller design, the proposed models are all linearized as a time-varying version for comparison.

Config. 1: A Two-axled SUV

In this case, a two-axled sport utility vehicle (SUV) is simulated and compared. It is the one used in experimental study of Chapter 6. Since it is a single vehicle unit with normal two axles configuration, there is only 'Axle Boolean Matrix' and can be written as,

$$T_c = \text{diag}(1, 1, 1, 1, 0, 0, 0, 0, 0, 0, 0, 0, 1, 1, 1, 1);$$

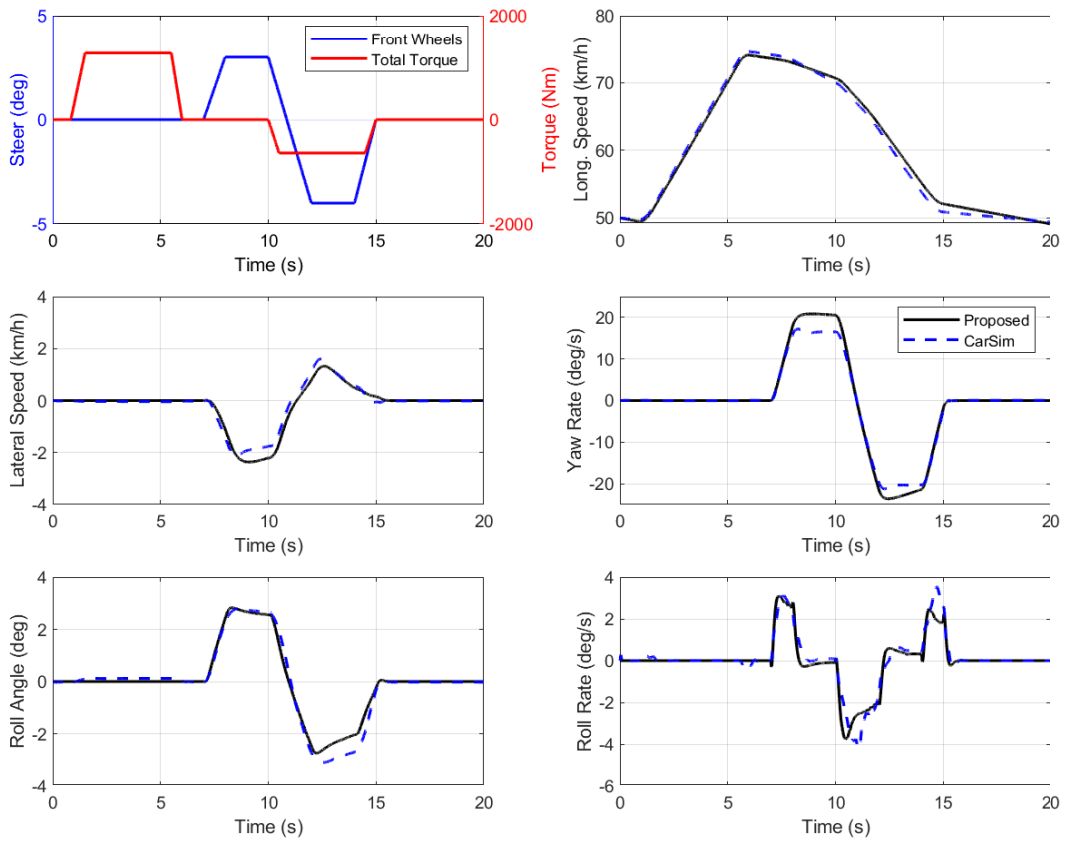


Figure 3.11: A two-axled SUV

For verification of the model, its responses to a left and right steer as input for the vehicle with an initial speed of 40km/h were compared. As shown in Figure 3.11, the results of longitudinal, yaw and roll dynamics responses are all quite similar to the results

of the CarSim model. In addition, the maximum tire slip angle is checked to reach 9 deg but the proposed model is very comparable with CarSim even at tire saturation area.

Config. 2: A Three-axled Bus

A bus with three axles where the front axle is for the steering system and rear two axles are connected to powertrain, is studied and evaluated. The bus is used in the simulation study of Chapter 5. Since it is a single vehicle unit with three axles configuration, there is only 'Axle Boolean Matrix' and can be written as:

$$T_c = \text{diag}(1, 1, 1, 1, 0, 0, 0, 0, 1, 1, 1, 1, 1, 1, 1);$$

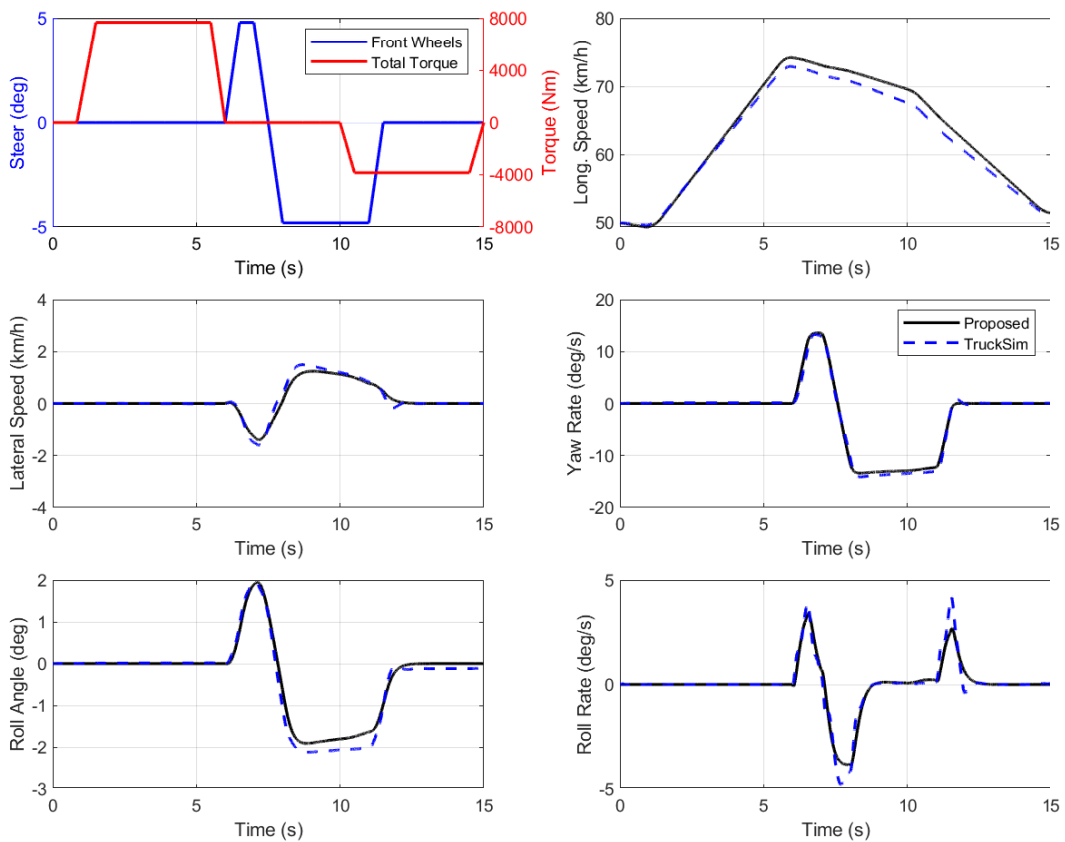


Figure 3.12: A three-axled bus

A flick maneuver which is usually for rollover test, with an initial speed of 50km/h, is conducted to the vehicle. As shown in Figure 3.12, the results of the configuration of the three-axle model are quite well-matched with the results of the TruckSim model. The longitudinal speed of the proposed model has a slightly steeper acceleration due to the ignorance of aerodynamics in the linearized model. What's more, it is checked that the maximum tire slip angles reach 7°. But the proposed model still shows a comparable behavior with TruckSim at whole duration of the maneuver .

Config. 3: An Articulated Bus

In this case, an articulated (three-axle) bus is simulated and compared. It is the one used in simulation study of Chapter 5. The tractor unit has two axles while the trailer unit has one. The 'Articulation and Axle Boolean Matrix' can hence be written as,

$$T_\varepsilon = I_{10 \times 10};$$

$$T_c^t = \text{diag}(1, 1, 1, 1, 0, 0, 0, 0, 0, 0, 0, 0, 1, 1, 1, 1);$$

$$T_c^i = \text{diag}(0, 0, 0, 0, 0, 0, 0, 0, 0, 0, 0, 0, 0, 1, 1, 1, 1);$$

For verification of the model, it used a left-and-right steer as input for the vehicle with an initial speed of 40km/h. The results of longitudinal, yaw and roll dynamics responses of each unit along with the articulation angle are presented in Figure 3.13. It is shown that the yaw rate, roll angle, and art. angle are all quite similar to the results of the TruckSim model. The small roll angle suggests the roll dynamics is very moderate. Due to the ignorance of aerodynamics of the proposed model, the longitudinal speed shows a slight mismatch with TruckSim. The lateral speed is seen the similar evidence because of the simplification of the model. However, it is a trade-off between model accuracy and implementability in controller design while the evaluation results are acceptable.

Config. 4: An Articulated Four-unit Truck

To show the reconfigurability of proposed methodology on articulated vehicles with more than two units, an articulated truck with four units is evaluated. It is a long truck

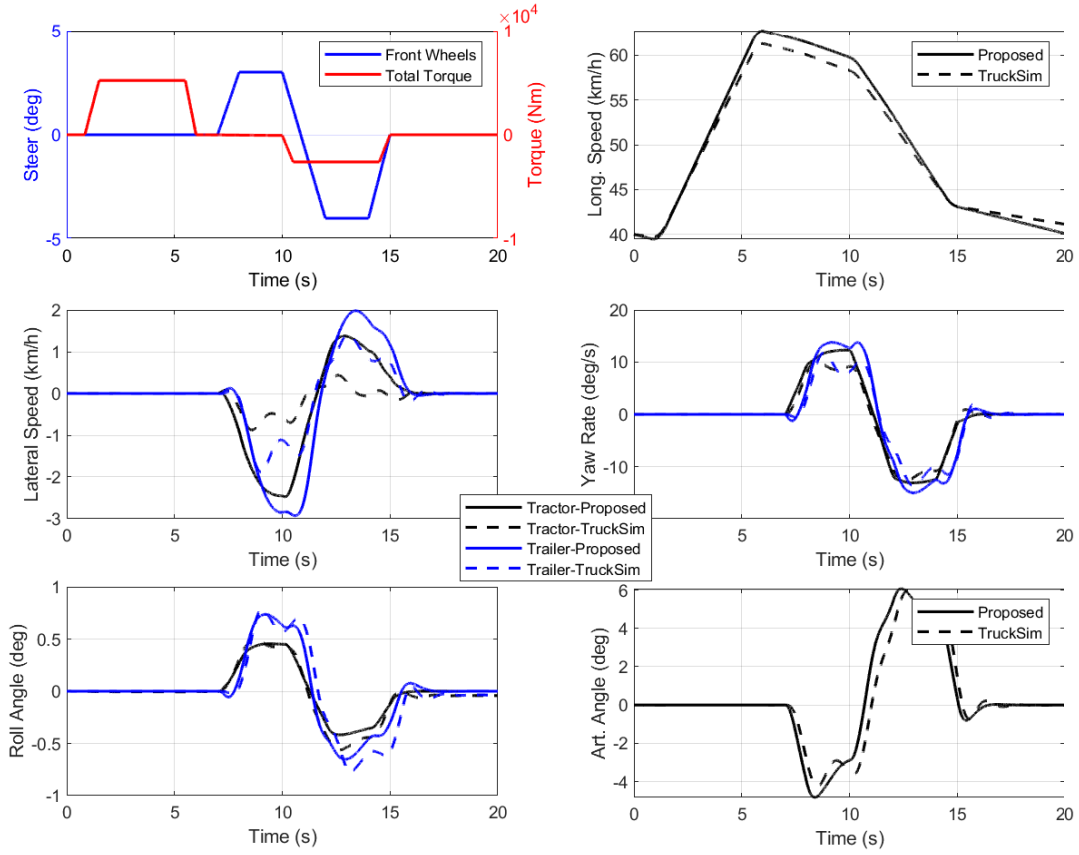


Figure 3.13: A articulated bus

with the configuration of ‘Tractor (driver unit)-Trailer #1-Dolly-Trailer #2’, (from left to right named as ‘Unit #1-Unit #2-Unit #3-Unit #4’). The tractor has three axle, where rear two axles are connected to powertrain. Trailer#1 and trailer #2 has two axle rear, where in between the one-axled dolly bridges together. Knowing the configuration, the The ‘Articulation and Axle Boolean Matrix’ can be written as,

$$T_{\varepsilon} = I_{(20 \times 20)};$$

$$T_c^{(1)} = \text{diag}(1, 1, 1, 1, 0, 0, 0, 0, 1, 1, 1, 1, 1, 1, 1, 1);$$

$$T_c^{(2)} = \text{diag}(0, 0, 0, 0, 0, 0, 0, 0, 1, 1, 1, 1, 1, 1, 1, 1);$$

$$T_c^{(3)} = \text{diag}(0, 0, 0, 0, 0, 0, 0, 0, 0, 0, 0, 0, 1, 1, 1, 1);$$

$$T_c^{(4)} = \text{diag}(0, 0, 0, 0, 0, 0, 0, 0, 1, 1, 1, 1, 1, 1, 1, 1);$$

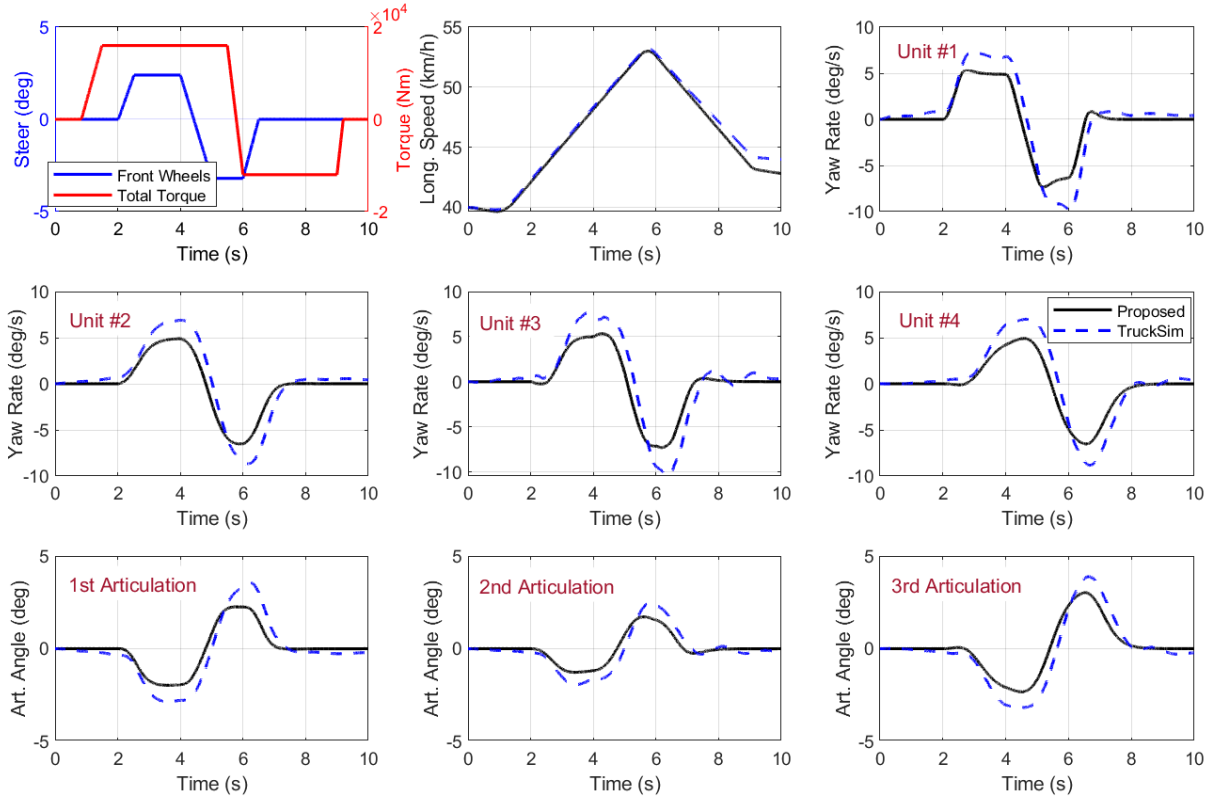


Figure 3.14: An articulated four-unit truck

Due to the complexity of the vehicle, it is very easy to trigger instability, for instance, trailer sway or rollover. As shown in Figure 3.12, a moderate maneuver with combined steering and drive/brake is applied to the vehicle. The yaw rate of each unit and the articulation angle at each articulation point are plotted and compared. It indicates a fair good behavior of the proposed model compared to TruckSim model, although applying to such a complex vehicle system. However, deviations are also seen in the yaw rates

and articulation angles where the maximum errors are listed in Table 3.2. This is mainly because the high complexity of a four units vehicle and the simplification of the proposed model, e.g. unchanged vertical tire forces used.

Table 3.2: Evaluation errors of an articulated four-unit truck

States deviation	1	2	3	4
Yaw rate	26.4%	27.5%	17.1%	28.5%
Art. angle	36.5%	32%	23.1%	N/A

3.6 Summary and Discussion

This chapter elaborated a detailed work on dynamics and modeling of multi-axle vehicles. The modeling started from a multi-axle vehicle without articulations, and used a three-layer modeling process, from corner forces to CG forces, and lastly to body dynamics, to arrive at a reconfigurable and general model. Moreover, the case of the articulated vehicle with any units is unified into a general form. This general model includes the longitudinal, lateral, yaw and roll dynamics of each unit of the vehicle.

The modeling framework discussed the active actuator system of active steering and active torque differential. However, other actuation system configurations, such as, active camber control, are also applicable in this modeling formulation. To fit the active camber control configuration, a camber model that connects the tire lateral force and camber angle is needed. For instance, a active camber system is introduced for a three-axled tilted vehicle rollover prevention control [59]. Similarly, when it comes to different power-train configurations, the dynamics of the power trains/actuators should be considered to have a full description of the system.

Model validity and accuracy is vital to the control design, which directly affects the system stability and the performance of the model-based controller. In the last section, a work of model evaluation was hence studied. To demonstrate the reconfigurability to

different vehicle configurations, four vehicle cases with different axle/articulation configurations were simulated and compared. Given the same vehicle steering and driving/braking torque inputs, dynamics responses of the proposed model were comparable with those of high-fidelity CarSim/TruckSim models. As a result, the modeling part laid a good foundation for reconfigurable controller design in the next chapter.

Chapter 4

Reconfigurable Controller Development

Now that the reconfigurable modeling has paved the way to model-based controller design, in this chapter, a framework of an optimization-based reconfigurable controller is developed in a very general form. For the sake of simplicity, the proposed controller focuses on multi-axle vehicles with two units, which actually covers the most common road vehicles. However, following concepts of reconfigurable modeling, one could extend the controller to any articulated vehicles with any units in greater detail. The majority of this chapter has been submitted to IEEE Journals in 2019 [88, 89].

The chapter is organized as follows. Section 4.1 provides an overview of the control framework. Section 4.2 studies different stability objectives in order to obtain good references for MPC tracking. Section 4.3 presents a high-level MPC controller, where a general prediction model is developed and a QP problem is formulated and solved. In Section 4.4, it uses a lower-level control allocation to distribute the virtual control calculations from the high-level controller. Real-time constraints, such as actuator limits, tire capacity, wheel slip control, and actuator failure are presented one by one in Section 4.5. Section 4.6 presents a study and guidelines for MPC tuning using a particular vehicle example. Section 4.7 summarizes the chapter and provides some concluding remarks.

4.1 Control Overview

To achieve the universality, reconfigurability, and integratability of the controller, a two-layer control structure was developed, illustrated in Figure 4.1. It could apply to any multi-axle vehicles with any control objectives in yaw and roll dynamics plane. However, depending on a specific application, part of the CG corrective forces, e.g. only the CG corrective yaw moment, and some of the objectives may be adopted.

The objective of the dual control strategy falls into two layers: At each time step, the high-level controller is to ensure the vehicle follows the reference from the driver and road, and guarantees stability and safety. In short, the high-level controller proposed in this chapter solves the following MPC problem:

$$\begin{aligned} \min \quad & \textit{tracking error} + \textit{CG corrections} + \textit{control oscillation} \\ & \textit{vehicle dynamics model} \\ \text{s.t.} \quad & \textit{input boundary} \\ & \textit{feasibility and stability} \end{aligned}$$

Once the optimal CG corrections are computed, lower level controller allocates the wheel steering, drive/braking torque optimal by solving the following control allocation problem:

$$\begin{aligned} \min \quad & \textit{mapping error} + \textit{control efforts} \\ \text{s.t.} \quad & \textit{input boundary} \end{aligned}$$

To explain control logic in Figure 4.1, the driver's steering and drive/brake torque commands are passed to the vehicle as a feed-forward input, and meanwhile, the summations go to the reference model module to generate desired states. To have a dynamic model prediction, the sensing and estimation module provides reliable state variables to the high-level MPC for model prediction. The MPC formulation minimizes the errors between the reference sequences and sequences predicted in the assumed control horizon using current state and driver inputs. Required CG corrections ΔF_x (for vehicle longitudinal control), ΔF_y (for vehicle lateral/roll control), and yaw moment ΔM_z (for vehicle yaw/roll control) at CG are computed on-line by solving an quadratic optimization problem. Now feeding them into

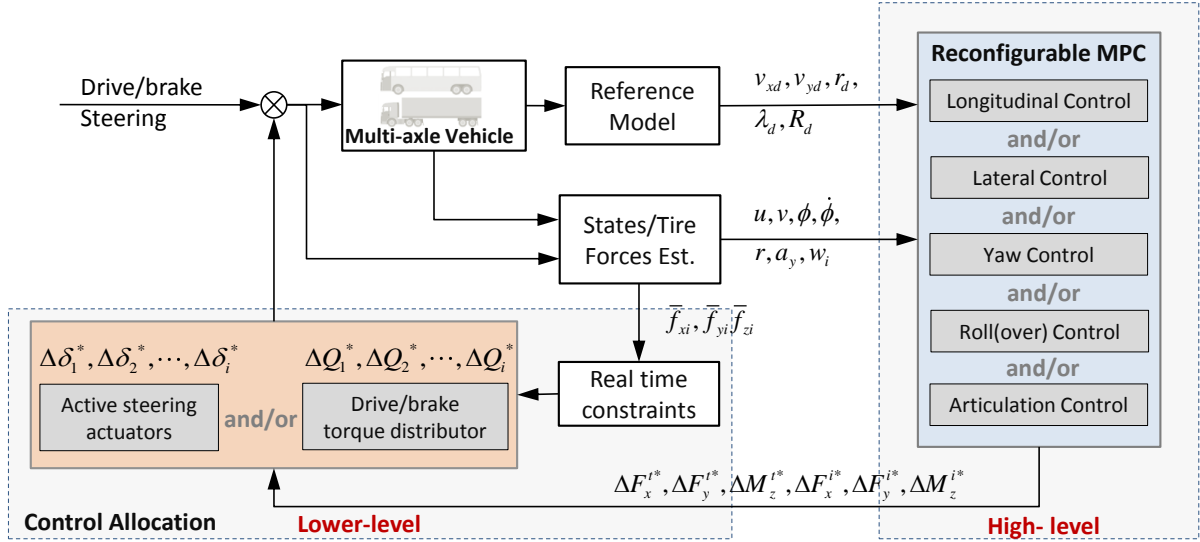


Figure 4.1: Control structure

the lower-level controller, the augmented torque or braking $(\Delta Q_1, \Delta Q_2, \dots, \Delta Q_i)$ or/and steering $(\Delta \delta_1, \Delta \delta_2, \dots, \Delta \delta_i)$ are optimally distributed by solving a constrained quadratic problem at each time step.

Remark. 1) Why two layers? Vehicles have various configurations but the virtual corrective CG forces are universal to any vehicles. This virtual control effort does not need prior knowledge about the actuators. Besides, active actuators could be different from vehicle to vehicle, even for the same operating vehicle, actuators may fail, i.e. wheel lock or brake failure. In such way, the lower layer controller has to handle active actuators reconfigurable, i.e., by setting T_w . In brief, the high-level controller represents universality while the lower-level, reconfigurability. Furthermore, in an MPC control algorithm, the computational cost grows significantly if using control action u , which may have more than 6 variables in multi-axle vehicles application. It is a huge burden in real time at automotive-grade hardware. 2) Control objectives. The controller could apply to any multi-axle vehicles pursuing selective control objectives, depends on specific applications and available actuators. For instance, a sedan may focus on wheel slip control and handling stability while a bus with high CG location considers rollover prevention as a top

priority. Autonomous vehicles could use longitudinal control (or cruise control) as well as meet stability constraints. Among articulated vehicles, it is essential for heavy trucks (articulated) to consider rollover prevention, jackknife prevention and off-tracking issues while a family car-trailer may emphasize the car stability control and trailer sway prevention. Therefore, the reconfigurability to control objectives can be achieved by adjusting the weights in high-level controller.

4.2 Stability and References

In this section, the desired vehicle responses are discussed and defined. The desired responses cover any multi-axle vehicles, e.g. the non-articulated and the articulated. It consists of the desired speed, desired lateral speed, the desired yaw rate, desired rollover index, and desired articulated angle if the target vehicle is articulated. These values serve as a reference set in an MPC tracking problem.

4.2.1 Longitudinal Control

Many researchers do not consider longitudinal speed control while focusing on lateral/yaw/roll stability. It is usually assumed as constant speed. However, this controller covers the longitudinal control, namely, speed tracking. For instance, a performance vehicle may want to maintain the speed (no speed drop) while negotiating a curve and active control is engaged. In the adaptive cruise control (ACC)/emergency braking control, the vehicle should keep a speed based on a driver's desire or environmental limits, such as collision avoidance. This is common in Advanced Driver-Assistance Systems (ADAS) or autonomous driving systems. Thus, the reference of longitudinal speed can be expressed as:

$$v_{xd} = \min(v_{dvr}, v_{env}, v_{cap}) \quad (4.1)$$

where v_{dvr} is the driver's desired speed, for instance, set from ACC. v_{env} is the speed constrained from the environment for safety's sake, such as road speed limit or collision avoidance. v_{cap} is the speed capacity of the vehicle, i.e. maximum speed. In addition, the

longitudinal controller should also limit the acceleration and deceleration of the vehicles. This can be realized in adding the slew term of the cost function of MPC formulation.

4.2.2 Lateral Stability

Vehicle slip angle is unavoidable. In non-critical conditions, the vehicle sideslip angle is small. However, large body slip is detrimental as tires may lose linear behaviors and approach adhesion limits. Usually, there are two approaches found from literature for lateral stability. One is to set the desired lateral slip to be zero all the time, for example, in [90], which is ideal but needs the active control system to be activated all the time. In the perspective of engineering practices, it is not cost-effective due to frequent control activation and energy consumption. To avoid this, the controller can be only activated when lateral speed exceeds a threshold [53]. Specifically, when the vehicle sideslip angle is small and in the safe range, the desired lateral velocity (v_{yd}) will be the same as the actual lateral speed, otherwise, set as zero:

$$v_{yd} = \begin{cases} v_y & |v_y| \leq v_{y,\max} \\ 0 & \text{otherwise} \end{cases} \quad (4.2)$$

where $v_{y,\max}$ is the maximum permissible lateral speed, which is derived from maximum sideslip angle. However, using a fixed boundary for lateral speed might not be most desired considering the full utilization of the tire capacity. Instead, this research borrows an envelop control concept [84] and uses a time-varying boundary. The controller only articulates the lateral speed while large body slip occurs in real time. The lateral speed bounds are defined by tires saturation ($\alpha_{i,sat}$). Converting tires slip angle expression in (3.21) into the lateral speed, it gives:

$$\begin{aligned} v_{yi,\max} &= v_x \alpha_{i,sat} - l_i r + v_x \delta_i, \quad (i = 1, \dots, 8) \\ v_{y,\max} &= \min(|v_{y1,\max}|, |v_{y2,\max}|, \dots, |v_{y8,\max}|) \end{aligned} \quad (4.3)$$

The vehicle speed v_x , yaw rate r and steering angle δ can be read from measurements or estimation. The maximum lateral speed will be determined by the most dangerous tire. In this manner, each tire sideslip condition is considered so that whole lateral stability is

enhanced. Similarly, the lateral stability envelope reduces frequent control activations and energy consumptions.

4.2.3 Steady State Handling

In this section, the stability of the tractor-trailer combination is investigated by using a linearized single-track model in Figure 4.2. The handling of the tractor unit is introduced firstly. For a single unit vehicle, namely, the front unit, it is well understood on deriving the relationship among the steering angle, turning radius, the wheelbase and tires slip angles [91]:

$$\delta - \alpha_f^t + \alpha_r^t = \frac{L^t}{R} \rightarrow \delta = \frac{L^t}{R} + (\alpha_f^t - \alpha_r^t) \quad (4.4)$$

Using the single-track model, the expression for the steer angle to negotiate a given curve is given:

$$\delta = \frac{L^t}{R} + \left(\frac{W_f^t}{C_f^t} - \frac{W_r^t}{C_r^t} \right) \frac{v_x^2}{gR} = \frac{L^t}{R} + K_{us}^t \frac{v_x^2}{R} \quad (4.5)$$

The steady state of yaw rate of the tractor is formulated as:

$$r_{ss} = \frac{v_x}{L^t + K_{us}^t v_x^2} \delta \quad (4.6)$$

where K_{us}^t is the understeer gradient of the tractor alone without considering load effects from the trailer unit. However, as shown in Figure 4.3, the trailer has a influence on the load distribution of the tractor. As a result, the understeer gradient changes due to the presence of trailer. The front and rear loads are modified as [92]:

$$W_{f,m}^t = W_f^t - \frac{l_h^t l_{78}^i}{L^t L^i} m^i g; \quad W_{r,m}^t = W_r^t + \frac{(l_h^t + L^t) l_{78}^i}{L^t L^i} m^i g \quad (4.7)$$

Assuming the cornering stiffness is constant, the modified understeer gradient is changed to be:

$$K_{us,m}^t = \left(\frac{W_{f,m}^t}{C_f^t} - \frac{W_{r,m}^t}{C_r^t} \right) / g = K_{us}^t - \left(\frac{C_r^t l_h^t + C_f^t (l_h^t + L^t)}{L^t L^i C_f^t C_r^t} \right) m^i l_{78}^i \quad (4.8)$$

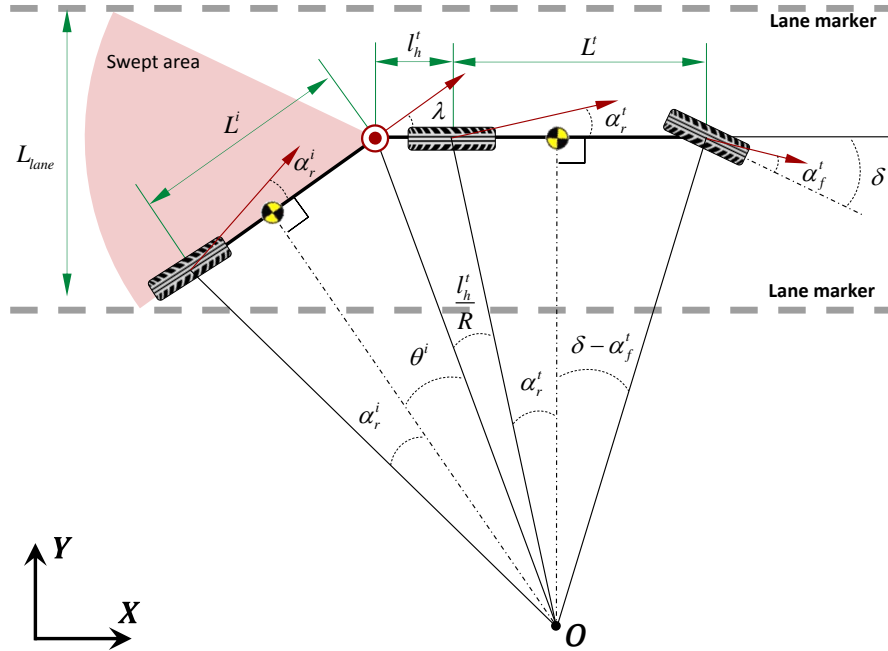


Figure 4.2: Steady-state handling model for a articulated vehicle (two-units)



Figure 4.3: Tractor weight distribution affected by the trailers [9]

If the geometry configuration of the tractor-trailer is determined, which usually is, the modified understeer gradient changes with the trailer mass (m^i) and CG location, indicated by l_{78}^i . As shown the blue solid line in Figure 4.4, compared to that of the tractor alone, the understeer gradient is reduced (from understeer to oversteer) when l_{78}^i is posi-

tive, namely the CG location center is ahead of the trailer axle, and getting bigger. On the contrary, it increases (from understeer to more understeer) when l_{78}^i is negative and moving away backwards from the trailer axle. However, this is concluded under the assumption of constant cornering stiffness. The reality is cornering stiffness also changes with the tractor normal loads. But compared to normal loads changes, the cornering stiffness change less proportional. Thus, the understeer gradient of the tractor keeps the same directional changes but much smaller than the value in calculation of (4.8). To include the considerations on normal load and its cornering stiffness changes, The black dash line in Figure 4.4 indicates a more precise and realistic understeer gradient variation. It shows approximate linear variation with trailer CG location.

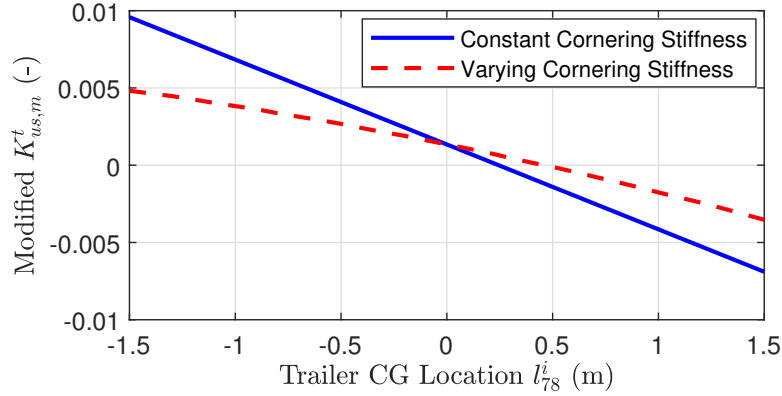


Figure 4.4: Tractor understeer gradient V.S. trailer CG location

For the sake of handling improvement, the steady state is used as the desired yaw rate for interpreting the driver's intention. Additionally, the maximum yaw rate that is subject to the limitation of maximum vehicle cornering force determined by the current tire-road friction coefficient [77]. Hence the desired yaw rate is given as follows:

$$r_d = \min\left(\left|\frac{v_x}{L^t + K_{us,m}^t v_x^2} \delta\right|, \left|\frac{0.85\mu g}{v_x}\right|\right) \cdot \text{sign}(\delta) \quad (4.9)$$

where $K_{us,m}^t$ is the modified understeer gradient of the vehicle. The factor 0.85 allows the lateral acceleration that comes from the derived of lateral speed to contribute 15%

to the total lateral acceleration [93]. In practical cases, L^t and $K_{us,m}^t$ vary due to vehicle axles/articulations configurations. Reported in [94], the equivalent wheelbase and understeer gradient of any multi-axle vehicles are derived using a dynamic equivalent approach.

4.2.4 Trailer Yaw Behavior

Trailer sway and jackknife are two major unstable modes of articulated vehicles that may lead to fatal accidents. The articulation should be actively controlled before losing stability. This section aims to develop a reference, namely, a desired articulation angle, for controller design. As shown in Figure 4.2, since the turning curve center O is perpendicular to the CG location of both units, it gives the angle relationship of the quadrangle [95]:

$$\theta^i + \frac{l_h^t}{R} + \alpha_r^t = \lambda \rightarrow \theta^i = \lambda - \frac{l_h^t}{R} - \alpha_r^t \quad (4.10)$$

Follow the similar approach in analyzing the steady-state handling behavior of a single vehicle unit, equation (4.10) could be written as a manner of:

$$\lambda - \frac{l_h^t}{R} - \alpha_r^t + \alpha_r^i = \frac{L^i}{R} \rightarrow \lambda = \frac{L^i + l_h^t}{R} + (\alpha_r^t - \alpha_r^i) \quad (4.11)$$

The equation shows a great similarity with equation (4.4). Under such condition, it is assumed the rear tire of the tractor unit is considered as the ‘steered tire’ for the trailer unit, and λ is the ‘steer angle’ of it:

$$\lambda = \frac{L^i + l_h^t}{R} + \left(\frac{W_r^t}{C_r^t} - \frac{W_r^i}{C_r^i} \right) \frac{v_x^2}{gR} = \frac{L^i + l_h^t}{R} + K_{us}^i \frac{v_x^2}{R} \quad (4.12)$$

The ratio of the articulation angle to the steer angle of the tractor unit in (4.5) is defined as the articulation angle gain, which is similar the yaw rate gain:

$$\frac{\lambda}{\delta} = \frac{(L^i + l_h^t) + K_{us}^i v_x^2}{L^t + K_{us}^t v_x^2} \quad (4.13)$$

where K_{us}^t is the understeer coefficient of the tractor unit while K_{us}^i , that of the trailer unit. To make sure both units are directional stable, both units are designed to be understeer. K_{us}^t and K_{us}^i are designed to be very small positive. They are calculated by the

axle cornering stiffness and its weight distribution. Figure 4.5 outlines five different cases on tractor-trailer steady state behavior and stability [95] and Table 4.1 summarizes the characteristics of each one. To put it shortly, this analysis suggests that the trailer mass and CG location's impact on tractor and trailer steady state behavior. It could conclude that the closer distance from CG to articulation point, the higher risk of jackknifing will be. In addition, a trailer sway is more likely to incur when the CG location is around trailer axle or in the back of the axle.

Table 4.1: Tractor-trailer steady state behavior

Case	Tractor	Trailer	Crit. Speed (v_{crt})	Description
I	understeer	understeer	N/A	Both directionally stable
II	understeer	oversteer	$\sqrt{-\frac{g(L^i+l_h^t)}{K_{us}^i}}$	Art. angle gain changes to negative when $v_x > v_{crt}$
III	oversteer	understeer	$\sqrt{-\frac{gL^t}{K_{us}^t}}$	Trailer jackknifing when $v_x \rightarrow v_{crt}$
IV	oversteer	oversteer	$\sqrt{-\frac{gL^t}{K_{us}^t}}$	Trailer jackknifing when $v_x \rightarrow v_{crt}$
V	oversteer	oversteer	$\sqrt{-\frac{g(L^i+l_h^t)}{K_{us}^i}}$	Trailer sway when $v_x \rightarrow v_{crt}$

Since the ISO coordinate system is used, shown in Figure 4.2, the sign of steering angle is negative while that of articulation angle is positive. The stable mode of the steady state of the articulation angle is used as the reference, which results in:

$$\lambda_d^{ss} = -\frac{(L^i + l_h^t) + K_{us}^i v_x^2}{L^t + K_{us}^t v_x^2} \delta \quad (4.14)$$

To avoid oscillation of small articulation angle from measurement bias and noise, the articulation angle is only controlled while its absolute value exceeds a threshold value (λ_{thre}) for experimentally validation, i.e. 5° . In addition, the reference should be also bounded by the tire-road friction coefficient which is similar to the tractor unit, and the

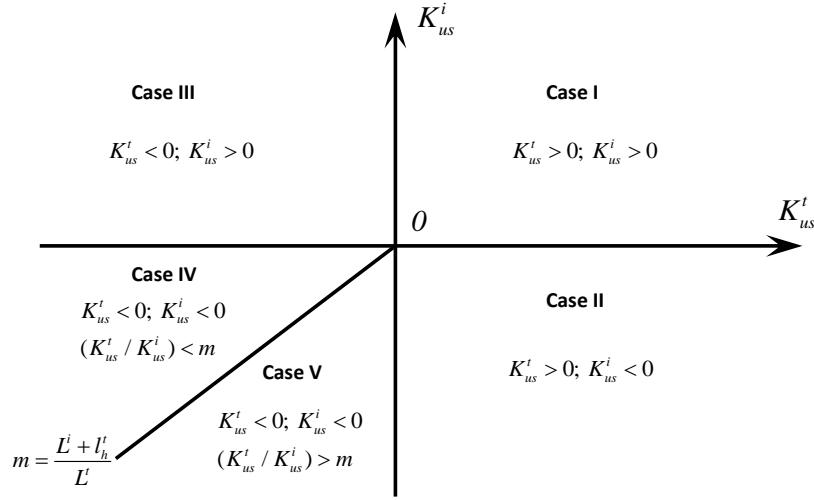


Figure 4.5: Five cases of tractor-trailer steady state behavior

driving lane boundaries assuming a high speed driving. Hence, the maximum articulation angle formulation in (4.12) due to friction coefficient is:

$$\lambda_{tire}^{max} = \frac{L^i + l_h^t}{L^t} \delta + K_{us}^i \mu g \quad (4.15)$$

Additionally, to avoid violating the lane markers shown in Figure 4.2, the maximum articulation angle due to lane geometry boundaries is constrained that:

$$\lambda_{lane}^{max} = \frac{L_{lane}}{2L^i} \quad (4.16)$$

Hence the desired articulation angle is given as follows:

$$\lambda_d = \begin{cases} \lambda & |\lambda| \leq \lambda_{thre} \\ -\min(|\lambda_d^{ss}|, \lambda_{tire}^{max}, \lambda_{lane}^{max}) \cdot sign(\delta) & \text{otherwise} \end{cases} \quad (4.17)$$

4.2.5 Rollover Stability

The imminent rollover detection is acquired by monitoring the lateral load transfers for both axles. In this research, un-tripped rollover is considered and a simplified rollover

index (RI) is used for vehicle rollover control. RI is a common coefficient that reflects the vehicle lateral load transfer. The formulation (2.1) based on tire normal forces can be rewritten from roll dynamics:

$$RI = \frac{2(mha_y + m_s g h_s \phi - I_{xx} \ddot{\phi})}{mgl_w} \quad (4.18)$$

where mha_y could be approximately substituted by $(m_s h_s + m_s h_r + m_u h_u) a_y$. Combining the roll dynamics equation in (3.30d), it gives:

$$RI = \frac{2(K_\phi \phi + C_\phi \dot{\phi} + m_s h_r a_y + m_u h_u a_y)}{mgl_w} \quad (4.19)$$

where the terms of $m_s h_r a_y + m_u h_u a_y$ are the effects of the un-sprung mass and the effects of overturning moments from the roll center to the ground. Previous studies typically ignored these terms for simplification. However, a comprehensive work deriving a new Rollover Index in [96] is used in this study, the final form of RI is obtained as a linear formulation associated with the roll angle and roll angle rate:

$$RI = c_1 \phi + c_2 \dot{\phi} \quad (4.20)$$

where,

$$c_1 = \frac{2}{mgl_w} (K_\phi (1 + \frac{m_s h_r + m_u h_u}{m_s h_s}) - (m_s h_r + m_u h_u) g),$$

$$c_2 = \frac{2}{mgl_w} C_\phi (1 + \frac{m_s h_r + m_u h_u}{m_s h_s}).$$

To calculate its value online, the constant coefficients c_1 and c_2 reflecting the vehicle's characteristics are previously obtained by substituting the vehicle's physical parameters. The state variables, namely, the roll angle and roll rate, are acquired from the sensors, i.e. IMU. Lateral Load Transfer is natural and ineluctable in cornering, it is unnecessary to minimize RI to be zero in normal conditions. In this study, the control action only activates when it exceeds a defined threshold. Due to the roll inertia effect and the control system delay, RI reaches ± 1 most probably when the tires have not yet left the road. Refer to the phase analysis of roll angle-rate in [97], the threshold (RI_{\max}) is achieved as the rollover index boundaries. The desired rollover index is hence defined as:

$$RI_d = \begin{cases} RI & |RI| \leq RI_{\max} \\ 0 & \text{otherwise} \end{cases} \quad (4.21)$$

Formulation (4.21) is a general expression for any multi-axle vehicles in this research. It should be noted that, in a tractor-trailer case, there will be two rollover indexes. The rollover index of the tractor unit is denoted as RI_d^t while the trailer unit is RI_d^i .

4.3 High-level: Reconfigurable MPC

4.3.1 A General Prediction Model

The prediction model's accuracy and complexity have a critical impact on the closed-loop optimization, i.e. computational cost and performance. The accuracy of this research is guaranteed using the nonlinear tire model meanwhile complexity is considered by linearizing the body dynamics and tire model. Regarding non-articulated vehicles, the prediction model is explicitly given in state space formulation (3.32). However, the final model of articulated vehicles is formulated in an indirect manner (3.41), which has difficulties to serve as a standard prediction model. A reformulation is therefore introduced.

For further simplification, assuming the articulation angle λ is small, the kinematic relationships and force constraints of the articulation point are linearized as follows:

$$v_x^i = v_x^t \quad (4.22a)$$

$$v_y^i = -v_x^t \lambda + (v_y^t - l_h^t r^t) - l_h^i r^i \quad (4.22b)$$

$$\dot{v}_y^i = -\dot{v}_x^t (r^i - r^t) + (\dot{v}_y^t - l_h^t \dot{r}^t) - l_h^i \dot{r}^i \quad (4.22c)$$

$$F_{x,h}^t + F_{x,h}^i = 0 \quad (4.23a)$$

$$F_{y,h}^t + F_{y,h}^i = 0 \quad (4.23b)$$

Note that the reaction yaw moment at articulation point in (3.40a) is ignored, which results in zero. By constructing the linearized equation (4.22), (4.23) and (3.40) to a matrix form, one could write the model of (3.41) as linearized form:

$$\text{state space form.} \quad \dot{x} = Ax + BF_{CG} + CF_H \quad (4.24)$$

2 units

$$\text{s.t.} \quad \begin{aligned} M_{(2 \times 10)} \dot{x} &= P_{(2 \times 10)} x \\ N_{(6 \times 8)} F_H &= Q_{(6 \times 10)} x \end{aligned}$$

where,

$$M_{(2 \times 10)} = \begin{bmatrix} 1 & 0 & 0 & 0 & 0 & -1 & 0 & 0 & 0 & 0 \\ 0 & 1 & -l_h^t & 0 & 0 & 0 & -1 & -l_h^i & 0 & 0 \end{bmatrix},$$

$$P_{(2 \times 10)} = \begin{bmatrix} 0 & 0 & 0 & 0 & 0 & 0 & 0 & 0 & 0 & 0 \\ 0 & 0 & -v_x^t & 0 & 0 & 0 & 0 & v_x^t & 0 & 0 \end{bmatrix},$$

$$N_{(6 \times 8)} = \begin{bmatrix} 1 & 0 & 0 & 0 & 1 & 0 & 0 & 0 \\ 0 & 1 & 0 & 0 & 0 & 1 & 0 & 0 \\ 0 & 0 & 1 & 0 & 0 & 0 & 1 & 0 \\ 0 & 0 & 1 & 0 & 0 & 0 & 0 & 0 \\ 0 & 0 & 0 & 1 & 0 & 0 & 0 & 1 \\ 0 & 0 & 0 & 0 & 0 & 0 & 0 & 1 \end{bmatrix},$$

$$Q_{(6 \times 10)} = \begin{bmatrix} 0 & 0 & 0 & 0 & 0 & 0 & 0 & 0 & 0 & 0 \\ 0 & 0 & 0 & 0 & 0 & 0 & 0 & 0 & 0 & 0 \\ 0 & 0 & 0 & 0 & 0 & 0 & 0 & 0 & 0 & 0 \\ 0 & 0 & 0 & 0 & 0 & 0 & 0 & 0 & 0 & 0 \\ 0 & 0 & 0 & 0 & 0 & 0 & 0 & 0 & 0 & 0 \\ 0 & 0 & 0 & 0 & -K_{t-i} & 0 & 0 & 0 & 0 & K_{t-i} \end{bmatrix}.$$

And the vector $F_H = [F_{x,h}^t \ F_{y,h}^t \ M_{z,h}^t \ M_{x,h}^t \ F_{x,h}^i \ F_{y,h}^i \ M_{z,h}^i \ M_{x,h}^i]^T$ represents the all forces/moments at the articulation point. The first constraint in (4.24) means there are two independent linear algebraic equations in terms of \dot{x} and x while the second one means six independent linear algebraic equations in terms of F_H^t and F_H^i . Multiply matrix M to both sides of (4.24), it gives:

$$M\dot{x} = MAx + MBF_{CG} + MCF_H \quad (4.25)$$

Combining (4.25) with the constraint $M\dot{x} = Px$, by taking the right-hand side of both equations, it gives:

$$MAx + MBF_{CG} + MCF_H = Px \Rightarrow MCF_H = (P - MA)x - MBF_{CG} \quad (4.26)$$

Next, integrating the constraint $N_{(6 \times 8)}F_H = Q_{(6 \times 10)}$ and (4.26) in one matrix operation form, it gives:

$$\left[\frac{N_{(6 \times 8)}}{(MC)_{(2 \times 8)}} \right] F_H = \left[\frac{Q_{(6 \times 10)}x}{((P - MA)x - MBF_{CG})_{(2 \times 1)}} \right] \quad (4.27)$$

To achieve a form that connects the F_H and state vector x and F_{CG} , here a trick of matrix transform is used, the right-hand side of (4.27) is equivalent to that:

$$\left[\frac{Q_{(6 \times 10)}x}{((P - MA)x - MBF_{CG})_{(2 \times 1)}} \right] = \left[\frac{Q_{(6 \times 10)}}{(P - MA)} \right] x - \left[\frac{0_{(6 \times 6)}}{MB} \right] F_{CG} \quad (4.28)$$

Since the matrix associated with F_H holds full rank, F_H can be expressed in terms of x and F_{CG} :

$$F_H = \underbrace{\left[\frac{N_{(6 \times 8)}}{(MC)_{(2 \times 8)}} \right]^{-1}}_J \underbrace{\left[\frac{Q_{(6 \times 10)}}{(P - MA)} \right]}_{K_1} x - \underbrace{\left[\frac{N_{(6 \times 8)}}{(MC)_{(2 \times 8)}} \right]^{-1}}_J \underbrace{\left[\frac{0_{(6 \times 6)}}{MB} \right]}_{K_2} F_{CG} \quad (4.29)$$

Lastly, substituting (4.29) back to (4.24), the state-space formulations becomes:

$$\dot{x} = Ax + BF_{CG} + C(JK_1x - JK_2F_{CG}) \Rightarrow \dot{x} = (A + CJK_1)x + (B - CJK_2)F_{CG} \quad (4.30)$$

where $F_{CG} = \begin{bmatrix} F_{CG}^{tT} & F_{CG}^{iT} \end{bmatrix}^T$. Applying the same procedure where F_{CG} is derived from a single vehicle unit, F_{CG} can be expressed in terms of tire model along with vehicle states and driver inputs. Eventually, it will achieve the full model configuration similar with (3.13).

4.3.2 Quadratic Programming Problem

The high-level MPC is designed to compute the corrective CG forces for stability's sake. MPC is naturally capable of handling multivariable systems, which simplifies the controller development when multivariables and different configurations need to be considered. Furthermore, states and actuator constraints are easily formulated into the optimization

problem. And MPC has inherent local robustness to disturbances and uncertainties [69]. Desired references of the longitudinal speed, lateral speed, the yaw rate, and articulation angle and the rollover index are generated and updated from the reference module:

$$y_d = \left[v_{xd}^t \quad v_{yd}^t \quad r_d^t \quad RI_d^t \quad \lambda_d \quad RI_d^i \right]^T \quad (4.31)$$

Note that reference vector (4.31) is the full state of a two-unit vehicle. When it comes to real implementation, the reference vector and prediction model may be simplified/reduced as to meet the desired objectives. For instance, a yaw-plane dynamics control for tractor-trailer gives a reference vector of $y_d = \left[v_{yd}^t \quad r_d^t \quad \lambda_d \right]^T$. In an MPC scheme, the vehicle dynamics model is used to predict the future states over a horizon and the control action sequence is achieved by repeatedly solving finite time optimal control problems in a receding horizon fashion. The optimization is formulated as a constrained quadratic programming problem.

The linear-time-varying(LTV) model is discretized using the Euler method (Zero Order Holder) with sampling period T_s :

$$x(k+1) = A_d x(k) + B_d v(k) + G_d w(k) + d(k) \quad (4.32a)$$

$$y(k) = C_d x(k) \quad (4.32b)$$

where the current control vector $v(k) = \left[\Delta F_x^t \quad \Delta F_y^t \quad \Delta M_z^t \quad \Delta F_x^i \quad \Delta F_y^i \quad \Delta M_z^i \right]^T$. $y(k)$ is the defined output used to track references. The cost function is defined in a finite horizon N_p and control horizon N_c ¹:

$$J(x_{0,t}, V_t) = \sum_{k=1}^{N_p} \|y_{t+k,t} - y_{d_{t+k,t}}\|_Q^2 + \sum_{k=0}^{N_c-1} \|v_{t+k,t}\|_R^2 + \|v_{t+k,t} - v_{t+k-1,t}\|_T^2 + \|y_{N_p}\|_P^2 \quad (4.33)$$

where $V_t = \left[v_{t,t}, \quad \dots \quad v_{t+N_c-1,t} \right]^T, \in \mathbb{R}^{6N_c \times 1}$, represents the optimization sequence at time t . Index $t+k, t$ denotes the predicted value at k steps ahead of the current time t . The first term in (4.33) is the tracking error of the references. The second term is the prospective CG forces and minimizes the control efforts. The third term is optional and enforces proximity to the previous step to prevent oscillation in control actions. The fourth is the

¹where the notation $\|x\|_Q^2 = x^T Q x$ is applied.

terminal cost, $P \succ 0$, used to guarantee a local stability, which is further explained in next section. The positive semi-definite Q , R and T are weighting matrices that reflect the importance of these terms in the cost function. Although not the focus of this research, it is worthy to mention here, regarding vehicle stability objectives, they can be prioritized by regulating the corresponding weights of Q . Generally, priority from high to lower should be, rollover prevention $>$ anti-excessive sideslip $>$ yaw rate tracking. By making certain rules, one could achieve the objective prioritization [98]. At each time step, the following finite horizon (N_p) optimal control problem is solved on-line:

$$\begin{aligned}
& \min_{V_t} && J(x_{0,t}, V_t) \\
& && x_{k+1,t} = A_d x_{k,t} + B_d v_{k,t} + G_d w_{k,t} + d_{k,t}, \quad k = 0, \dots, t + N_p - 1 \\
& && y_{k,t} = C_d x_{k,t}, \quad k = 1, \dots, t + N_p \\
& \text{s.t.} && y_{\min} \leq y_{k,t} \leq y_{\max}, \quad k = 1, \dots, t + N_p \\
& && v_{\min} \leq v_{k,t} \leq v_{\max}, \quad k = 0, \dots, t + N_c - 1 \\
& && v_{k,t} = v_{k-1,t} + \Delta v_{k,t}, \quad k = 0, \dots, t + N_c - 1 \\
& && \left\| y_{N_p-1,t} - y_{dN_p-1,t} \right\|_Q^2 + \left\| u_{N_c-1,t} \right\|_R^2 \leq \gamma
\end{aligned} \tag{4.34}$$

Iteration Algorithm:

1. Acquire the new state $x(t)$, driver input $w(t)$, reference state $y_d(t)$;
 2. Obtain V_t^* by solving the QP optimization problem (4.34) ;
 3. Apply $v(t) = v_{0,t}^*$ (the first element of V_t^*) to the vehicle;
 4. $t \leftarrow t + 1$. Go to 1.
-

Remark. The last constraint in (4.34) refers to the terminal constraint to guarantee the stability of the LTV-MPC scheme, where detailed work could be found in [99]. The Batch approach in [70] is used to formulate the problem as a standard QP problem. The objective function can be expressed as a function of the initial state $x_{0,t}$ and sequences of reference, driver input. The solver, *qpOASES*, based on a structure-exploiting active-set method, provides fast and reliable solutions and is used in this research [100]. The corrective control vector should be bounded by the maximum CG forces/moment that a specific vehicle can generate. The high-level controller hence completes the calculation of optimal corrective GG forces.

The Batch approach is used to find the optimal solution for the MPC controller. This section presents how a standard QP problem is formulated step by step. Firstly, for computation's sake, the prediction model (4.32) is can be written as:

$$x(k+1) = A_d x(k) + B_d v(k) + d_w(k) \quad (4.35)$$

where, $d_w(k) = G_d w(k) + d(k)$; Using the model of (4.32), the prediction state can be expressed as:

$$\begin{aligned} \underbrace{\begin{bmatrix} y_{1,t} \\ y_{2,t} \\ \vdots \\ \vdots \\ y_{N_p,t} \end{bmatrix}}_Y &= \underbrace{\begin{bmatrix} CA \\ CA^2 \\ \vdots \\ \vdots \\ CA^{N_p} \end{bmatrix}}_{S_x} x_{0,t} + \underbrace{\begin{bmatrix} CB & 0 & \cdots & \cdots & 0 \\ CAB & CB & 0 & \cdots & 0 \\ \vdots & \ddots & \ddots & \ddots & \vdots \\ \vdots & \ddots & \ddots & \ddots & \sum_{i=0}^{(N_p-1)-N_c} CA^i B \\ CA^{N_p-1} B & CA^{N_p-2} B & \cdots & \cdots & \sum_{i=0}^{N_p-N_c} CA^i B \end{bmatrix}}_{S_v} \underbrace{\begin{bmatrix} v_{0,t} \\ v_{1,t} \\ \vdots \\ \vdots \\ v_{N_c-1,t} \end{bmatrix}}_V \\ + \underbrace{\begin{bmatrix} C & 0 & \cdots & \cdots & 0 \\ CA & C & 0 & \cdots & 0 \\ \vdots & \ddots & \ddots & \ddots & 0 \\ \vdots & \ddots & \ddots & \ddots & 0 \\ CA^{N_p-1} & CA^{N_p-2} & \cdots & \cdots & C \end{bmatrix}}_{S_d} \underbrace{\begin{bmatrix} d_{w0,t} \\ d_{w0,t} \\ \vdots \\ \vdots \\ d_{w0,t} \end{bmatrix}}_{D_w} \end{aligned} \quad (4.36)$$

Note that in the prediction expansion (4.36) the N_p and N_c denote the output prediction horizon and control horizon. It is assumed that the control input keeps constant while $N_c \leq t \leq N_p$. Its selection is discussed in the later section. Write the expansion (4.36) in the following compact form:

$$Y = S_x x_{0,t} + S_v V + S_d D_w \quad (4.37)$$

The reference outputs are assumed to be constant over the prediction horizon:

$$Y_d = \begin{bmatrix} y_{d,t}^T & y_{d,t}^T & \cdots & y_{d,t}^T \end{bmatrix}^T \quad (4.38)$$

The weighting matrices are constructed as \bar{Q} , \bar{R} and \bar{T} over the horizon:

$$\bar{Q} = \text{blockdiag}(Q, Q, \dots, Q) \quad (4.39a)$$

$$\bar{R} = \text{blockdiag}(R, R, \dots, R) \quad (4.39b)$$

$$\bar{T} = \text{blockdiag}(T, T, \dots, T) \quad (4.39c)$$

Substituting (4.37) and (4.38) into the cost function (4.33) with the ignorance of terminal cost, it yields:

$$\begin{aligned} J(x_{0,t}, V_t) &= (Y - Y_d)^T \bar{Q} (Y - Y_d) + V^T \bar{R} V + (V - V_p)^T \bar{T} (V - V_p) \\ &= V^T (S_x^T \bar{Q} S_x + \bar{R} + \bar{T}) V \\ &\quad + 2V^T (S_v^T \bar{Q} S_x x_{0,t} + S_v^T \bar{Q} S_d D_w - S_v^T \bar{Q} Y_d - \bar{T} V_p) + \textit{The rest} \end{aligned} \quad (4.40)$$

The lower and upper boundaries are constructed as:

$$LB = \begin{bmatrix} v_{\min}^T & v_{\min}^T & \dots & v_{\min}^T \end{bmatrix}^T \quad (4.41a)$$

$$UB = \begin{bmatrix} v_{\max}^T & v_{\max}^T & \dots & v_{\max}^T \end{bmatrix}^T \quad (4.41b)$$

The problem is formulated as a standard compact form:

$$\begin{aligned} \min_V \quad & \frac{1}{2} V^T H V + V^T g(x_{0,t}, y_{dt}, w_{0,t}) \\ \text{s.t.} \quad & LB \leq V \leq UB \end{aligned} \quad (4.42)$$

where H is the Hessian Matrix, g is the Gradient Vector that can be extract from (4.40) as follows,

$$\begin{aligned} H &= 2(S_x^T \bar{Q} S_x + \bar{R} + \bar{T}), \\ g &= 2(S_v^T \bar{Q} S_x x_{0,t} + S_v^T \bar{Q} S_d D_w - S_v^T \bar{Q} Y_d - \bar{T} V_p). \end{aligned}$$

4.3.3 Feasibility and Stability

Many research work can be found on feasibility and stability of MPC controlled systems and it has reached a relatively mature stage [101]. The constraints shown in (4.34) may pop

up infeasibility in real-time optimization. This may be due to the disturbance [102], for instance, side-wind to a vehicle or modeling and signal errors. It may also happen when the optimization is not completely solved due to the limitation of computation. Therefore, in industrial applications, a common approach is to soften the hard constraints by introducing slack variables and a small corresponding penalty term in the cost function. Generally, only the output constraints are softened as input constraints are supposed to be feasible all the time in a good formulation [69].

Closed-loop stability of MPC has been widely studied and Morari [102] pointed out that the stability has been well addressed from a theoretical perspective, although not from a practical application. Most researchers use the monotonicity property of the cost function to establish stability and the good news is found that it could be used as Lyapunov function to establish condition for asymptotically stability. Mathematically, to establish asymptotic stability, it needs to show that:

$$J^*(x(k+1)) - J^*(x(k)) < 0 \quad \forall x \neq 0 \quad (4.43)$$

where $J^*(x(k))$ is the total cost of (4.33) when substituting the optimal control sequence V^* and current state $x(k)$. In [99], it developed the conditions for the uniform asymptotical stability of a LTV-MPC system. A proof whose arguments is sketched here. To simplify the exposition it assumes that $N_p = N_c$.

Proof.

First, the following terminal triple is introduced to provide sufficient conditions for stability [103]. (1) a terminal constraint set X_f (could be Y_f). It is invariant under the terminal control law; (2) a feasible terminal control law K_f . It should hold in the terminal constraint set; (3) a terminal state weighting P in the terminal cost of the finite horizon optimization problem.

Assumption 1: The stage cost $l(x, v)$ is strictly positive and is 0 only for $l(0, 0)$, where $l_f(\cdot)$ is the terminal cost, and $l(\cdot)$ is the remainder of the cost function.

Assumption 2: There exists a local control law $K_f(x)$ for which the terminal set X_f is invariant (namely, closed loop trajectories starting inside X_f remain in that set), and the

state and input constraints are satisfied (i.e., for $x \in X_f$ it holds that $K_f(x) \in V$).

Assumption 3: Terminal cost $l_f(x)$ is a Lyapunov function inside X_f .

One needs to design the above ingredients properly for stability, where multiple ways exist. The most straightforward and common one is to leverage the linear quadratic regulator (LQR) problem. Hence, P is selected from algebraic Riccati equation solution of the state space formulation (4.35). K_f is set to be the associated LQR gain. A typical choice for the terminal constraint X_f is the maximal positive invariant set for the closed-loop system of (4.35) using the LQR gain. As a result, assumptions 1 -3 hold. Note that this approach is also workable for output tracking problem after proper modifications.

To prove the closed-loop stability of the LTV-MPC system, it needs to show the optimal cost function $J^*(x(k))$ is strictly decreasing along closed loop trajectories. Consider the optimal sequence $\left[v_0^* \ v_1^* \ \cdots \ v_{N_p-1}^* \right]^T$, the corresponding optimal cost function from (4.40) can be rewritten:

$$J^*(x(k)) = \sum_{k=0}^{N_p-1} l(x_k^*, v_k^*) + l_f(x_{N_p}^*) \quad (4.44)$$

Using the sub-optimal control sequence $\left[v_1^* \ v_2^* \ \cdots \ K_f(x_{N_p}^*) \right]^T$ for $x(k+1)$, the sub-optimal cost function is obtained as follows:

$$J'(x(k+1)) = \sum_{k=1}^{N_p} l(x_k^*, v_k^*) + l_f(\hat{x}_{N_p+1}) \quad (4.45)$$

where $\hat{x}_{N_p+1} = (A_d + B_d * K_f)x_{N_p}^*$, and K_f is a LQR feedback control law. Namely, it can rewrite $J'(x(k+1))$ as follows:

$$J'(x(k+1)) = J^*(x(k)) - l(x_0^*, v_0^*) - l_f(x_{N_p}^*) + l_f((A_d + B_d K_f)x_{N_p}^*) + l(x_{N_p}^*, K_f x_{N_p}^*) \quad (4.46)$$

In an LQR formulation, assumption 3 always holds that $l_f(x)$ is a Lyapunov function since the P_f gives the largest infinite-horizon predicted cost over all. Thus, the summation of the last three terms in the above expression is nonpositive. It results in leaving us with the expression:

$$J^*(x(k+1)) \leq J'(x(k+1)) \leq J^*(x(k)) - l(x_0^*, v_0^*) \quad (4.47)$$

where, because Q and R are positive definite, the right-hand side is strictly negative. Thus, it indicates that the optimal cost function $J^*(x(k))$ is strictly decreasing along closed loop trajectories, and thus that they will converge to the origin, establishing asymptotic stability of the MPC for the origin.

4.4 Lower-level: Control Allocation

In this section, calculations by high-level MPC are applied through corner modular, i.e. drive/braking and steering. Multi-axle vehicles are usually over-actuated mechanical systems, i.e. brake system in more than two wheels; active steering system. The lower-level controller should be able to handle redundancy and various configuration of active actuators. The technique of Control Allocation (CA) is leveraged to cope with such redundant actuation systems [54, 73]. As a result, CA offers an optimal distribution on actuator commands, meanwhile minimization of the CG corrective forces errors.

To achieve a dynamics stability, the requested corrective CG forces calculated by the high-level MPC are denoted by:

$$v^* = \left[\Delta F_x^{t*} \quad \Delta F_y^{t*} \quad \Delta M_z^{t*} \quad \Delta F_x^{i*} \quad \Delta F_y^{i*} \quad \Delta M_z^{i*} \right]^T \quad (4.48)$$

Using the mappings of aforementioned modeling, the actual CG forces generated by lower-level CA are denoted by,

$$v = \left[\Delta F_x^t \quad \Delta F_y^t \quad \Delta M_z^t \quad \Delta F_x^i \quad \Delta F_y^i \quad \Delta M_z^i \right]^T = B_p u \quad (4.49)$$

where $B_p = L_c T_c L_w T_w B_1$, is the **control effectiveness matrix (or mapping matrix)**, that connects all the possible actuator configurations of the vehicle. That is why CA offers the great convenience to adapt different actuation configurations. u is the lower-level control actions, e.g. torques or steerings defined in (3.27).

CA is formulated as a convex quadratic programming with linear constraints. Therefore, at each time step, the lower level controller solves the following optimization problem,

$$\begin{aligned} \min_u \quad & \xi \|v^* - B_p u\|_{W_e}^2 + \|u\|_{W_u}^2 \\ \text{s.t.} \quad & A_{eq} u = b_{eq} \\ & lb \leq u \leq ub \end{aligned} \quad (4.50)$$

where, the first term in the objective function of (4.50) is to minimize the CG forces error, while the second term is to minimize the control efforts of the actuation. lb, ub are the lower and upper bounds, W_e, W_u are positive definite weighting matrices or scalar, which give a compromise between three costs. ξ is used to emphasize the importance of minimizing the allocation error, that typically set very large. The equality constraint ($A_{eq}u = b_{eq}$) could be useful while considering some engineering practices. For instance, active steering strategy usually makes the steering angles of the left wheel and right wheel equal. W_e, W_u may be time-varying, depending on the driver inputs or road conditions. It reflects how the available actuators will be preferred and utilized for a integrated control strategy. This brings up a interesting topic, actuators prioritization, which is omitted for sake of brevity.

Remark. Actuators Prioritization. W_e, W_u may be time-varying, depending on the driver inputs or road conditions. It reflects how the available actuators will be preferred and utilized. For instance, 1) to maintain good path tracking and good road conditions, i.e. high and changeless tire-road coefficient, the active steering correction is prioritized for better driving comfort and a smaller speed drop. 2) In an emergency obstacle avoidance, e.g. sudden lane change, together with heavy braking, it should make the best of braking (wheel slip ratio control). 3) Cases in high speed and sharp steering may trigger a rollover event, such that a reduction in the lateral forces by using integrated control may be preferable [40].

4.5 Real-time Constraints

The lower-level controller distributes the virtual optimal control action calculated from MPC, into the available actuators on the vehicle. In this section, operating system constraints, including actuator constraints, tire capacity and wheel slip limits and actuator failure are formulated one by one. In terms of the active steering angle calculated from the lower-level controller, the boundaries are written in a general form:

$$lb_i(2) = \max(-\delta_i^{perm}, -\delta_i^{tire}, -\delta_i^{fail}) - \delta_i \quad (4.51a)$$

$$ub_i(2) = \min(\delta_i^{perm}, \delta_i^{tire}, \delta_i^{fail}) - \delta_i \quad (4.51b)$$

where $lb_i(2)/ub_i(2)$ denotes the lower/upper boundary of the steering angle according to $u_i = \begin{bmatrix} \Delta Q_i & \Delta \delta_i \end{bmatrix}^T$. δ_i is the wheel steering angle mapped and measured from driver's steering request. δ_i^{perm} represents the maximum steering angle in the permissible range, limited by the physical design. δ_i^{tire} is bounded by lateral tire force saturation, where more steering produces no additional lateral force. δ_i^{fail} handles steering failure occurrence, explained in section of 'Actuator Failure'. $lb_i(1)/ub_i(1)$ denotes the lower/upper boundary of the torque:

$$lb_i(1) = \max(Q_i^{brake}, -Q_i^{tire}, Q_i^{slip-lb}, -Q_i^{fail}) - Q_i \quad (4.52a)$$

$$ub_i(1) = \min(Q_i^{drive}, Q_i^{tire}, Q_i^{slip-ub}, Q_i^{fail}) - Q_i \quad (4.52b)$$

where Q_i is the estimated torque of the driver's request. Various real-time constraints are explained below.

Drive/Brake Limits

The lower-level control allocation is reconfigurable to different actuation applications. It could be differential braking, or torque vectoring or hybrid control (some wheels provide positive drive torque, others provide negative brake torque), listed in Table 4.2. The maximum deliverable drive/brake torque depends on the vehicle's powertrain and braking system capacity.

Table 4.2: Possible application and its boundaries

Application Type	Q_i^{drive} (Positive)	Q_i^{brake} (Negative)
Differential Braking	0	Max-brake torque
Torque Vectoring	Max-drive torque	0
Hybrid Control	Max-drive torque	Max-brake torque

Tire Capacity

As shown in Figure 4.6, it is a friction ellipse model for tire i with a combined slip, where lateral and longitudinal slip occur simultaneously at such situation. The capacity

of the tires to generate longitudinal and lateral forces at the contact patch is limited by a ‘friction ellipse model’ [78]:

$$\left(\frac{f_{xi}}{f_{xi}^{\max}}\right)^2 + \left(\frac{f_{yi}}{f_{yi}^{\max}}\right)^2 \leq 1 \quad (4.53)$$

where $f_{xi}^{\max} = \mu_x f_{zi}$, represents the maximum longitudinal forces without lateral slip while $f_{yi}^{\max} = \mu_y f_{zi}$, represents the maximum lateral tire forces without longitudinal slip. f_{zi} is the tire vertical force and μ_x, μ_y are the corresponding tire-road friction in x and y direction.

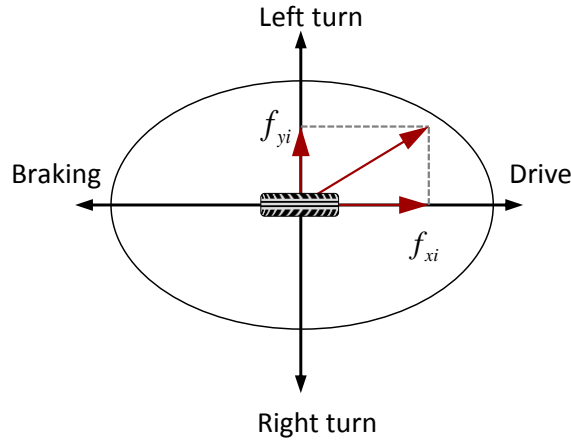


Figure 4.6: A friction ellipse model of tire i

Since the friction ellipse model tells how much longitudinal force is still available to use for active torques, the maximum torque the tire can provide can be described by:

$$Q_i^{tire} = \left(f_{xi}^{\max} \sqrt{1 - \left(\frac{f_{yi}}{f_{yi}^{\max}}\right)^2} \right) \times R_{eff} \quad (4.54)$$

In order to obtain the tire capacity constraints in real time, the estimates of tire forces are required, extensive works can be found in the literature [104, 105].

Wheel Slip Prevention

One might note the wheel slip control objective is not included in the high-level MPC controller formulation. Some researchers integrated the body dynamics and wheel dynamics into one MPC formulation, see [53, 56]. As a result, it gives optimal solution even considering the conflicts between body control and wheels control. In deployment, estimators often experience processing delays or absolute inaccuracies, which can cause unwanted control actions. Here a purely wheel speed based longitudinal approach is used. Although not optimal, it has the benefit of direct measurement feedback via wheel encoders [52]. First, wheel slip ratio is defined as:

$$s_i = \frac{R_{eff}\omega_i - v_{xi}}{\max(R_{eff}\omega_i, v_{xi})} \quad (4.55)$$

where typical values of $|s_i|$ lay in the range of 0.1 to 0.2, at where longitudinal tire force reach the peak. These slip ratio references are chosen to strengthen the wheel-slip prevention control through a proportional controller. The longitudinal force constrained by anti-slip is given,

$$f_{xi}^{\max-slip} = f_{xi}^{\max} - K_s s_i; f_{xi}^{\min-slip} = -f_{xi}^{\max} - K_s s_i \quad (4.56)$$

where, by tuning proportional gain K_s , performance is regulated. As before, accounting for combined 'friction ellipse model', the final bounds from wheel slip prevention are defined as:

$$Q_i^{slip-lb} = \left(f_{xi}^{\min-slip} \sqrt{1 - \left(\frac{f_{yi}}{f_{yi}^{\max}} \right)^2} \right) \times R_{eff} \quad (4.57a)$$

$$Q_i^{slip-ub} = \left(f_{xi}^{\max-slip} \sqrt{1 - \left(\frac{f_{yi}}{f_{yi}^{\max}} \right)^2} \right) \times R_{eff} \quad (4.57b)$$

Actuator Failure

Although the 'Actuator Boolean Matrix T_w ' readily determines the configuration of the active actuators, actuator failures may occur. For example, a braking actuator or power-assisted steering locked in a faulty position. Control allocation has the ability to handle fault-tolerant control [73]. Thanks to updating constraints in real time, once a fault is detected, CA will systematically set the lower and upper boundaries to the failure value

Q_i^{fail} , which could be a locked value or zeros assuming a complete failure. There is no need to redesign the control laws as the system can detect the failure and then utilize the rest of the actuators automatically to maintain the stability objectives. The advantage of the reconfigurable control to actuator failures is evaluated in a case study.

4.6 Controller Parameters Tuning

A typical MPC has many parameters to be tuned or selected, but controller tuning is not that challenging. Because, fundamentally speaking, MPC control problem is formulated as a QP optimization problem in the time domain. There are a great number of research can be found on MPC tuning methods and industrial applications, where an excellent review is elaborated in [106]. Generally, there are three significant goals when tuning a MPC controller [107]: (1) developing appropriate model predictions over the horizon; (2) a compromise between robustness and performance ; (3) a feasible computational cost. Differ to slow process applications, i.e. chemical process, the fast closed-loop system requires a higher computation in running MPC in real time, so the goal (3) is included.

The controller parameters tuning varies from plants to plants. In this section, a tractor-trailer is taken, see Figure 3.9 and Figure 6.1, and the parameters of tractor-trailer#1 in Table 6.1, as an example for tuning study. The model has 3 DoFs that considers the yaw and lateral dynamics of the tractor, and the yaw dynamics of the trailer. The high-level MPC control input is the corrective yaw moment at CG of the tractor and the trailer, respectively. The lower-level control input is the differential brake torques applied.

Sample Time & Prediction Horizon

The controller sampling time T_s is for use in the discrete-time formulation to predict the future states. It is different from the system sampling time. If T_s is too big, the model might lose accuracy, and when a disturbance comes in, the controller will not be able to react to disturbance fast enough. On the contrary, if the sample time is too small, the controller can react much faster and setpoint changes, but costs high computations. Therefore, there is a trade-off. In order to have accurate predictions (4.36), T_s should

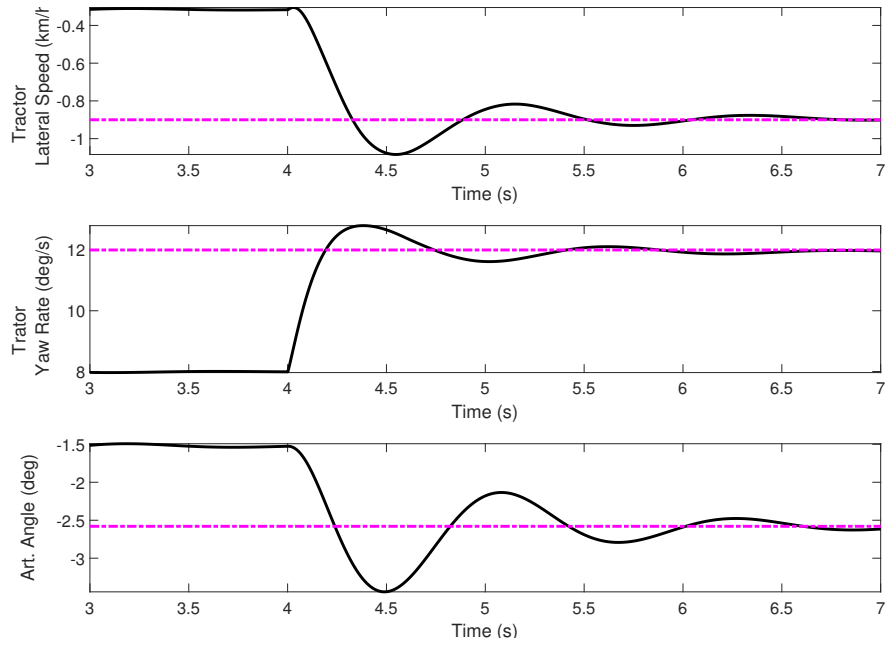
be small enough that allows 3-10 steps in the settling of a fastest dynamics [69]. Others recommend that the sampling time is between 10% to 25% of the system rise time [108]. In Figure 4.7, the tractor-trailer in CarSim is simulated by feeding a step corrective CG yaw moment to the tractor and trailer, respectively. The lateral speed and yaw rate of the tractor, and the articulation angle are presented to understand the system responses and rise times, which are summarized in Table 4.3. Rise time 1 denotes that a step corrective CG yaw moment to the tractor shown in Figure 4.7a while rise time 2 denotes that to the trailer shown in Figure 4.7b. Compromising all suggested sampling times, this research chose 0.015/0.02s for controller design used in experimental study.

Table 4.3: Rise time of tractor-trailer responses

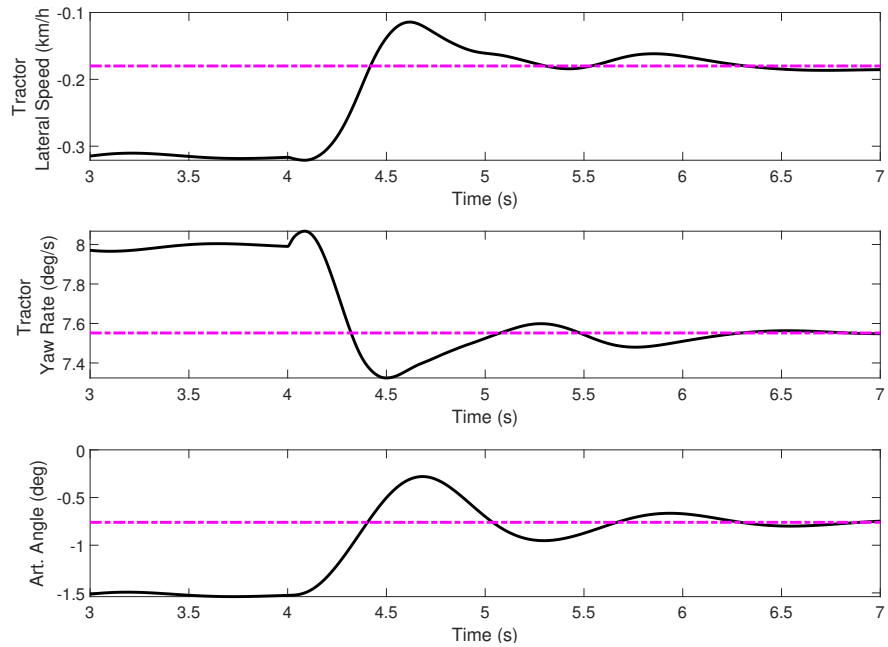
Vehicle output	Rise time1	Suggested T_s	Rise time2	Suggested T_s
v_y^t (tractor)	0.20s	0.01s-0.02s	0.22s	0.011s-0.022s
r^t (tractor)	0.15s	0.0075s-0.015s	0.15s	0.0075s-0.015s
λ (articulation)	0.18s	0.009s-0.018s	0.30s	0.015s-0.03s

There are various techniques found in the literature to tune the prediction horizon. A basic principle is N_p should be large enough to capture the significant dynamics of system process [109]. A heuristic method from [110], sets N_p be 10, as a default setting and good results are achieved in the application of a continuous stirred tank reactor (CSTR). A similar method from Wojsznis et al [111] suggested tuning the prediction horizon large enough so that control performance is not significantly changed when one further increases it. A reasonable guideline for N_p suggested by Maurath et al [109] is to cover 80-90% of the rise to a new steady state giving a step input to the open-loop system, where in [108] a similar recommendation is seen. Thus, in this example, by referring the step input responses of Figure 4.7, it is calculated that $N_p = 10$ for tractor differential braking control strategy and $N_p = 13$ for trailer differential braking control strategy. However, to compromise the computational cost, a prediction horizon of 10 steps is used for both control strategies.

Control Horizon



(a) A step CG yaw moment to the tractor



(b) A step CG yaw moment to the trailer

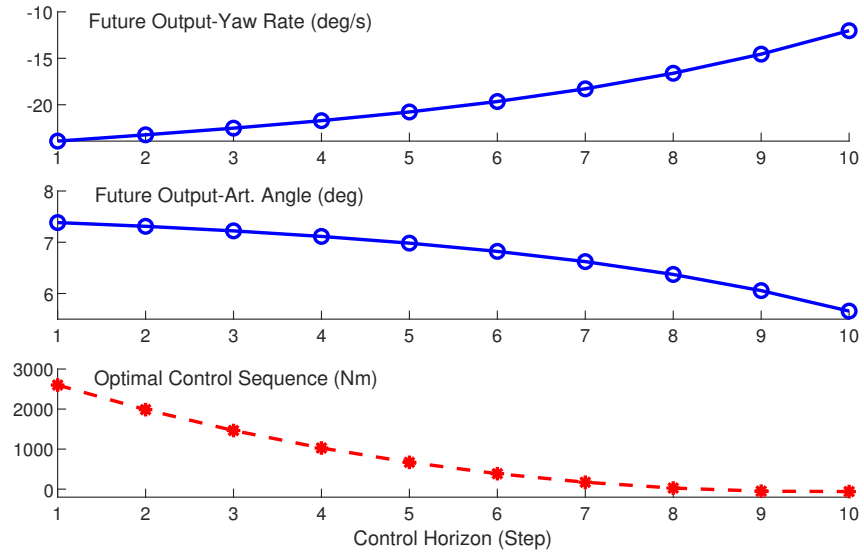
Figure 4.7: Tractor-trailer open loop responses

The future control actions lead to the predicted future output, the number of control moves to time step N_c are called the control horizon. The smaller the control horizon, the fewer the computations. However, the minimum horizon will not give us the best control maneuvers. This leads to a trade-off. If the control horizon is increased, it results in a more robust but more aggressive controller as well as larger computational cost. On the contrary, decreasing the control horizon creates more the conservativeness and saves computations but with the price of reducing robustness [106].

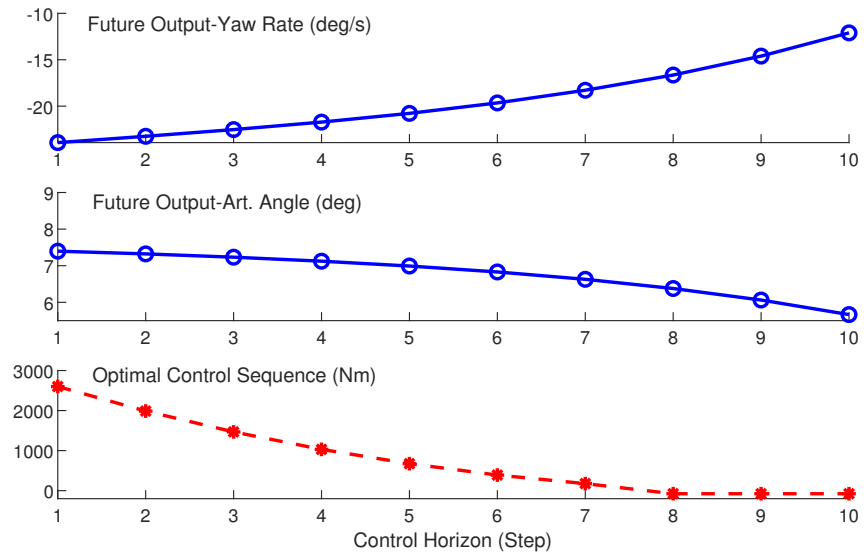
It is ideal to set N_c large enough to cover all significant adjustments of the control sequence in order to cope with a set-point change. Georgiou et al.[112] chose the time that takes for the output response to reach 60% of steady state as control horizon, which results in around 6 in our example. One suggested the control horizon be 10% to 20% of the prediction horizon meanwhile greater than 3 [108]. To find a proper control horizon that saves computations meanwhile without much sacrifice on control performance, it compared the future states over the prediction horizon corresponding to the control sequence over the control horizon. As discussed, the prediction horizon is set to be 10, Figure 4.8 and Figure 4.9 compares the future outputs over prediction horizon at control horizon $N_c = 10, 8, 5, 3$, respectively. It is shown decreasing the control horizon from 10 to 5, has little influence on the states prediction and the remaining moves have only minor effect. However, in the case of $N_c = 3$, the first element of the control sequence has a significant difference to others. Thus, $N_c = 5$ is chosen for simulation and experimental study.

Weights

There are weights on the outputs and weights on the control efforts as basic tuning. Weights tuning depends on system requirements and control desires. For instance, if one emphasizes the tracking accuracy and wants a more aggressive control performance, more weights should be put on the tracking error side, i.e., weighting matrix Q . If robustness and smooth control performance and energy saving are important, one could increase the weighting matrix R to realize such goal. In this research, a normalized tuning method is used for weight tuning [113]. First, weighting matrix Q and R can be written as diagonal

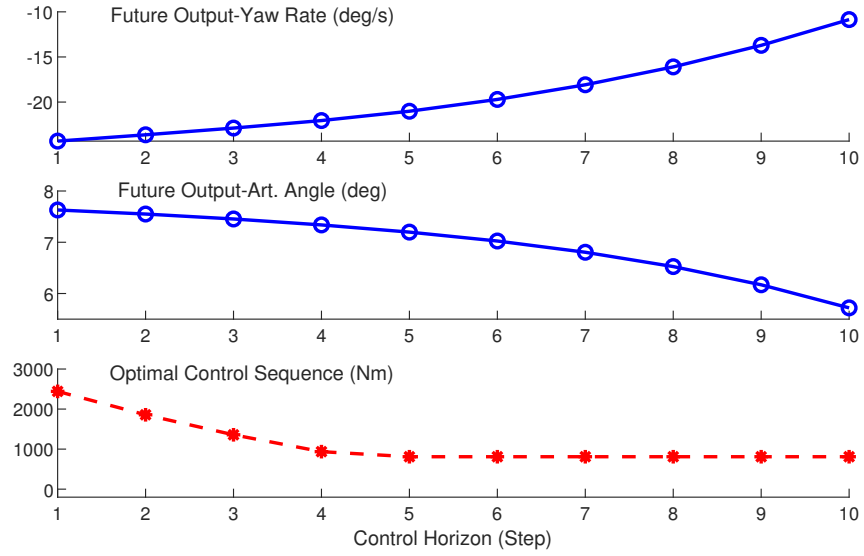


(a) $N_p = 10, N_c = 10$

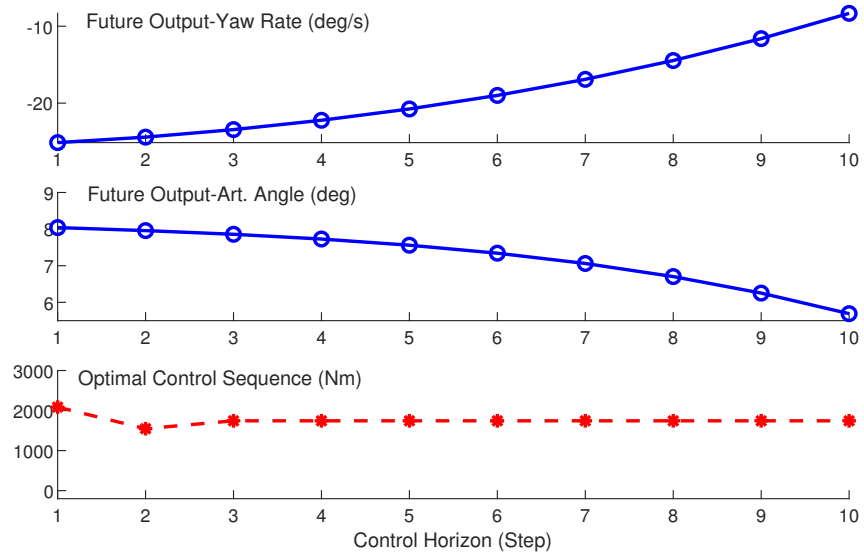


(b) $N_p = 10, N_c = 8$

Figure 4.8: Predicted outputs over different control horizon-1



(a) $N_p = 10, N_c = 5$



(b) $N_p = 10, N_c = 3$

Figure 4.9: Predicted outputs over different control horizon-2

weights:

$$Q = \begin{bmatrix} q_1 & & 0 \\ & \ddots & \\ 0 & & q_n \end{bmatrix}; R = \begin{bmatrix} r_1 & & 0 \\ & \ddots & \\ 0 & & r_n \end{bmatrix}. \quad (4.58)$$

Starting from Q , where q_1, \dots, q_n corresponds to different states to be tracked, the allowable tracking errors of each state are considered, for instance, assuming the first output is vehicle speed and its allowable error is 0.5m/s. To normalize $(y_1 - y_{d1})q_1(y_1 - y_{d1})$ be 1, it results that $(0.5)q_1(0.5) = 1$, which gives us $q_1 = (1/0.5)^2$. Assuming the third output is articulation angle and its allowable error is 2 deg, namely, $2 * \pi/180$ in radians. It is normalized that $(y_3 - y_{d3})q_3(y_3 - y_{d3}) = 1$, which is $(\pi/90)q_3(\pi/90) = 1$. Thus, the weight q_3 is $(90/\pi)^2$. Following this procedure, one could tune the r_1, \dots, r_n using the boundaries of the control inputs. To achieve a robust and satisfying performance, Trial and error is necessary to see the changes and balance of the control responses. In addition, when it comes to production implementation, a fine tuning process is needed that considers all possible situations, such as, road slope, bank angle, uncertainties from road friction and side wind.

4.7 Summary and Discussion

In this chapter, an optimization-based reconfigurable control framework for any multi-axle vehicles was presented. Stability objectives of yaw and roll planes were studied in order to provide good references for stability control. Especially, the steady-state of tractor yaw rate and articulation angle were analyzed considering the load effect of the trailer. In the high-level MPC, a reconfigurable yet universal and explicit prediction model is the key to synthesize a QP problem. In the light of dynamics and modeling in Chapter 3, vehicles with multi units were unified into a general prediction model and a general MPC controller was formulated. The feasibility and stability of the LTV-MPC were discussed.

In the lower-level control allocation, the virtual corrective CG forces were optimally distributed by solving a static QP problem. This layer captured the diversity of vehicle configurations so the reconfigurability is achieved through modifying the effectiveness (or

mapping) matrix and constraints. Different constraints for steering and torque corrections were studied in the optimization problem. Thus, wheel dynamics control and tire capacity reservation are guaranteed.

In addition, a comprehensive work on MPC tuning with a specific vehicle example was presented from theoretical and practical perspectives. Simulation results were presented for comparison and analysis. It covered sampling time, model prediction horizon, control horizon selection, and weights tuning.

Chapter 5

Applications and Simulations

In this chapter, a comprehensive simulation-based study is presented to evaluate the feasibility and effectiveness of the controller. Section 5.1 introduces a controller formulation and simplification process when a specific application is given. The reconfigurable controller is applied to several different applications. Section 5.2 presents a three-axled bus for longitudinal and yaw control and rollover prevention by integrated torque vectoring control (TVC) and differential braking system (DBS). Section 5.3 present an articulated bus for yaw control and sway prevention by active trailer steering and differential braking system, respectively. Section 5.4 presents a more complex articulated truck for jackknifing and rollover prevention by differential braking system of the tractor. Furthermore, Section 5.5 investigates the case of actuator failure and controller robustness. Section 5.6 summarizes the chapter and provides some concluding remarks.

5.1 Matrix Size Reduction

MPC needs larger computational load and memory caches than classical controls. There are challenges while implemented within auto-grade electronic control units (ECUs). In addition to selecting a fast and robust QP solver, another key issue is the dimension of the system matrices and the number of control inputs. While applying the proposed controller

to a specific case, in practice, the configuration of the vehicle to be controlled is prior knowledge, such as axle/articulation configuration; drive mode and steering system; control objective; active control system. Therefore, it is necessary to adjust the matrix dimension for computation's sake. The controller algorithm flowchart in Figure 5.1 suggests how it works while giving a vehicle for dynamics control. In offline mode, once the target vehicle is chosen, the vehicle configurations, stability objectives, and physical constraints are surely acquired. Therefore, 'Boolean Matrices', namely, T_e, T_c and T_w are defined. Dimensions of model matrices(A_d, B_d, G_d, d_d and C_d), the mapping matrix (B_p), and vectors (x, y, v and u) are simplified and determined. All matrices are configured to be the proper size before execution. In online mode, it follows the two-layer control framework as introduced previously. A diverse group of applications and simulations summarized in Table 5.1 is used to demonstrate as well as verify the proposed framework. From Application I to III, a open loop simulation environment (without the driver in the loop) is used while Application IV considers the driver in the loop. Although driver in the loop is recommended that could compare the vehicle stability and trajectory, the research focuses on stability control. In addition, the experimental validation takes account of the driver in the loop.

Table 5.1: Applications description

App.	Vehicle	Driver and Maneuver	μ	Control Objective	Actuators
I	Three-axled bus	1)DLC, with initial speed of 100 km/h	0.5	-Longitudinal control -Yaw tracking control	TVC +
		2)Fishhook steer,initial speed of 80 km/h	0.75	-Rollover prevention -Yaw tracking control	DBS
II	Articulated bus	Sine steer with constant speed of 80 km/h	0.75	-Trailer sway control -Yaw tracking control	ATS
III	Articulated bus	Sine steer with constant speed of 85 km/h	0.75	-Trailer sway control -Yaw tracking control	DBS
IV	Articulated truck	1) Double lane change, initial speed of 80 km/h	0.75	-Rollover prevention	Tractor
		2) Brake in a step turn, initial speed of 65 km/h	0.5	-Jackknifing prevention	DBS

The parameters of the high-level MPC are selected based on the tuning study of Section 4.6. As a result, this simulation study set the sample time of the controller equal to 15 ms

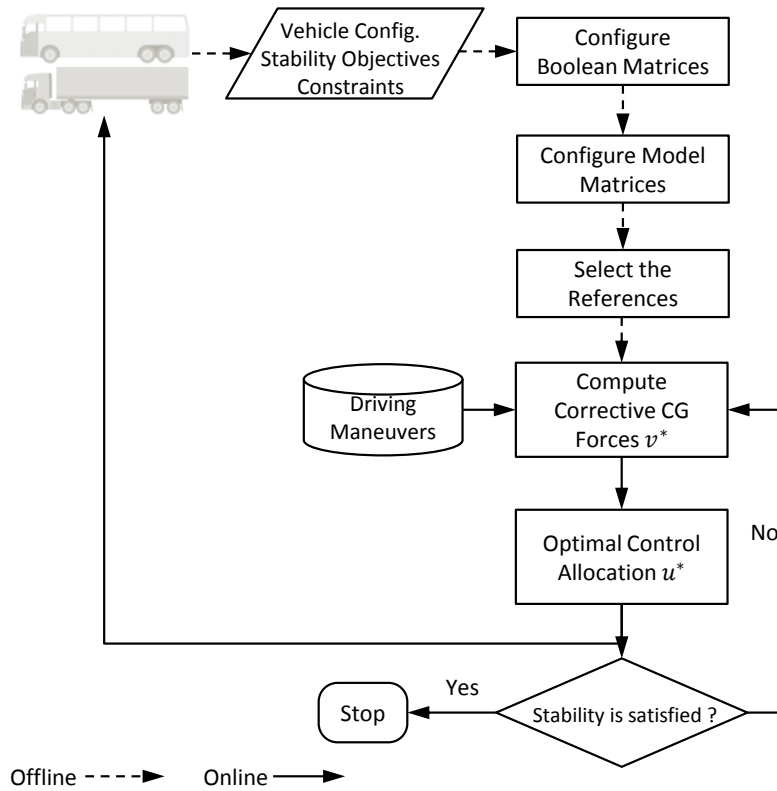


Figure 5.1: Controller algorithm flowchart

for model discretization and set the prediction horizon equal to 10 steps while the control horizon, 5 steps. These selections are resulted from the compromise between computation cost for real-time implementations and holding an acceptable control performance. The entries of weighting matrices vary from applications to applications. They are not listed for each application and configuration, but following the tuning procedure introduced in Section 4.6, the weights are obtained and used in simulations.

5.2 Three-axled Bus with TVC&DBS

This case aims to evaluate the proposed control framework applying to a multi-axle bus that are is articulated. Built in TruckSim environment, the bus has three axles (axle #1, #3 & #4), with two rear axles drive from independent electric motors and hence is capable of rear torque vectoring control (TVC), shown in Table 5.1 and Figure 5.2. Besides, the bus has differential braking system (DBS) for all wheel actuators. With the knowledge of its configuration, the 'Articulation, Axle and Actuator Boolean Matrix' can be written as,

$$T_c = \text{diag}(1, 1, 1, 1, 0, 0, 0, 0, 1, 1, 1, 1, 1, 1, 1, 1);$$

$$T_w = \text{diag}(0, 0, 0, 0, 0, 0, 0, 0, 1, 0, 1, 0, 1, 0, 1, 0).$$

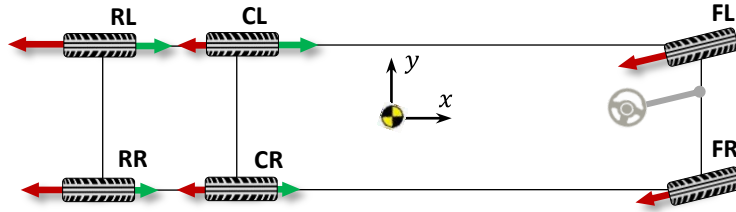


Figure 5.2: A three-axled bus with rear torque vectoring

Since the vehicle configuration is given and control objectives are targeted, matrix dimensions of state space model (4.32) are simplified and specified: $A_d \in \mathbb{R}^{5 \times 5}$; $B_d \in \mathbb{R}^{5 \times 1}$; $G_d \in \mathbb{R}^{5 \times 5}$; $d \in \mathbb{R}^{5 \times 1}$; $x = [v_x \ v_y \ r \ \phi \ \dot{\phi}]^T$; $v = [\Delta F_x \ \Delta M_z]^T$; $y = [v_x \ v_y \ r \ RI]^T$. Regarding the mapping equation (4.49), the sizes are obtained that $B_p \in \mathbb{R}^{2 \times 6}$; $u = [\Delta Q_1 \ \Delta Q_2 \ \Delta Q_3 \ \Delta Q_4 \ \Delta Q_5 \ \Delta Q_6]^T$, where ΔQ_1 and ΔQ_2 can only be braking torque (negative) while ΔQ_3 to ΔQ_6 can be drive torque (positive) or braking torque (negative).

The Double Lane Change (DLC) maneuver with speed keeping described in Table 5.1 and top-left corner of Figure 5.3 is performed for this simulation. The rollover threshold (RI_{max}) in equation (4.21) is set to be 0.7 (see the 'magenta dashed line' in the subplot

labelled rollover index). The main objective is to control the vehicle from yaw instability and meanwhile holding the speed at 100km/h for cruise control. As shown in Figure 5.3, in the 'OFF' case, the rollover index indicates a very stable roll dynamics condition but the yaw rate deviates reference state shown oversteer and the speed dropped naturally without driver's engagement. To prevent this and stabilize the bus, CG correction, including ΔF_x and ΔM_z are engaged in control 'ON' and they are optimally and smoothly distributed in each wheel, see ΔQ in the figure. As a result, the speed is accurately cruised and yaw rate is well tracked to the reference even during a higher speed compared that without control.

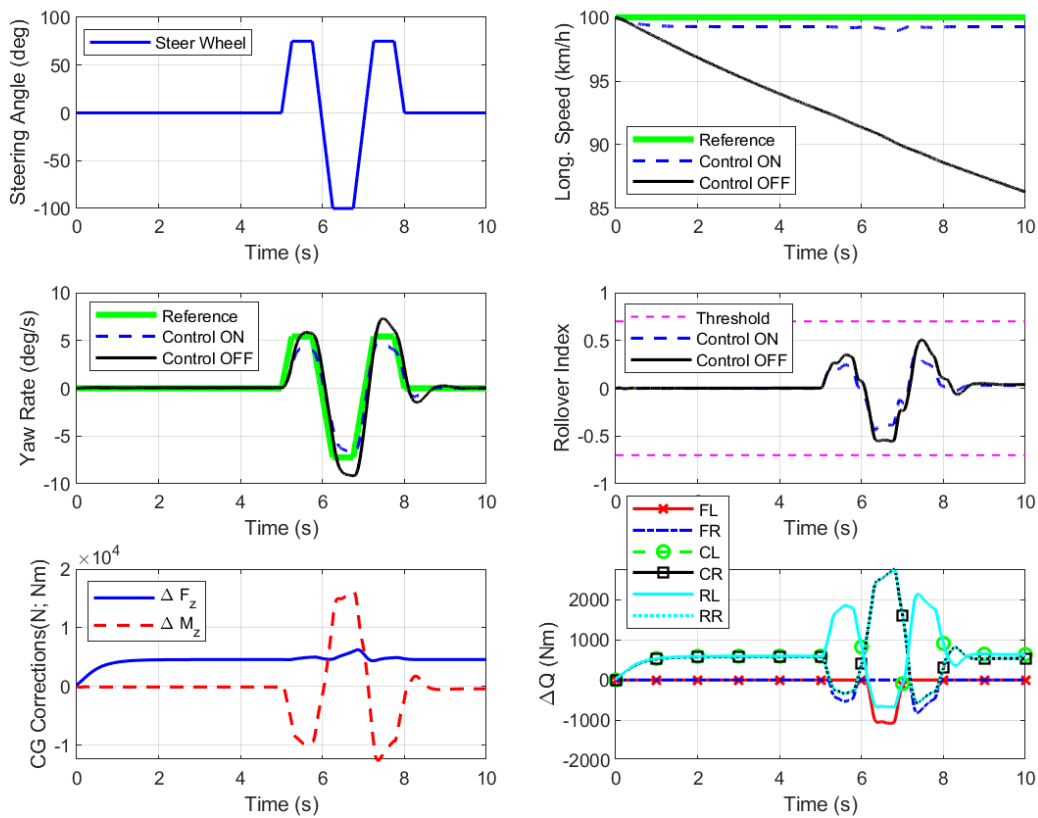


Figure 5.3: Results of longitudinal (cruise control) and yaw control in App. I

The fishhook steer maneuver described in Table 5.1 and top-left corner of Figure 5.4, which is widely used for rollover test is used for this simulation. The over-steer and rollover

risk are triggered at this severe condition. The main objective is to control the vehicle from rollover, and secondary yaw instability. One should note, in order to eliminate the effect of speed drop, a uniform brake is applied to all wheels, only for 'Control OFF' case. It gives almost same deceleration behavior(from 80km/h to 50km/h) between 'OFF' and 'ON', so results are fairly compared. As compared in Figure 5.4, the 'OFF' case shows a significant offset to reference states. In addition, marginal rollover happens from 2.8th sec to 5.5th sec, which means the bus is in a critical situation. Note that the rollover index in this case is calculated from the indirect approach using roll dynamics in (4.20), thus it could exceed ± 1 . Through active control of hybrid active torque, the rollover index is maintained within ± 1 throughout the maneuver. The lateral acceleration results show similar evidence that the risk of rollover is reduced significantly. The objectives priority successfully takes both roll and yaw stability into account. It is interesting to note that the system did not control the rollover index with the desired threshold (± 0.7) all the time. This demonstrates the challenge of severe rollover control even if the best efforts of torque vectoring and differential braking are applied.

5.3 Articulated Bus with ATS/DBS

Trailer sway is a serious threat for tractor semi-trailers safety. In this case, the controller aims to tackle the problem. An articulated bus is developed in TruckSim by modifying the templates of it. The vehicle has three axles (axle #1& #4 of unit 1, and axle #4 of unit 2), with the axle #4 of unit 1 drive powered by traditional combustion engine; Feasible actuation systems involve active trailer steering (ATS) and differential braking system (DBS) [114]. The ATS system has the capacity of -8° to 8° , shown in Table 5.1 and Figure 5.5. With such prior-knowledge of the configuration, the 'Articulation, Axle and Actuator Boolean Matrix' can be written as,

$$T_\varepsilon = I_{10 \times 10};$$

$$T_c^t = \text{diag}(1, 1, 1, 1, 0, 0, 0, 0, 0, 0, 0, 0, 1, 1, 1, 1);$$

$$T_c^i = \text{diag}(0, 0, 0, 0, 0, 0, 0, 0, 0, 0, 0, 0, 0, 1, 1, 1, 1);$$

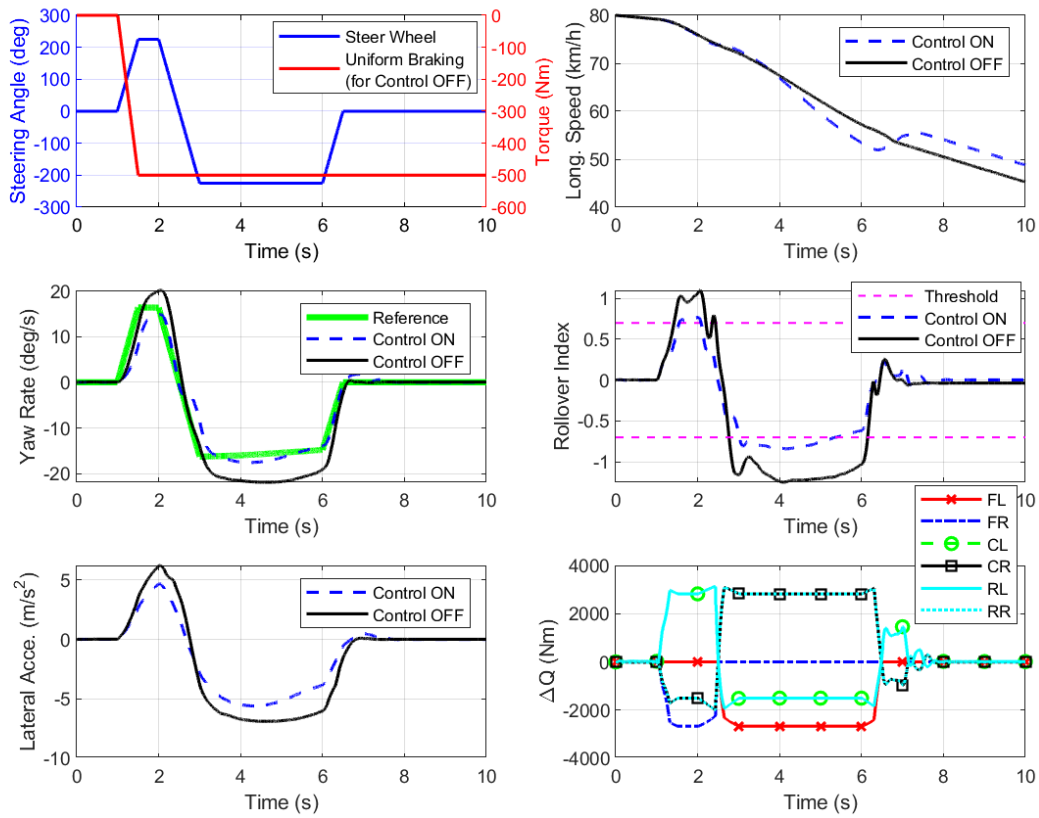


Figure 5.4: Results of yaw and rollover control in App. I

$$T_w^t = \text{diag}(0, 0, 0, 0, 0, 0, 0, 0, 0, 0, 0, 0, 0, 0, 0, 0);$$

$$T_w^i = \text{diag}(0, 0, 0, 0, 0, 0, 0, 0, 0, 0, 0, 0, 0, 0, 1, 0, 1).$$

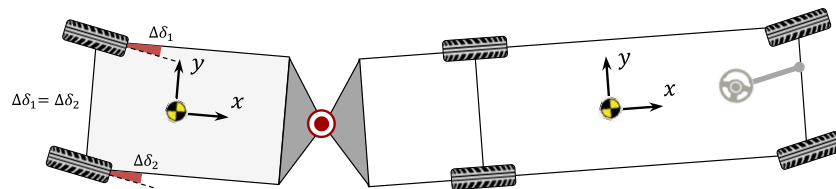


Figure 5.5: An articulated bus with active trailer steering

Since the vehicle configuration is given and control objectives are targeted, matrix dimensions of state space model of (4.32) are specified: $A_d \in \mathbb{R}^{4 \times 4}$; $B_d \in \mathbb{R}^{4 \times 2}$; $G_d \in \mathbb{R}^{4 \times 4}$; $d_d \in \mathbb{R}^{4 \times 1}$; $x = [v_y^t \ r^t \ v_y^i \ r^i]^T$; $v = \Delta M_z^i$; $y = [v_y^t \ r^t \ \lambda]^T$. Regarding the mapping equation (4.49) and control input, where $B_p \in \mathbb{R}^{1 \times 2}$; $u = [\Delta\delta_1 \ \Delta\delta_2]^T$ and $\Delta\delta_1 = \Delta\delta_2$.

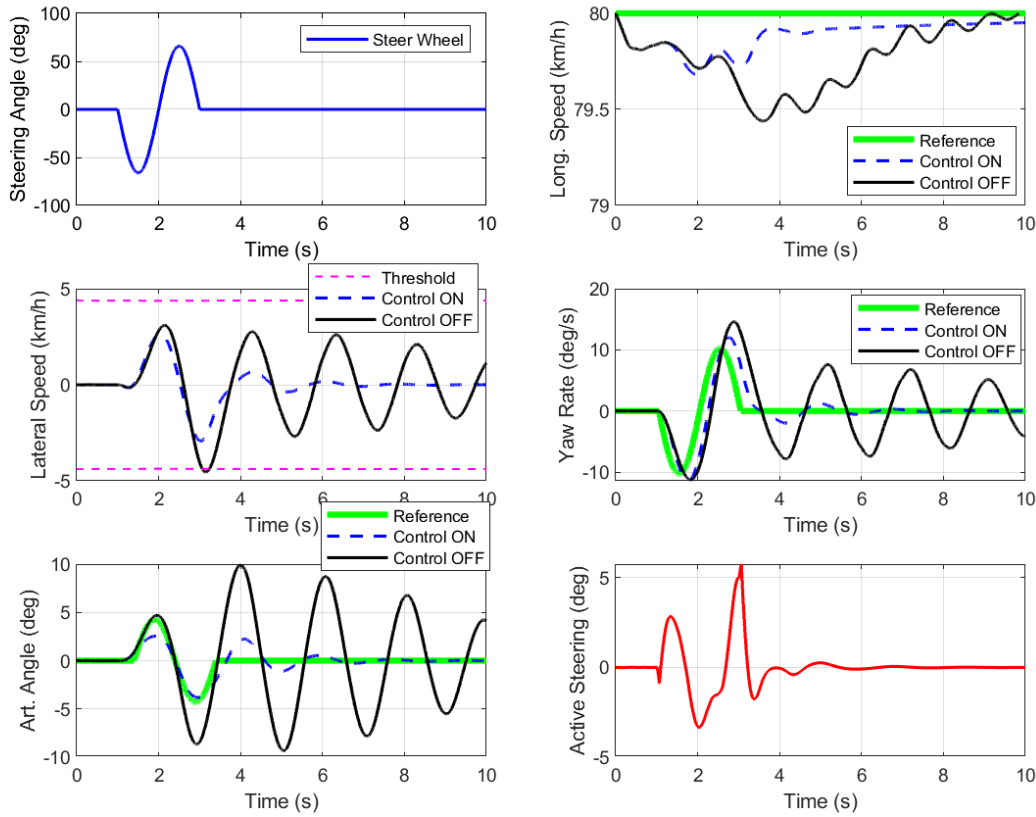


Figure 5.6: Results of yaw and sway control of App. II

A sharp sine impulse steer, with the amplitude of 75 deg and period of 2s, described in and the top-left corner of Figure 5.6 is performed for this simulation. A constant speed is held for both OFF and ON modes for fair comparison purpose. In the control 'OFF' mode, a severe trailer sway and tractor yaw oscillation are triggered. The articulation angle reached as big as 10 deg and damped very slow. Note that, the maximum articulation angle is translated to be around 3m of the arc length that the rear end swept, which is

very dangerous due to the violation to its driving lane. In addition, neither the leading unit(tractor) is stable in yaw motion. Through active trailer steering, the articulation angle is well tracked throughout the maneuver and the sway stopped after the 5th second. As the secondary objective, the tractor yaw rate tracking shows similar evidence that the vehicle is stabilized. From the result of the active steering angle, it is notable that small steering adjustments (3° to 5°) are only needed but the stabilization impact is huge. Additionally, the active trailer steering angles are very smooth and without oscillations.

In this case, the same articulated bus in App. II but configured with differential braking is built in TruckSim. The main purpose of this application is to compare the performance of various differential brake systems, as well as demonstrate the reconfigurability of the framework. With the prior-knowledge of the configuration in Table 5.1 and Fig. 5.7, the 'Articulation and Axle Boolean Matrix' are kept same as App. II, but 'Actuator Boolean Matrix' is modified as,

$$T_w^t = \text{diag}(1, 0, 1, 0, 0, 0, 0, 0, 0, 0, 0, 0, 0, 1, 0, 1, 0);$$

$$T_w^i = \text{diag}(0, 0, 0, 0, 0, 0, 0, 0, 0, 0, 0, 0, 0, 0, 1, 0, 1, 0).$$

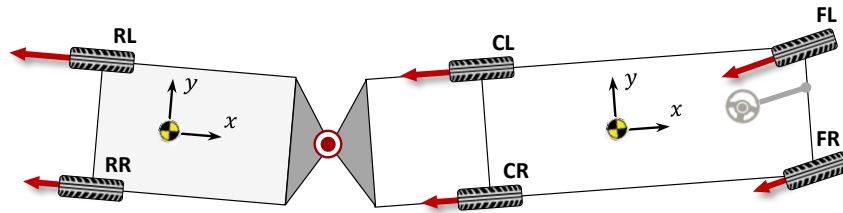


Figure 5.7: An articulated bus with differential braking system

Given the vehicle configuration and control objectives, matrix dimensions of state space model (4.32) are specified: $A_d \in \mathbb{R}^{4 \times 4}$; $B_d \in \mathbb{R}^{4 \times 2}$; $G_d \in \mathbb{R}^{4 \times 4}$; $d_d \in \mathbb{R}^{4 \times 1}$; $x = [v_y^t \ r^t \ v_y^i \ r^i]^T$; $v = [\Delta M_z^t \ \Delta M_z^i]^T$; $y = [v_y^t \ r^t \ \lambda]^T$. For the mapping equation (4.49), there are three versions of the control strategies listed and named in Table 5.2. For 'Controller A' where $B_p \in \mathbb{R}^{1 \times 4}$; $u = [\Delta Q_1 \ \Delta Q_2 \ \Delta Q_3 \ \Delta Q_4]^T$; 'Controller B'

where $B_p \in \mathbb{R}^{1 \times 2}$; $u = [\Delta Q_5 \quad \Delta Q_6]^T$; 'Controller C' where $B_p \in \mathbb{R}^{2 \times 6}$;

$u = [\Delta Q_1 \quad \Delta Q_2 \quad \Delta Q_3 \quad \Delta Q_4 \quad \Delta Q_5 \quad \Delta Q_6]^T$; Thanks to the reconfigurability of the proposed framework, it can easily design the different controllers and compare the performance.

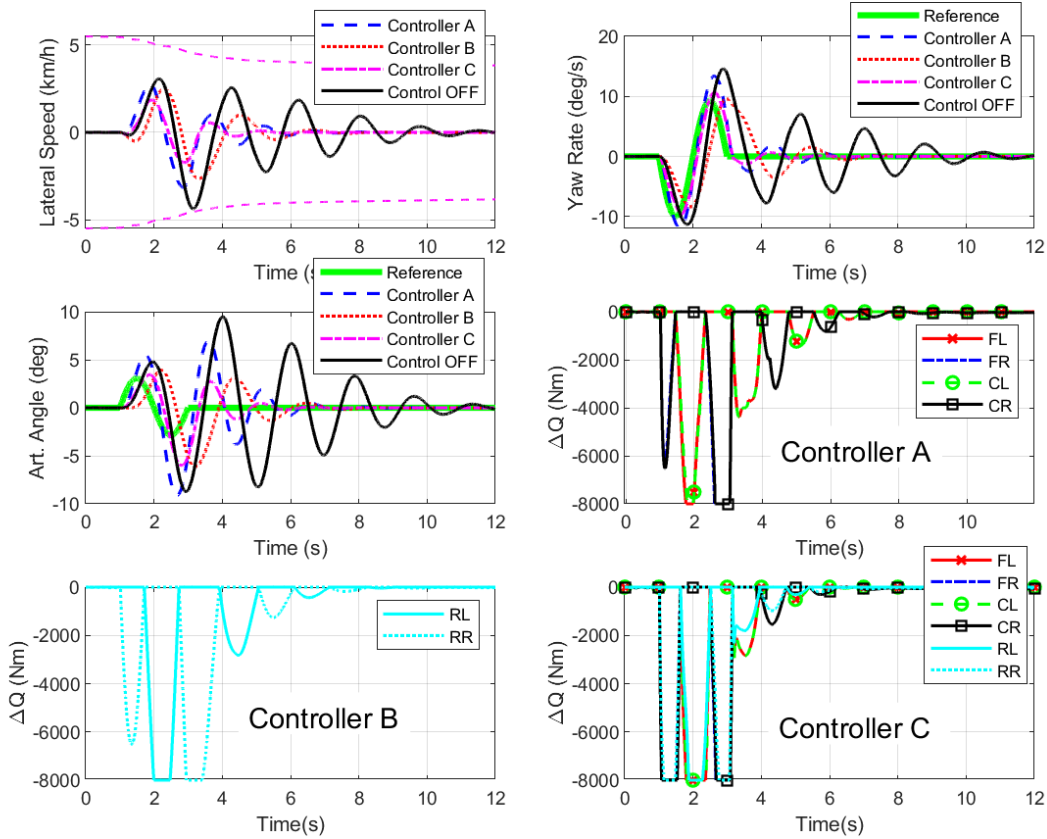


Figure 5.8: Results of yaw and sway control of App. III

Similar to the case with ATS, a sharp sine steer, with the amplitude of 75 deg and period of 2s (Table 5.1), is applied to the bus. In the control 'OFF' mode, the bus experienced severe trailer sway, the articulation angle reached as big as 10 deg, and the vehicle gets stable gradually. The tractor yaw rate oscillates in the same way and time range. By engaging active control systems, namely, Controller A, B, C, the stabilization is achieved in various extent, described in Table 5.2. The trailer sway is effectively restrained in terms

of maximum articulation angle and sway duration. Interestingly, the comparison finds that Controller A is more effective on yaw rate tracking control while Controller B is more effective on sway stabilization but with a delay. This makes sense intuitively, as Controller A uses the differential braking of the tractor while Controller B uses that of the trailer. Additionally, Controller C shows the very good comprehensive performance on both control objectives.

Table 5.2: Performance of different controller of App. III

Controller	Active Actuators	Max. λ	Duration of Sway	Art. Angle Tracking	Yaw Rate Tracking
OFF	No active actuators	10 °	1 st – 11 th	Trailer sways	Oversteer
A	Differential braking on tractor	8.5°	1 st – 6.5 th	Limited	Effective
B	Differential braking on trailer	6°	1 st – 6.5 th	Reduced with a delay	Reduced with a delay
C	Integrated differential braking	6°	1 st – 6.5 th	Effective	Effective

5.4 Articulated Truck with DBS

Many tractor trailer combinations have the changeable trailer. However, the scope of this work assumes the trailer configuration, e.g., axles, is constant and its information is known, measured/estimated. In this case, a commercial truck with full payload is built in TruckSim. As mentioned, truck dynamics is complex and challenging for active controls. In this case, the controller aims to prevent the likelihood of trailer rollover and jackknifing, which are the most common threats to highway safety of long trucks. Articulated truck built in TruckSim has four axles(axle #1,#2 & #4 of unit 1, and axle #3 & #4 of unit 2), with tractor rear axles drive from a combustion engine and is capable of the tractor differential braking, shown in Table 5.1 and Figure 5.9. With the prior knowledge of the configuration, the 'Articulation, Axle and Actuator Boolean Matrix' can be written as,

$$T_\epsilon = I_{10 \times 10};$$

$$T_c^t = \text{diag}(1, 1, 1, 1, 0, 0, 0, 0, 1, 1, 1, 1, 1, 1, 1, 1);$$

$$T_c^i = \text{diag}(0, 0, 0, 0, 0, 0, 0, 0, 1, 1, 1, 1, 1, 1, 1, 1);$$

$$T_w^t = \text{diag}(1, 0, 1, 0, 0, 0, 0, 0, 1, 0, 1, 0, 1, 0, 1, 0);$$

$$T_w^i = \text{diag}(0, 0, 0, 0, 0, 0, 0, 0, 0, 0, 0, 0, 0, 0, 0, 0).$$

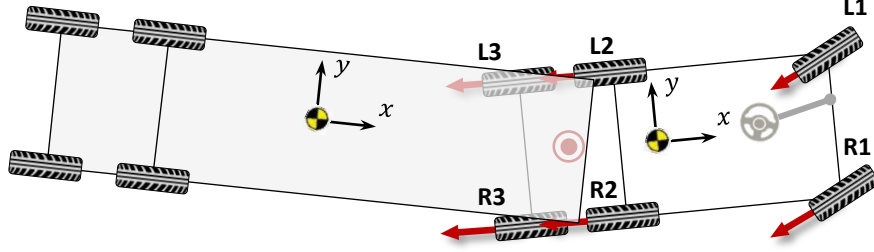


Figure 5.9: An articulated truck with differential braking system

Again, with the knowledge of the vehicle configuration and control objectives, matrix dimensions of state space model (4.32) are specified: $A_d \in \mathbb{R}^{8 \times 8}$; $B_d \in \mathbb{R}^{8 \times 1}$; $G_d \in \mathbb{R}^{8 \times 6}$; $d_d \in \mathbb{R}^{8 \times 1}$; $x = [v_y^t \ r^t \ \phi^t \ \dot{\phi}^t \ v_y^i \ r^i \ \phi^i \ \dot{\phi}^i]^T$; $v = \Delta M_z^t$; $y = [r^t \ \lambda \ RI^i]^T$. For the mapping equation (4.49), where $B_p \in \mathbb{R}^{1 \times 6}$; $u = [\Delta Q_1 \ \Delta Q_2 \ \Delta Q_3 \ \Delta Q_4 \ \Delta Q_5 \ \Delta Q_6]^T$; Note that, in this case, the high-level controller only generates the yaw moment of tractor and the lower-level controller computes the active brake commands, where, from left to right and front to back, are indicated by L1, R1 to L3, R3 in Figure 5.9.

In the maneuver of double lane change (DLC) in Figure 5.10, a driver is in the loop using a path-following model of TruckSim. The driver performed a harsh DLC to avoid potential obstacles on a highway. The weights of Q are set to emphasize rollover prevention. The rollover threshold (RI_{max}) is set to be 0.6 (see the ‘magenta dashed line’). If no active control engaged, the trailer rollover likelihood is seen at 5th-6th, and 7th-8th second. When differential braking is engaged, the maximum load transfer ratio of the trailer is reduced by approximately 32.6% from -0.92 to -0.62. In addition, the lateral acceleration shows similar evidence on rollover prevention. Although the weights of yaw rate and articulation angle (in Q) are set very small, the tractor yaw rate and articulation are also reduced as a notable side effect because of the corrective yaw moment and speed drop.

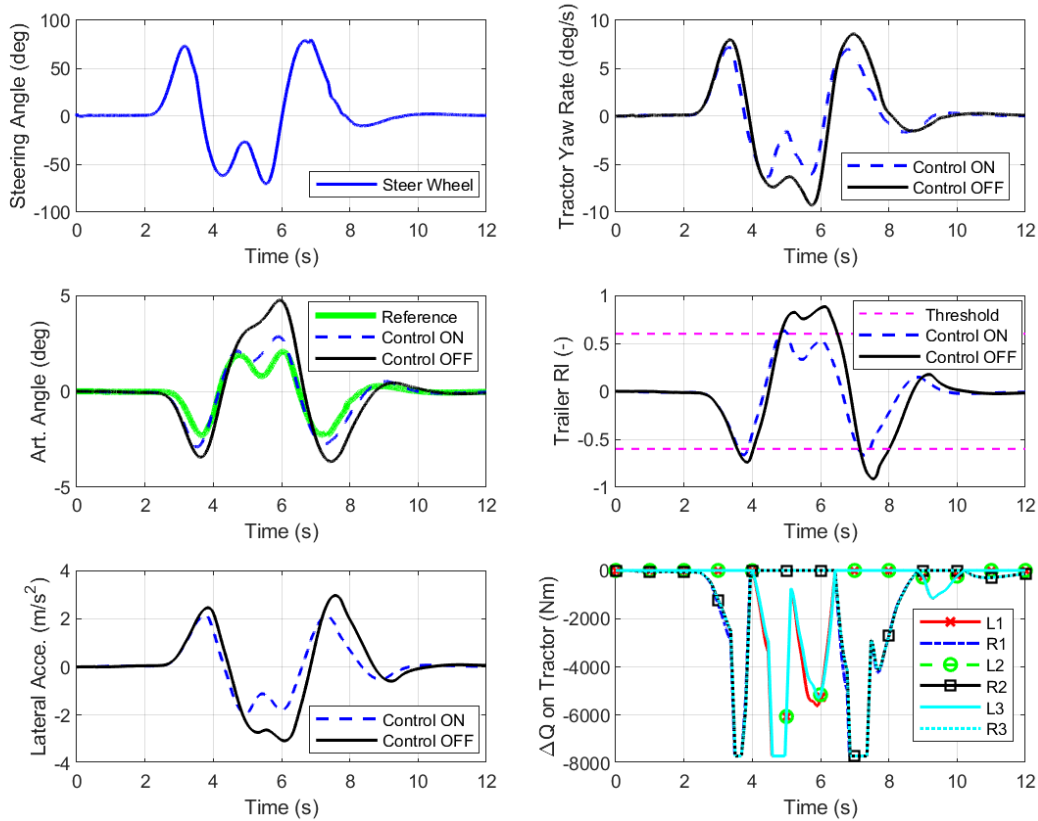


Figure 5.10: Results of rollover prevention of App. IV

In the second case, to trigger a jackknife, a step steer and a step brake of 1200Nm at each wheel are applied. The tires are in a high slip or saturation scenarios at the low road friction coefficient condition. And the huge inertia of the trailer due to the full load contributes to the likelihood of jackknife. As shown in Figure 5.11, in Control OFF Mode, the articulation angle keeps increasing and diverging, indicating a jackknife is very likely to happen. Moreover, the trailer RI stayed in the high value during the turn. However, the engagement of differential braking prevents the truck from jackknife successfully, where the articulation angle is reduced to follow the reference and maintain in a very small range and RI is dropped to a relatively safe area in practice.

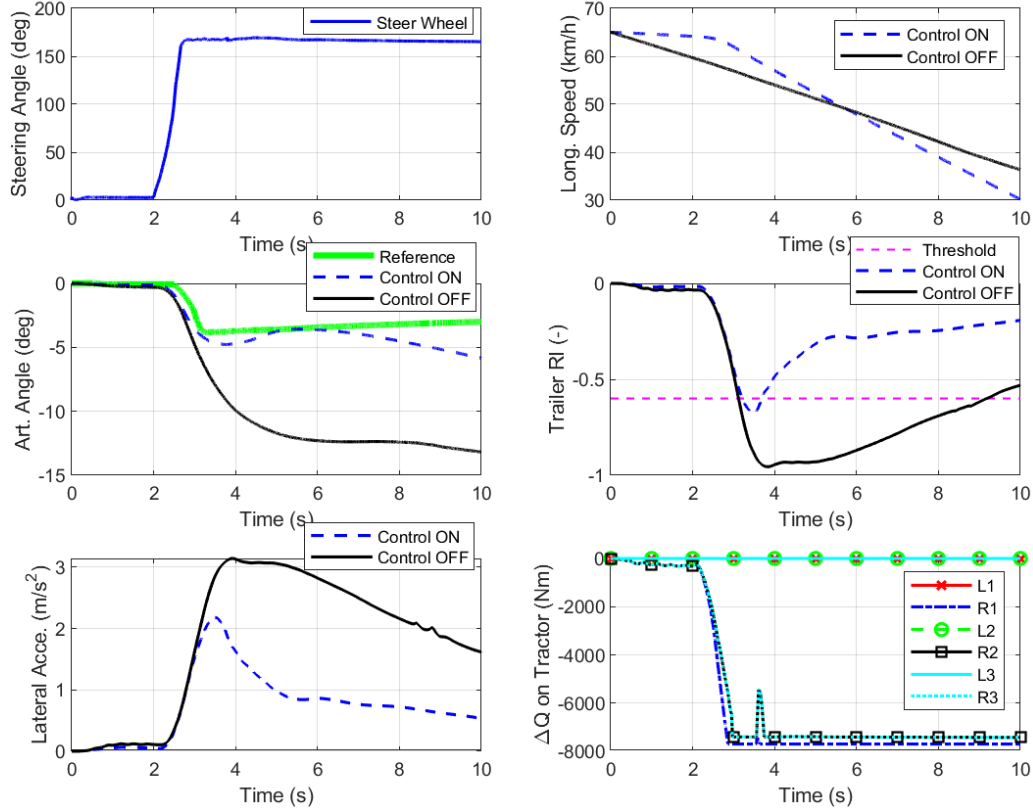


Figure 5.11: Results of jackknife prevention of App. IV

5.5 Actuator Failure and Robustness

In this case, the same bus and fishhook maneuver used in App. I are used. However, the front-left (FL) wheel braking actuator suddenly fails at 4th sec, namely, no braking torque can be applied on the FL wheel, shown in Figure 5.12. However, thanks to the real-time updating of the actuators' constraints, the reconfigurable controller successfully prevented the instability by reconfiguring the individual wheel brake torques. The rollover index and yaw rate are greatly reduced with slightly less performance than the unfailed case in Figure 5.4. From the corrective torques, central-right (CR) and rear-right (RR) driving torque are increased from 2800Nm to 3200 Nm while central-left (CL) and rear-left (RL)

braking torque go down from -1500Nm to -3200Nm, in order to generate a reverse yaw direct moment to compensate FL brake failure. It is observed that the bus is about to lose stability at the failure moment but quickly pulled back through braking redistribution.

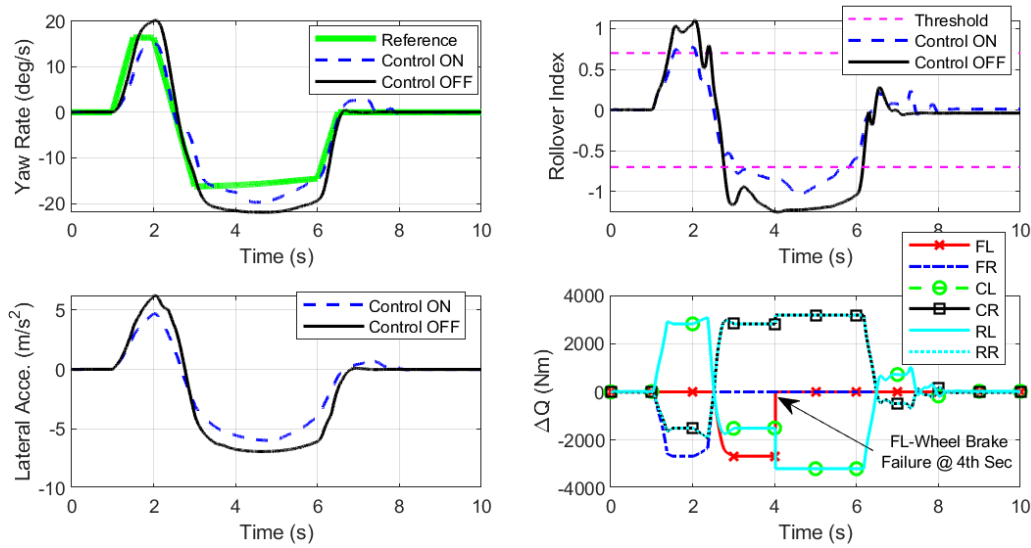


Figure 5.12: Fault-tolerance control of fishhook maneuver in App. I while a brake actuator failed

Road condition, namely, tire-road friction coefficient (μ) is important but challenging and expensive to estimate. In our control system, it should be noted that the controller does not require a tire-road friction estimation, instead, it uses a constant coefficient, i.e. $\mu = 0.9$ for all simulations. Comprehensive results show the controller robust to road condition, for instance, when the actual μ is 0.75 or 0.5. In addition, the model-based controller also needs to handle the uncertainty and the reasonable variation of the vehicle. For a better comparison, the same bus and fishhook maneuver in App. I are used. However, in this case, the tire cornering stiffness used in the controller has 30% degradation and actual bus (in TruckSim) has some variations on dynamics parameters due to the payload, e.g. passengers. Specifically, the bus mass increased by 1500kg, the CG location is 10cm higher, and the distance between the front axle to CG is 50cm longer. As a result, the bus becomes more challenging to control and this can be seen from the bus responses in Figure 5.13 without control compared to these in Figure 5.4. However, when the active control

engaged, the bus is stabilized from oversteer and rollover and the performance is almost comparative to these in Figure 5.4.

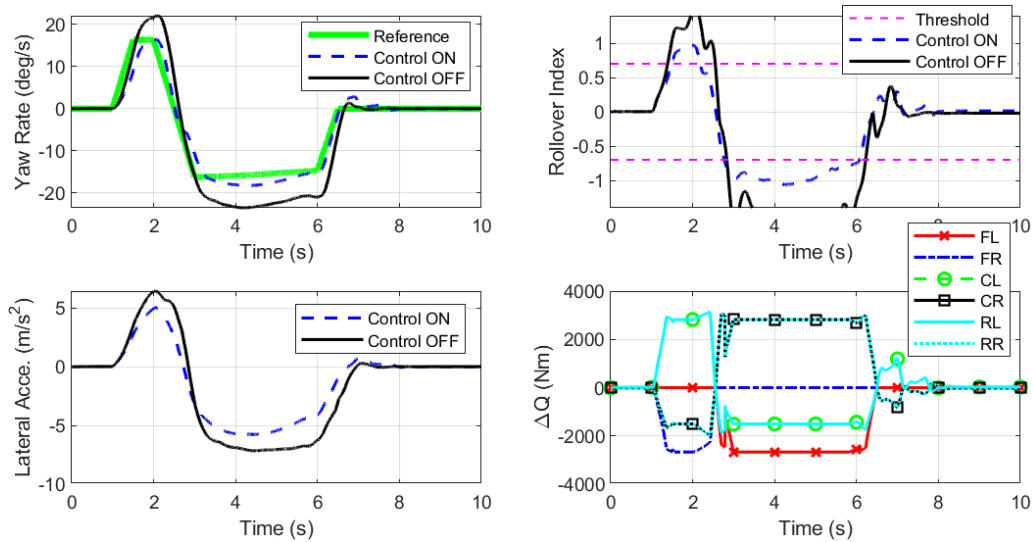


Figure 5.13: Robustness performance of fishhook maneuver in App. I to tires and vehicle parameters variations

5.6 Summary and Discussion

In this chapter, the universality, reconfigurability, and performance of the proposed controller were evaluated through several different applications and configurations. Three different vehicles with different active actuation systems, namely, three-axled bus, articulated bus, and truck, are built and modified in CarSim/TruckSim environment to provide high-fidelity models for simulation. Since vehicles have different dynamic characteristics and tendency of instability, different control objectives are specialized and emphasized.

To develop the controller for each application, the ‘Boolean Matrices’ and gains were selected properly without reformulating the controller. In addition, to reduce the computational burden, the model formulation is simplified and customized for each case. It

is shown that the proposed framework is capable of handling different vehicles and configurations. More importantly, at severe maneuvers, such as DLC, fishhook, sine steer, the vehicles without control experienced serious safety issues, i.e., rollover, yaw deviation, lateral instability, or trailer sway and jackknife in articulated vehicles. In contrast, the active controller is effective and successfully stabilize the vehicles from those undesired phenomena. Additionally, the controller can handle situations of actuator failures and, to some extent, has the robustness to vehicle and road variations and uncertainties.

Chapter 6

Experimental Study

Due to difficulties and challenges in applying the proposed control framework to different vehicles and configurations experimentally, experimental studies are conducted on a tractor-trailer, whose active brake system can be configured for different control actuations. To validate the reconfigurability and effectiveness of the controller, different control actuation systems are used and tested.

The chapter is organized as follows. Section 6.1 introduces the experimental facilities for field tests, which covers the vehicle, sensor, and controller implementation platform. Section 6.2 presents a work of cornering stiffness identification for the trailer tires because the information is not available. In Section 6.3, comprehensive test results and discussions with different control strategies are presented. Section 6.4 summarizes the chapter and provides some concluding remarks.

6.1 Experimental Facilities

Tractor

The test tractor is a pure electric 4 wheel independent drive Chevrolet-Equinox (2011), seen in Figure 6.1. It is a SUV, highly modified from its gasoline version in ‘Mechatronic Vehicle Systems Laboratory’ and the electric motors are configured at each corner. It

allows each wheel to be controlled independently, which applies to for different driveline configurations, such as FWD, RWD and 4WD. More importantly, the configuration provides great benefits on active torque vectoring and differential (regenerative) brake control. Each motor has up to ± 1600 Nm and an ABS module is available on this vehicle for wheel slip prevention. The main parameters of the tractor are listed in Table 6.1.

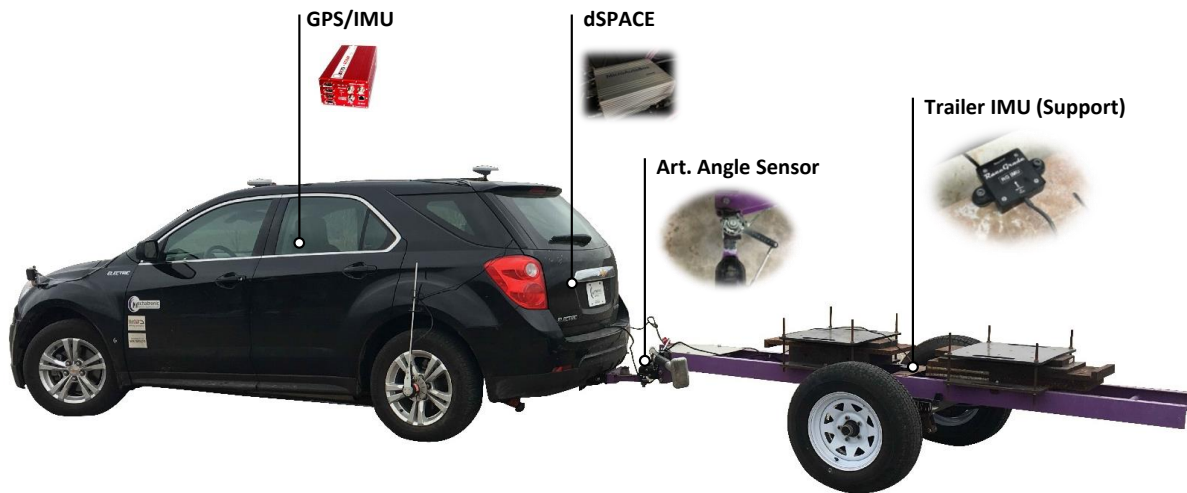


Figure 6.1: Test tractor (Equinox) and customized trailer, and main hardware

Trailer

The trailer, seen in Figure 6.1, for test was designed and made by the previous graduate student of 'Mechatronic Vehicle Systems Laboratory' for the active hitch control [115]. To cope with the significant effect of configuration variation, the trailer is designed to be adjustable in payload and CG location. It can be seen from Figure 6.1 that there are two removable/addable clump weights between the trailer axle and the trailer axle can be fixed at different position over the frame through bolting. Trailer #1 and #2 are configured as stable and unstable configuration by changing the payload and its distribution. The main parameters of two are listed in Table 6.1. In addition, the trailer is equipped with electronic drum brake system that can be controlled independently. It gives freedom to test the trailer differential brake strategy. For the sake of safety, brakes are activated once

the articulation angle exceeds a certain value and trailer becomes unmanageable.

Table 6.1: Dynamics parameters of tractor trailer

Symbol	Description	Unit	Tractor	Trailer#1	Trailer#2
m^t/m^i	Total mass	kg	2270	650	700
I_{zz}^t/I_{zz}^i	Yaw moment of inertia	kg.m ²	4600	900	1200
l_{12}^t/l_{12}^i	Distance of 1st axle to CG	m	1.42	N/A	N/A
l_{34}^t/l_{34}^i	Distance of 2nd axle to CG	m	N/A	N/A	N/A
l_{56}^t/l_{56}^i	Distance of 3rd axle to CG	m	N/A	N/A	N/A
l_{78}^t/l_{78}^i	Distance of 4th axle to CG	m	1.44	0.21	-0.1889
l_w^t/l_w^i	Average track width	m	1.59	1.32	1.32
l_h^t/l_h^i	Distance of hitch point to CG	m	2.54	1.89	1.889
R_{eff}^t/R_{eff}^i	Wheel effective radius	m	0.34	0.40	0.40
K_{us}^t/K_{us}^i	Understeer coefficient	-	0.004	—	-1.28e-04

Sensors/Hardwares

In order to implement the controller to the tractor trailer, sensing is a critical part of providing vehicles states and feedbacks for closed-loop control. Most of the sensors are pointed and illustrated in Figure 6.1. Steering wheel angle sensor, located in the steering column, is to provide steering angle and rate of turn. This sensor is common in most vehicles for vehicle stability control. A GPS (Global Positioning System) navigation system is installed on the tractor to measure the longitudinal speed and lateral speed of the vehicle accurately. A 6-axis IMU (Inertial Measurement Unit) is mounted inside of the tractor, close to the CG location. To acquire the information of trailer yaw motion, articulation angle sensor is needed. It is mounted right at the articulation point to provide articulation angle and its rate. Although not requisite, an additional auto-grade IMU is mounted in the trailer as supported module. The sensor intends to provide trailer yaw rate, lateral acceleration, etc. All these measurements and controller calculations to the vehicle are communicating through a dSPACE MicroAutoBox II, shown in Figure 6.1. The proposed controller is developed in Matlab/Simulink environment and then compiled in the platform of dSPACE to realize the real time implementation and control.

Controller Description

Following the procedure in Section 5.1, the vehicle state-space formulation can be simplified and customized. With the prior knowledge of the configuration of the experimental tractor-trailer, the ‘Articulation, Axle, and Actuator Boolean Matrix’ are modified as,

$$T_\varepsilon = I_{(10 \times 10)};$$

$$T_c^t = \text{diag}(1, 1, 1, 1, 0, 0, 0, 0, 0, 0, 0, 0, 1, 1, 1, 1);$$

$$T_c^i = \text{diag}(0, 0, 0, 0, 0, 0, 0, 0, 0, 0, 0, 0, 1, 1, 1, 1);$$

$$T_w^t = \text{diag}(1, 0, 1, 0, 0, 0, 0, 0, 0, 0, 0, 0, 1, 0, 1, 0);$$

$$T_w^i = \text{diag}(0, 0, 0, 0, 0, 0, 0, 0, 0, 0, 0, 0, 1, 0, 1, 0).$$

Given the vehicle configuration and control objectives, matrix dimensions of state space model of (4.32) are specified: $A_d \in \mathbb{R}^{4 \times 4}$; $B_d \in \mathbb{R}^{4 \times 2}$; $G_d \in \mathbb{R}^{4 \times 4}$; $d_d \in \mathbb{R}^{4 \times 1}$; $x = [v_y^t \ r^t \ v_y^i \ r^i]^T$; $v = [\Delta M_z^t \ \Delta M_z^i]^T$; $y = [v_y^t \ r^t \ \lambda]^T$.

For the mapping equation (4.49), there are three versions of the control strategies can be listed. ‘Controller A’ is with tractor differential braking, where $B_p \in \mathbb{R}^{1 \times 4}$; $u = [\Delta Q_1 \ \Delta Q_2 \ \Delta Q_3 \ \Delta Q_4]^T$; ‘Controller B’ is with trailer differential braking, where $B_p \in \mathbb{R}^{1 \times 2}$; $u = [\Delta Q_5 \ \Delta Q_6]^T$; ‘Controller C’ is with integrated differential braking of tractor and trailer, where $B_p \in \mathbb{R}^{2 \times 6}$; $u = [\Delta Q_1 \ \Delta Q_2 \ \Delta Q_3 \ \Delta Q_4 \ \Delta Q_5 \ \Delta Q_6]^T$. Thanks to the reconfigurability of the proposed framework, the different controllers can be easily designed without reformulation.

There are some states can not be used directly due to noises and corruption. Therefore, estimations are used instead, where the vehicle longitudinal speed and lateral speed are estimated for prediction model. The art. angle and its rate go through a median filter and then feed to the controller. The tire forces (longitudinal forces, lateral forces and normal forces) of the tractor are estimated for constructing the tire constraints by using the work from [104]. Since the trailer is usually a passive system with limited sensors, the trailer tire constraints are only bounded by brake capacity.

Table 6.2: Parameters of reconfigurable controller

Symbol	Description	Value
T_s	Controller sample time (s)	0.01
N_p	Steps of the prediction horizon	10
N_c	Steps of the control horizon	5
α^{sat}	Tire saturated side slip angle ($^\circ$)	7.5
q_1	Weight of lateral speed tracking error	32.4
q_2	Weight of yaw rate tracking error	900
q_3	Weight of art. angle tracking error	3600
r_1	Weight of tractor yaw moment	5e-07
r_2	Weight of trailer yaw moment	2e-06
$\Delta M_{z,min}^t / \Delta M_{z,max}^t$	Bounds of tractor yaw moment (Nm)	-5000/5000
$\Delta M_{z,min}^i / \Delta M_{z,max}^i$	Bounds of trailer yaw moment (Nm)	-1500/1500
W_e	Weight of CG forces mapping error	diag([50,50])
W_u	Weight of control efforts	0.02*diag([1,1,1,1,2,2])
Q_{brk}^t / Q_{brk}^i	Tractor/trailer brake limits (Nm)	-1500/-800

6.2 Cornering Stiffness Identification

The trailer dynamics parameters are obtained from 3D Solidworks model or direct measurement offline and it can be customized to change its dynamics characteristics, such as the mass and CG center. But the tire cornering stiffness is a challenge to acquire. An optimization-based estimation approach is proposed using nonlinear least squares algorithm. First, a cost function consisting of the sum of the squared measurement errors is defined:

$$J = \left\| Y_{exp.} - \hat{Y}_{sim.} \right\|_W^2 \quad (6.1)$$

where,

$$Y_{exp.} = \begin{bmatrix} v_y^t & r^t & r^i & \lambda \end{bmatrix}^T ; \hat{Y}_{sim.} = \begin{bmatrix} \hat{v}_y^t & \hat{r}^t & \hat{r}^i & \hat{\lambda} \end{bmatrix}^T$$

$Y_{exp.}$ is the given tractor-trailer experimental data of the conducted maneuver, see the configuration of Tractor-Trailer#1 in Table 6.1. It includes the tractor (Equinox) lateral speed and yaw rate, the trailer yaw rate and articulation angle under a specific steer and drive inputs. Then, it uses the same driver inputs (steer, drive/brake) for the high-fidelity tractor-trailer model in CarSim to achieve the similar dynamics responses, which is $\hat{Y}_{sim.}$. W is the weighting matrix tuning the cost of each state error.

The cornering stiffness identification problem is formulated as

$$\begin{aligned}
 \min_{C_{\alpha}^i} \quad & J \\
 & Y_{exp.} = \text{Experimental Data} \\
 \text{s.t.} \quad & \hat{Y}_{sim.} = f(\text{CarSim}, C_{\alpha}^i, \text{Driver Inputs}) \\
 & lb \leq C_{\alpha}^i \leq ub
 \end{aligned} \tag{6.2}$$

To obtain the simulation data $\hat{Y}_{sim.}$, an estimation work is built CarSim and Matlab/Simulink, shown in Figure 6.2. The tractor-trailer is modified in CarSim but leaving the driver commands and trailer lateral tire forces as inputs. The trailer tire uses the brush model formulated in (3.19) to generate lateral tire forces. A Levenberg-Marquardt algorithm is applied for iteration till the cost function (6.1) is minimized, which means the optimal cornering stiffness is identified (1.39e05N/rad). In Figure 6.3, the CarSim results using the identified corner stiffness of the trailer are compared to the experimental results. It is shown a very good match in SUV-lateral speed and yaw rate and fair match in trailer yaw rate and articulation angle. Therefore, the identified cornering stiffness is used in the model-based controller as for experiments study.

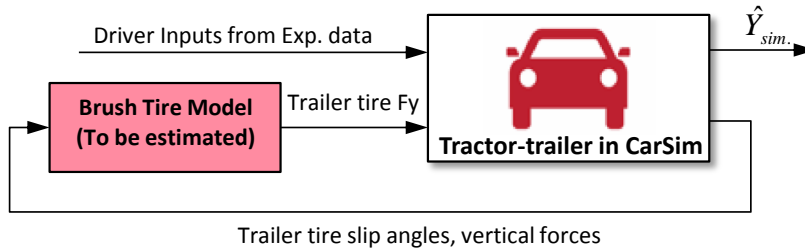


Figure 6.2: The estimation scheme for computing $\hat{Y}_{sim.}$.

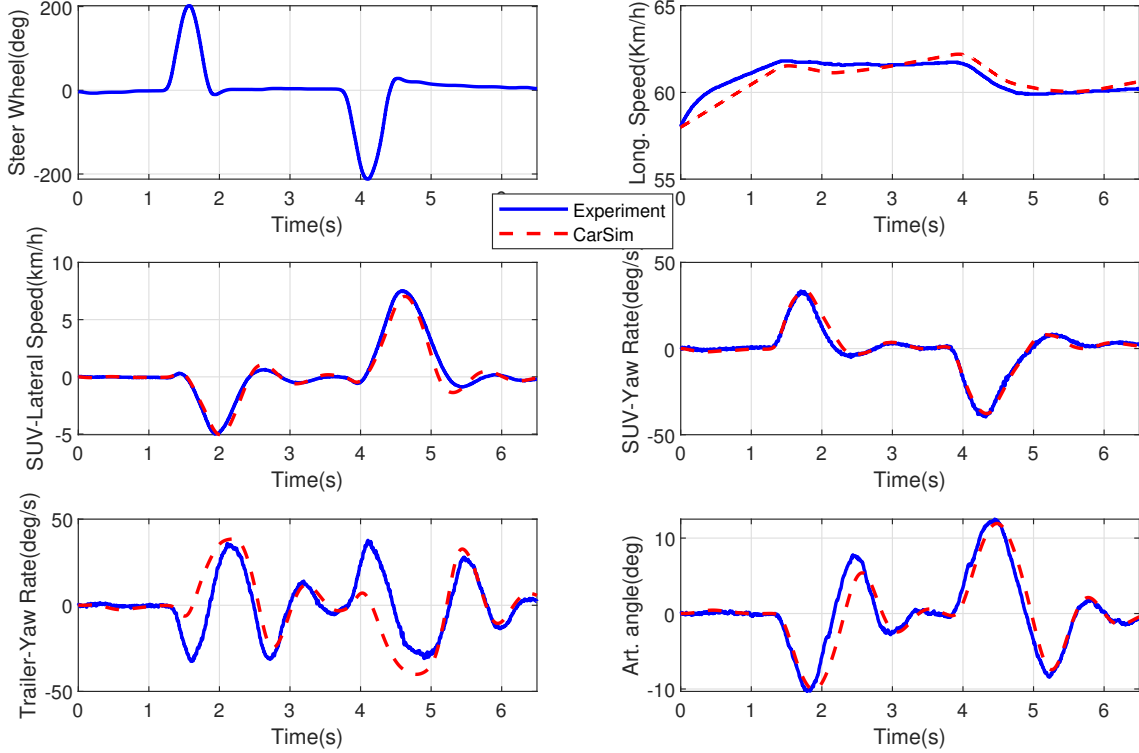
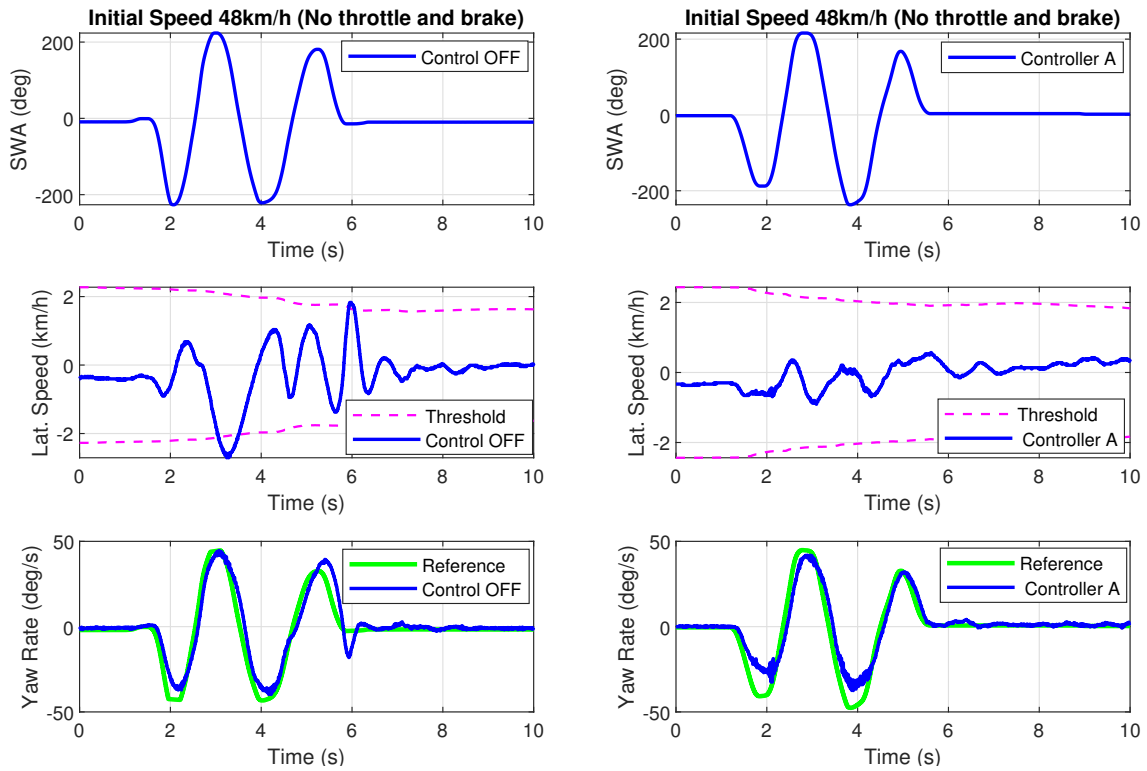


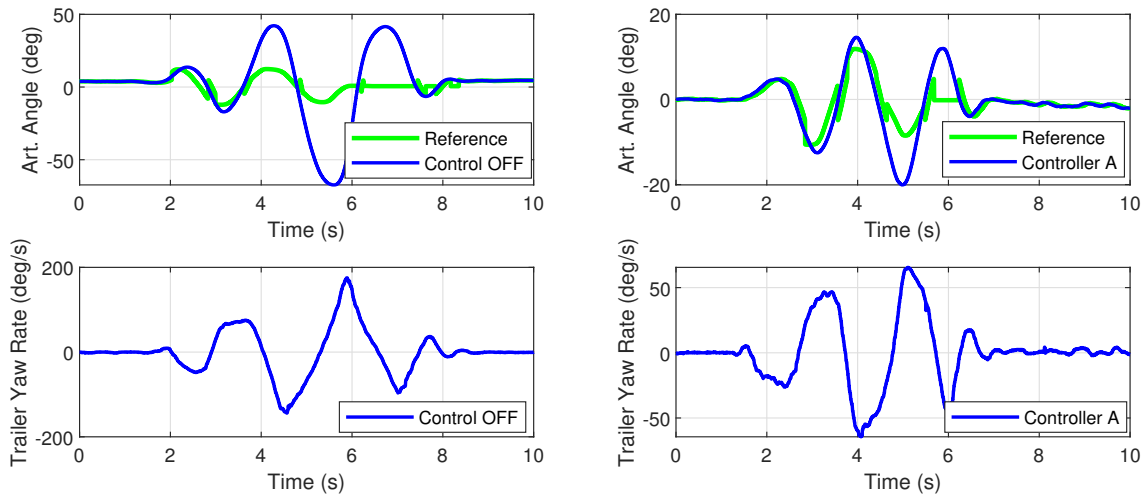
Figure 6.3: Fitting results using optimized C_{α}^i

6.3 Experimental Results

The control objective is to maintain a good lateral and yaw stability for the tractor unit and prevent the trailer from sway. The unstable configuration of Trailer #2 is used in tests as it is more likely to trigger a trailer sway at low speeds. In all tests, a continuous sine steer and double lane change, as two major maneuvers, are conducted on a half-wet pavement, which means the tire-road friction coefficient ' μ ' is around 0.7. Thus, the controller is expected to be robust to road friction variation. For each case with active controller engaged, a highly-similar but open-loop (Control OFF) maneuver is performed for comparison purpose.



(a) Tractor comparative results



(b) Trailer comparative results

Figure 6.4: Tractor-trailer responses for Control OFF and Controller A in sine steer

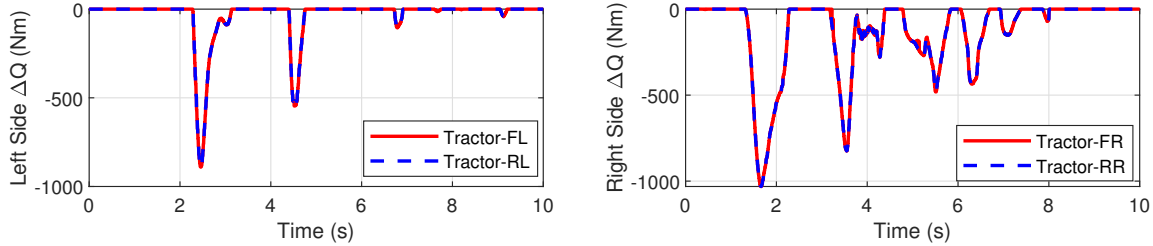
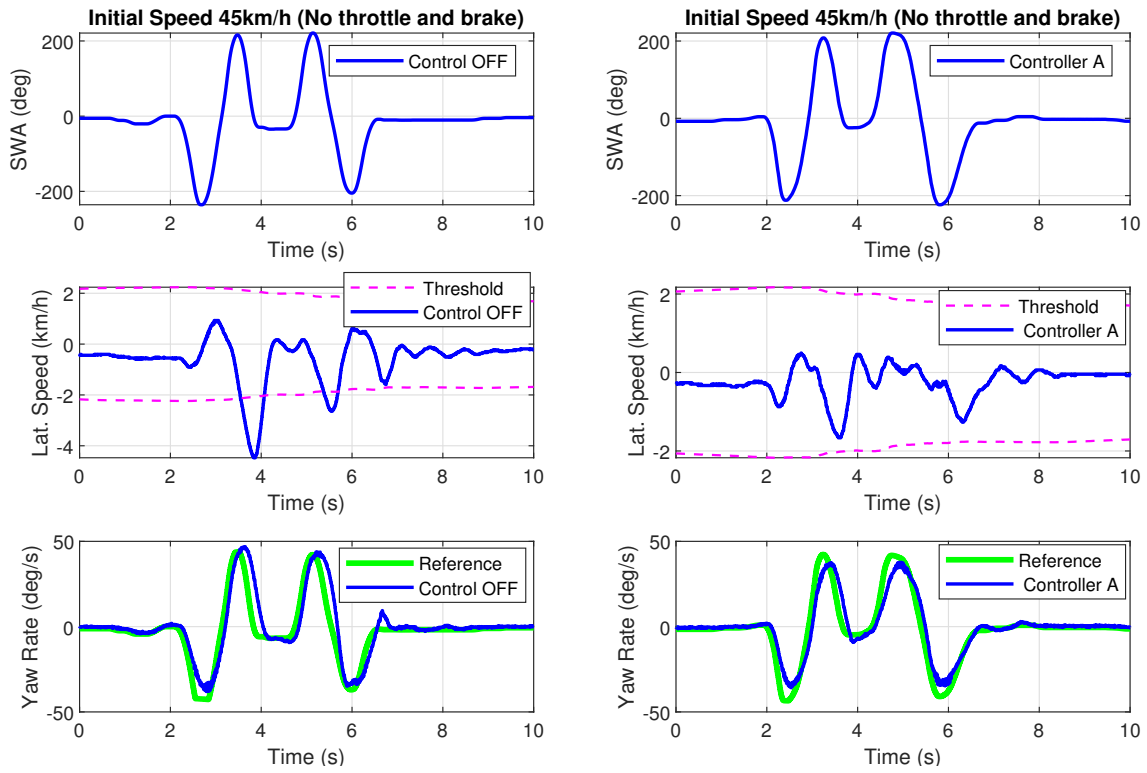


Figure 6.5: Corrective torques by Controller A in sine steer

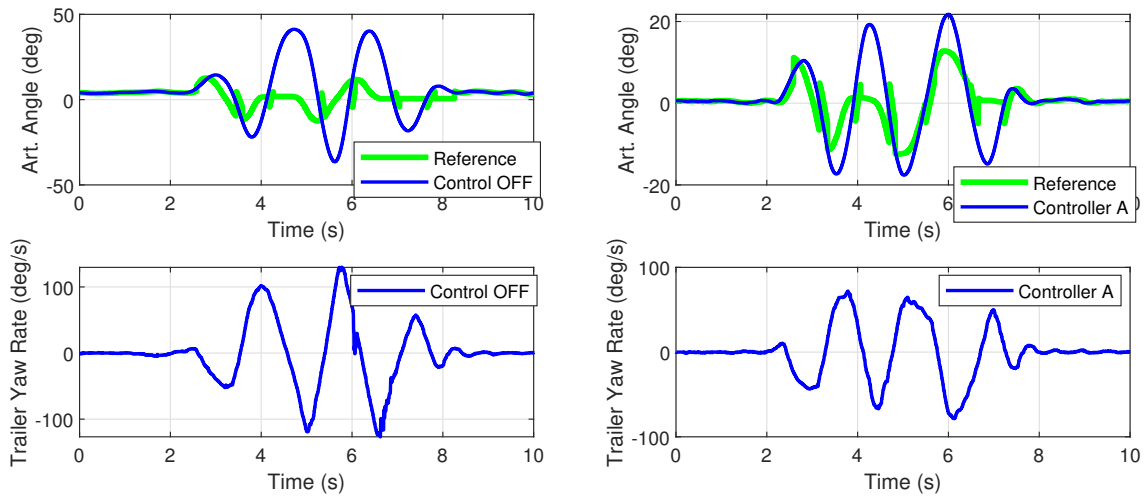
6.3.1 Tractor Differential Braking

The tests with tractor differential braking system are firstly implemented. To realize this strategy and only calculate the corrective torque from ΔQ_1 to ΔQ_4 , one could modify the gains and bounds of the MPC and CA listed in Table 6.2. Both sine steer and DLC maneuvers are performed and compared in the cases of with and without the controller. The vehicle test is filmed by a drone, and one could find the visualized and intuitive comparison from the footage in Appendix B.

Figure 6.4 and Figure 6.5 give the results of sine steer maneuver. In Figure 6.4, it is easy to find all subfigures at left column denote the ‘Control OFF’ maneuver while these at right column denote the ‘Controller A’ engaged. At the very top of the figure, it is shown the driver performed sine steering and dropped the throttle and brake at the same speed of 48km/h. The steering angles applied for both maneuvers are almost the same in spite of small discrepancies. Figure 6.4a compares the lateral speed and yaw rate of the tractor while Figure 6.4b compares the articulation angle and yaw rate of the trailer. In the Control OFF case, the lateral speed is generally much larger than this in Controller A and even exceeds the permissible boundary at 3rd and 6th second. The lateral speed with Controller A remains very small and far less than the boundary limit. The yaw rate behaved stable and similar in both cases and it suggested that the tractor is more understeer than the reference derived from an understeer characteristic. This is mainly due to load transfer effect of the unstable trailer. Looking at the trailer results in Figure 6.4b, while no control engaged, the art. angle deviated from the reference very much after 3.5th second and reached to almost 40° then reached to the peak value of -65° at 5.5th



(a) Tractor comparative results



(b) Trailer comparative results

Figure 6.6: Tractor-trailer responses for Control OFF and Controller A in DLC

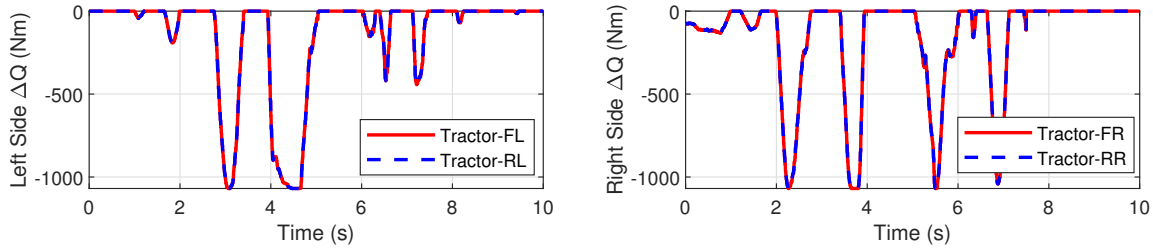
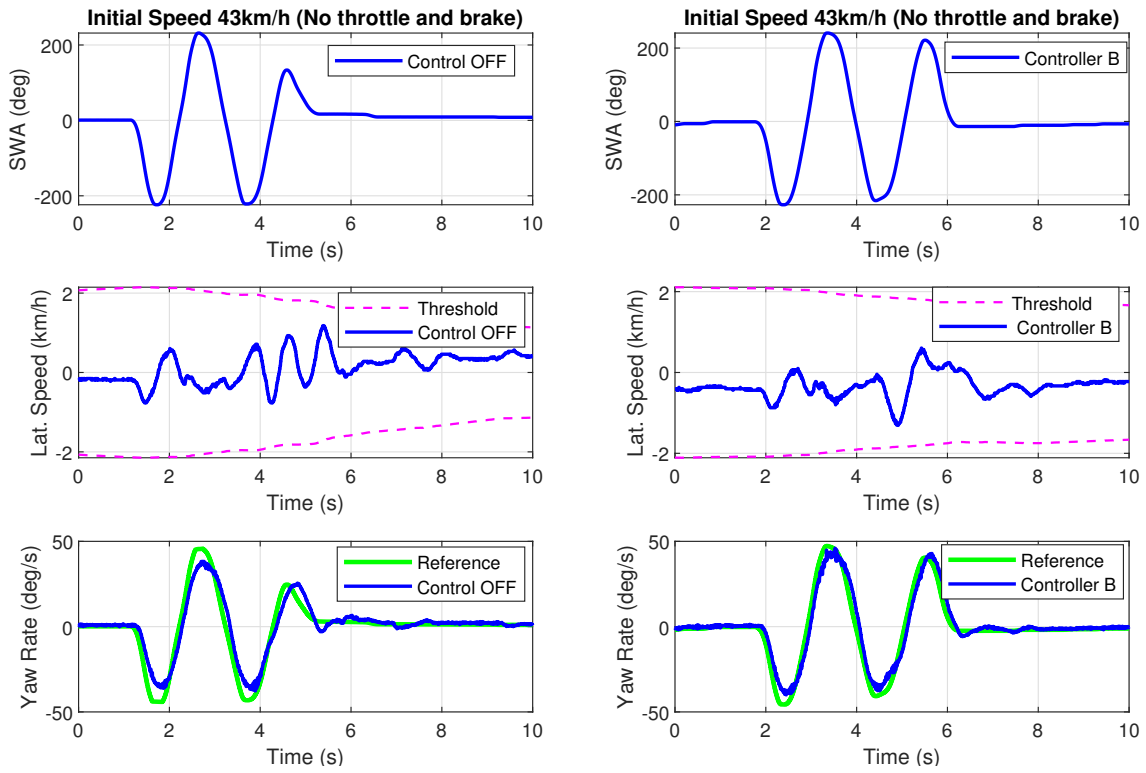


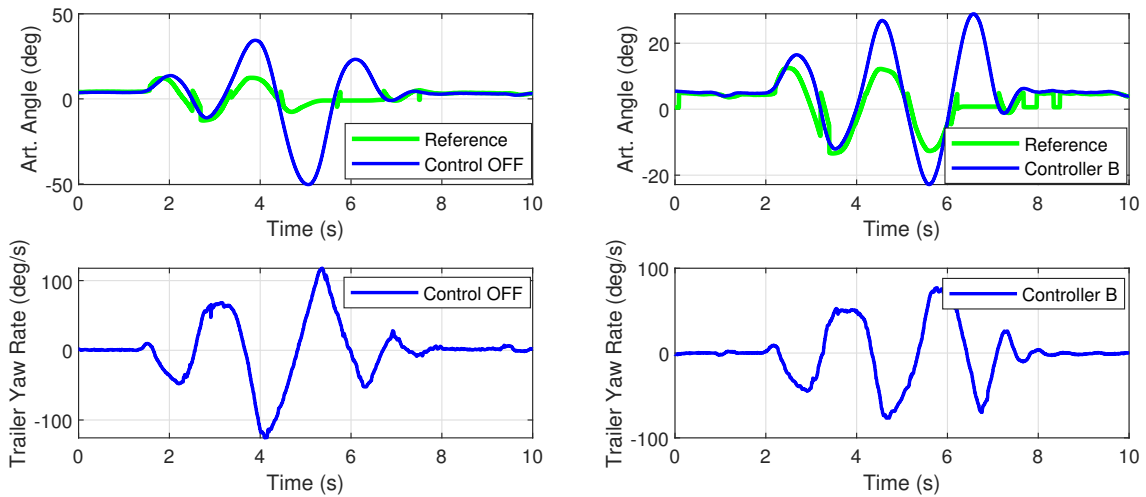
Figure 6.7: Corrective torques by Controller A in DLC

second. The whole trailer sway lasted from 2nd to 8th second. Trailer yaw rate shows similar evidence that the range went -150 to 190 deg/s. Clearly, this is a very unstable and dangerous situation. On the contrary, in the Controller A case, it is shown that art. angle is significantly reduced to less than 20° and lasted till the 6.5th second. The trailer yaw is also within a reasonable range that is similar to the tractor yaw rate. The corrective (braking) torques of the tractor are shown in Figure 6.5. It can be seen that the torques are smooth and the transition from side to side are consistent. Besides, the torques requested are within the actuator and tire capacity thanks to the real-time constraints.

Figure 6.6 and Figure 6.7 present the results of DLC maneuver. For safety concern, the initial speed is set at 45 km/h and the driver applied the similar steering angles of DLC, shown in the top position of the figure. Figure 6.4a compares the lateral speed and yaw rate of the tractor while Figure 6.4b compares the articulation angle and yaw rate of the trailer. In Control OFF case, the lateral speed exceeded the bounds and reached to -4 km/h at 4th second, which is equivalent to -6° of CG sideslip angle. The tires may experience saturation and the yaw motion is stable with a slight oversteer at some time points. These two responses with controller engaged behaved better and kept in stable margin. Again, the significant improvement is seen in trailer responses thanks to the requested differential torques shown in Figure 6.7. Trailer art. angle is reduced from 40° to 20° and its yaw rate is around 40% decreased, and thus the sway is stabilized successfully.



(a) Tractor comparative results



(b) Trailer comparative results

Figure 6.8: Tractor-trailer responses for Control OFF and Controller B in sine steer

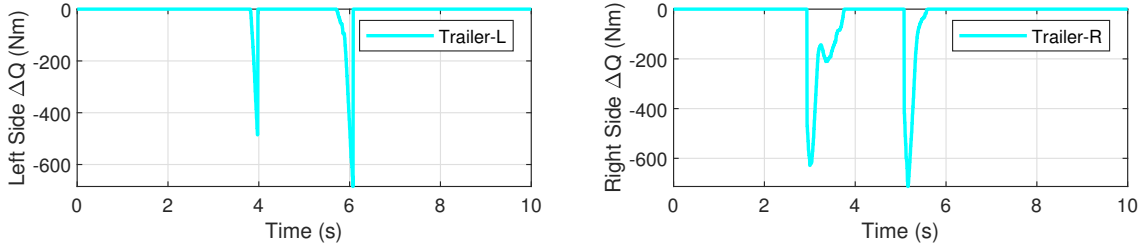


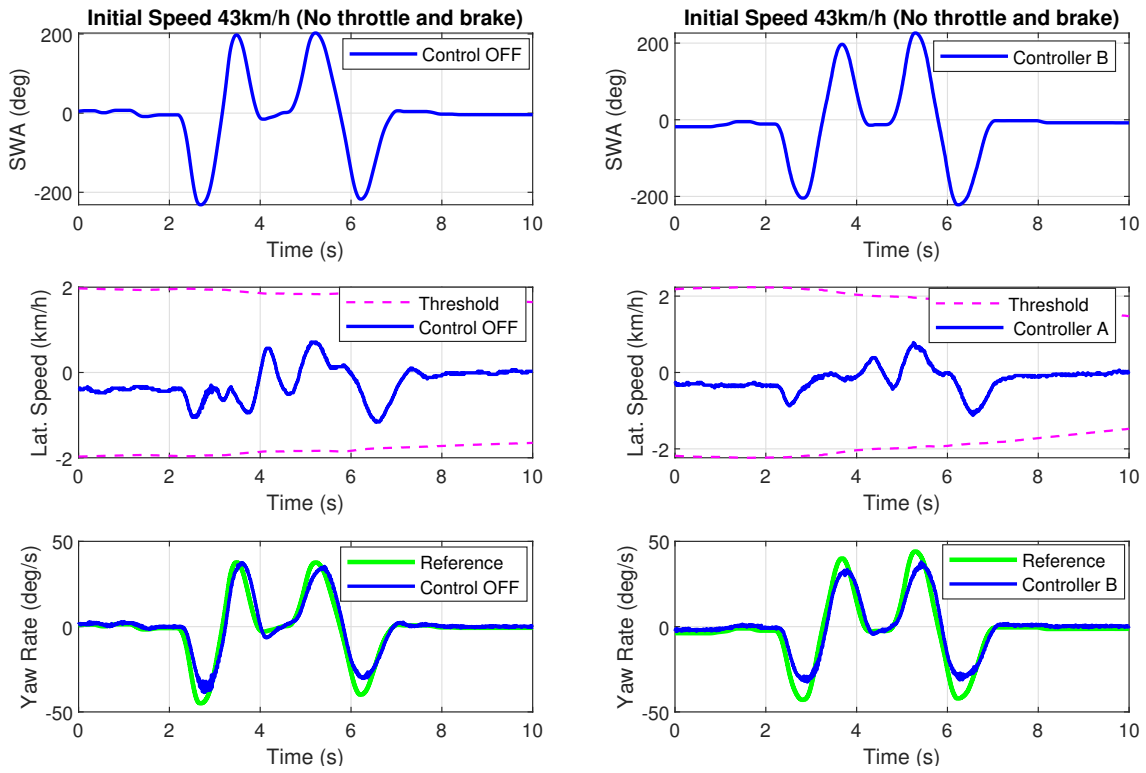
Figure 6.9: Corrective torques by Controller B in sine steer

6.3.2 Trailer Differential Braking

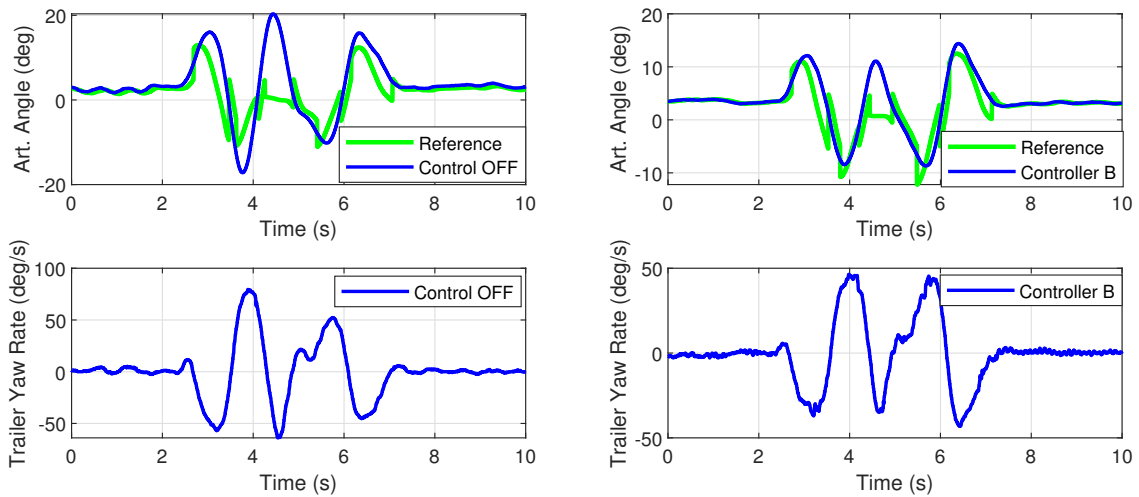
Thanks to the reconfigurability of the proposed controller, one could easily move from the tractor differential braking to trailer differential braking without reformulating the problem again. To realize this strategy (Controller B) and only calculate the corrective torque of ΔQ_5 and ΔQ_6 , one could modify the gains and bounds of the MPC and CA listed in Table 6.2. Both sine steer and DLC maneuvers are performed and compared in the cases of with and without the controller. Besides, the maneuvers can also be used to compare to those with Controller A.

Figure 6.8 and Figure 6.9 give the results of sine steer maneuver. In Figure 6.8, all subfigures at left column denote the ‘Control OFF’ maneuver while these at right column denote the ‘Controller B’. The sine steering angles and initial speed of 43km/h are shown at the top of the figure. A slower initial speed is used to prevent the trailer from total instability considering the limited capacity of trailer braking. As a result, lateral speed and yaw rate of the tractor in Figure 6.8 are stable and well tracked. Figure 6.8b compares the articulation angle and the yaw rate of the trailer. The art. angle went unstable and diverge from 0° to -50° when no control engaged. However, with the active differential braking of Controller B, the art. angle is controlled within 20° and trailer yaw rate is reduced around %20. The trailer corrective (braking) torques are shown in Figure 6.9. It can be seen that the torque actions are less than 700Nm and activated in short time slots, but the control is effective in sway prevention.

Figure 6.10 and Figure 6.11 present the results of DLC maneuver. The initial speed is set at 43 km/h and the driver applied the similar steering angles of DLC, shown in the



(a) Tractor comparative results



(b) Trailer comparative results

Figure 6.10: Tractor-trailer responses for Control OFF and Controller B in DLC

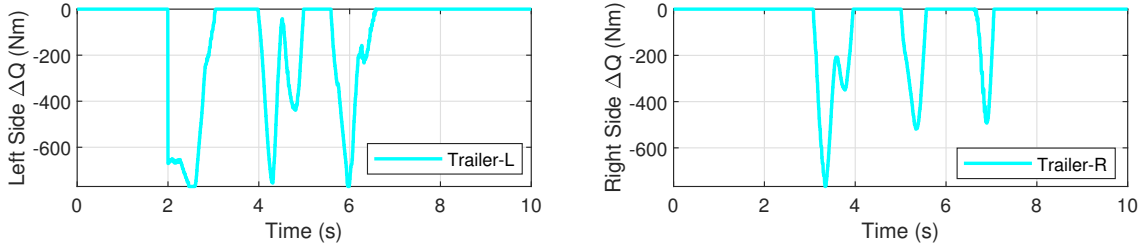


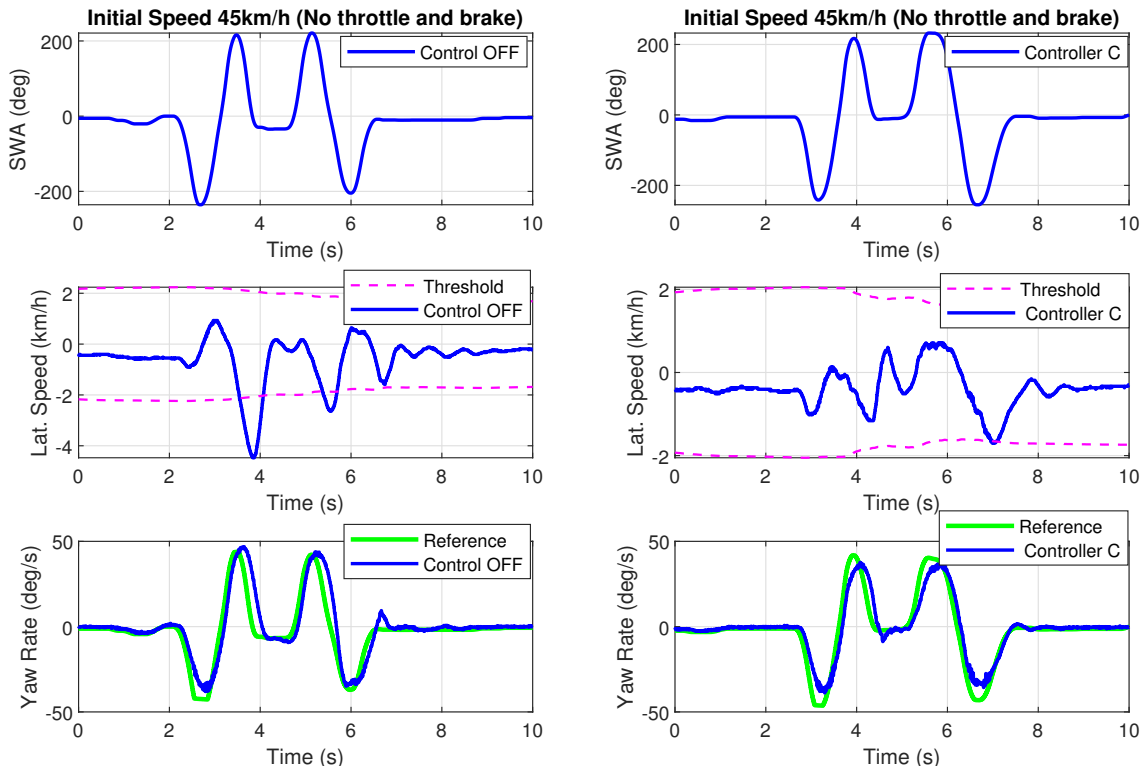
Figure 6.11: Corrective torques by Controller B in DLC

top position of the figure. In Control OFF case, both tractor and trailer show stable and non-critical dynamics responses, but the art. angle fails to follow the reference and trailer yaw rate is too large. With the engagement of Controller B, the art. angle is controlled within 10° and follows the reference generally very well. The trailer rate is reduced by around 30%. One may note the there is a constant deviation suggested in art. angle when no steering is applied (driving straight). This is from the sensor error due to the bended linkage in Figure 6.1. However, the art. angle reference is set only when art. angle exceeds a certain threshold, which avoids undesired control. Thus, in Figure 6.11, there are no unnecessary torque adjustments at the first and last 2 seconds.

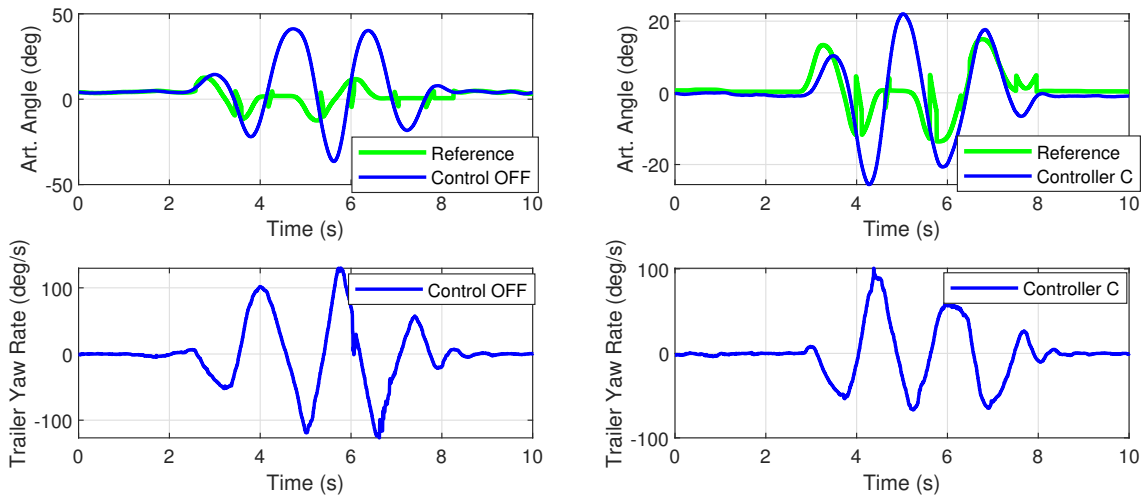
Compared to Controller A of the same/similar maneuvers, it indicates that Controller A generally outperforms Controller B in reducing art. angle and handling the more critical situation. This is because Controller A has a much larger brake capacity than B. And it uses the regenerative brake of the electric motor instead of the hydraulic brake system, which gives instant and very accurate torque feeding. In contrast, the trailer brake system can only provide limited torque. In addition, a linear mapping relationship is used to translate the requested torque to percentage value when it is actually nonlinear and has an actuator delay.

6.3.3 Integrated Differential Braking

In this integrated differential braking strategy, six corrective torques of ΔQ_1 to ΔQ_6 are applied and the gains and bounds of the MPC and CA are listed in Table 6.2. Only the DLC maneuver is tested in the cases of with and without the controller for comparison.



(a) Tractor comparative results



(b) Trailer comparative results

Figure 6.12: Tractor-trailer responses for Control OFF and Controller C in DLC

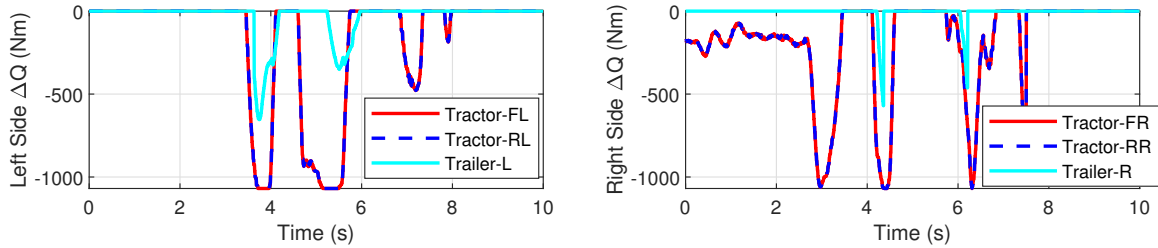


Figure 6.13: Corrective torques by Controller C in DLC

Figure 6.12 and Figure 6.13 present the results of DLC maneuver. The Control OFF result is exactly the same to these in Figure 6.6 as the same maneuvers are used for demonstration and it is discussed in the previous subsection. This helps to compare the effectiveness of Controller A and C in the same 'OFF' maneuver. First, the Controller C stabilized the tractor lateral within the bounds and prevent the trailer from sway with around 20° , which is similar to the performance seen in Controller A of Figure 6.6. However, looking at the details, the lateral speed, art. angle and trailer yaw rate achieved by Controller A slightly outperformed those achieved by Controller C. Although this is just one single case, which cannot draw a conclusion, it may be explained by torques corrections in Figure 6.13. From 3.5th to 4.5th second, the vehicle is turning right and the art. angle is negatively increasing. To pull the trailer back from sway and large angle, brake torques at the left side of the tractor are expected, which is actually shown in Figure 6.13. Meanwhile, brake torque at the right side of the trailer should be applied but it applied the left side torque. This causes a problem of canceling out one another's efforts and the performance is thus degraded. In addition, unwanted brakes are generated in the tractor from 0 to 2.4th second as shown in right side of Figure 6.13, this may be due to the deviation of the vehicle states, such the lateral speed as shown in the Controller C of Figure 6.12 (a).

6.4 Summary and Discussion

In this chapter, an experimental study was presented to validate the reconfigurability and performance of the proposed controller. Test facilities and platform, such as the

vehicle, sensors, and hardware were introduced. Given that both tractor and trailer are equipped with differential braking systems, three potential braking strategies were used and validated. To develop the respective controller for each strategy, the benefits of the reconfigurable control framework were taken that one can quickly formulate the control problem by setting the ‘Boolean Matrices’ and gains properly. To reserve a good dynamics model of the tractor-trailer, the cornering stiffness of the trailer was identified through an optimization formulation and using test data. The identified cornering stiffness used in CarSim simulation showed a good accuracy compared to real-time test results.

Experimentally, three control strategies were compared with sine steer and DLC maneuvers. As presented, the controllers were all working properly and smoothly. The controllers provided best braking torques in critical situations to maintain lateral/yaw stability of the tractor and prevented the sway of the trailer. And even the trailer braking system with limited capacity can control the trailer from sway effectively. In particular, it is observed that the performance of the tractor differential braking was very promising and outperformed the other two. It gave us more confidence to use the tractor actuation system to control both units since most trailers are passive systems.

Chapter 7

Conclusions and Future Work

This thesis presented a reconfigurable and universal modeling and control framework to address challenges of configuration diversity, multiple dynamics control objectives, and actuation redundancy of multi-axle vehicles. In contrast to most of the existing stability control systems, this framework provides freedom and flexibility, and reconfigurability on dynamics control that significant modifications and major retuning can be avoided when applying to different vehicles.

7.1 Conclusions

First, a reconfigurable modeling methodology was developed. To this aim, it started from a multi-axle vehicle without articulations using a three-layer modeling process. It defined '*Actuator Boolean Matrix*' to determine the configuration of the active actuation and '*Axle Boolean Matrix*', the configuration of axles. As a result, a reconfigurable model was formulated, in where longitudinal, lateral, yaw, and roll motions were included along with a nonlinear brush model and load transfers were considered and evaluated. Moreover, the dynamics of articulated vehicles with any units was modeled and unified in an intuitive manner. The '*Articulation Boolean Matrix*' was defined to judge the availability of the articulation. When any axle, articulations, and/or active actuator was added or removed,

it can easily and quickly formulate the corresponding dynamics model. Model evaluation was conducted with different vehicles and the model was proved to be accurate and reliable compared with these in CarSim/TruckSim platform.

Second, based on the model proposed, a reconfigurable and hierarchical control framework was developed using optimization-based techniques. In the hierarchical (two-layer) control system, the high-level MPC controller represents universality to calculate corrective CG force while the lower-level CA controller, reconfigurability, is responsible for distributing the control actions to active actuators, such as steering or torque (brake) at wheels. Particularly, vehicles with multi units were unified into a general prediction model as to achieve a general MPC formulation for any vehicles with any configurations. The feasibility and stability of the LTV-MPC were discussed and proved. The main benefit of the proposed framework is that there is no need to reformulate the control problem when a new vehicle with new configurations is given.

Third, different stability objectives and dynamics behavior were studied to provide reliable references for MPC tracking. In particular, effects on tractor due to the existence of trailer and trailer articulation stability were analyzed. Furthermore, a comprehensive study in MPC tuning was presented using a specific vehicle example so that sampling time, prediction horizon, control horizon and weights were tuned and selected. In the lower-level control allocation, the optimization was constrained by actuator limits, tire capacity, wheel slips, and actuators failure case in real time.

Fourth, the control system was evaluated through diverse applications and simulations under adverse driving conditions. It highlighted the reconfigurability that each control formulation was accomplished by setting the ‘Boolean Matrices’, demonstrated that the proposed system is universal and reconfigurable for very different vehicles and configurations. More specifically, the simulation study covered different vehicles, control objectives, and active actuation, robustness and actuator failures. It is shown that a single universal controller is effective to handle all these cases.

Finally, the proposed control system was validated with an experimental study. It was implemented in dSPACE Autobox and tested on an articulated vehicle (tractor-trailer) in real-time with multiple differential braking configurations. Examined with uncontrolled

maneuvers for both sine steer case and double lane change case, it showed that the controller has a very promising performance in yaw control and trailer sway prevention. Furthermore, the promising reconfigurability of the controller was also proved when moving from this configuration to another one.

7.2 Future Work

Vertical Dynamics Inclusion

This thesis considered longitudinal and lateral tire forces when deriving vehicle dynamics. However, it could also include normal force and active normal force of tires in future work, for instance, vertical control from active/semi-active suspension. Thus, looking back to tires forces equation of (3.1), the tire normal force may be added:

$$F_{zi} = (f_{zi} + t_{zi}\Delta f_{zi})$$

where f_{zi} is the tire normal force and Δf_{zi} is the augmenting normal force applied by the active controller, e.g. active suspension. Similarly, The symbol t_{zi} is defined as ‘Actuator Boolean Parameter’ to determine the availability of active vertical actuators. This inclusion creates an additional CG vertical force, CG roll moment and pitch moment, which provides a great opportunity and freedom on ride and comfort, and roll/rollover control.

Advanced Prediction Model

A nonlinear brush tire model is used in this work to represent the tire lateral force. The derating effect from tire longitudinal force is neglected, which means the lateral force is only calculated from tire slip angles. However, longitudinal force, especially in large slip ratios, has a significant impact on tire lateral forces. Regarding the body dynamics equations, it is accurate enough for a single unit vehicle, but for an articulated vehicle the articulation angle is assumed small and kinematic and forces constraints are simplified. This may bring a limitation to the MPC prediction model when angles are large, such as a jackknifing situation. Therefore, considering a reliable combined-slip tire model and nonlinearities of body dynamics is a worthy future direction. The model can be linearized at each step

for computational sake. In return, the MPC will have a more solid prediction ability and control performance, particularly in combined slip situations and large articulation angle.

Control Objectives/Actuators Prioritizing

The MPC formulation (high-level) and CA formulation (lower-level) in this thesis provide freedom and flexibility to investigate objectives and actuators prioritization further. For instance, when rollover and yaw instability coincides, rollover prevention demands a higher priority. The controller is expected to be ‘aware’ of the difference and engage active controls with prioritization. In addition, if two or more actuation types exist, how should the best configuration of actuators for a specific situation be selected? For example, to maintain good path tracking in good road conditions, the active steering correction is prioritized for better driving comfort and a smaller speed drop. In an emergency obstacle avoidance, e.g. sudden lane change, it should make the best of differential braking.

Experiment Improvements

The controller implementation may be further improved. For instance, unwanted braking corrections at low speeds and driving in a straight line. In practice, the robust estimation and filters of longitudinal and lateral speed are needed in order to provide reliable states. In addition, the actuator dynamics and delay are very prominent factors that need to be taken into account when designing the stability control controller. In the future, if stabilizer facilities are equipped, the performance on slippery road conditions and robustness of the controller, such as with respect to trailer load distribution, are expected to be validated.

References

- [1] P. Fancher and C. Winkler. Directional performance issues in evaluation and design of articulated heavy vehicles. *Vehicle System Dynamics*, 45(7-8):607–647, 2007.
- [2] D. Williams. Multi-axle vehicle dynamics. *SAE Technical Paper*, No. SP-2337, 2012.
- [3] Statistics Canada. Transportation, 2017. <https://www150.statcan.gc.ca/n1/pub/11-402-x/2012000/pdf/transport-eng.pdf>, (Accessed: 2019-05-20).
- [4] Transport Canada. Transportation in canada 2016. https://www.tc.gc.ca/media/documents/policy/comprehensive_report_2016.pdf, (Accessed: 2019-05-20).
- [5] American Public Transportation Association. Public transportation benefits, 2018. <https://www.apta.com/news-publications/public-transportation-benefits/>, (Accessed: 2019-05-20).
- [6] U-M Transportation Research Institute. Dynamics of heavy duty trucks. <http://isd.engin.umich.edu/nexus/professional-programs/dynamics-of-heavy-trucks/index.htm>, (Accessed: 2019-05-20).
- [7] NHTSA. 2017 fatal motor vehicle crashes: Overview. <https://crashstats.nhtsa.dot.gov/Api/Public/ViewPublication/812603>, (Accessed: 2019-05-20).
- [8] U.S. Department of Transportation. Large trucks and buses crash facts 2016. <https://www.fmcsa.dot.gov/sites/fmcsa.dot.gov/files/docs/safety/data-and-statistics/398686/ltbcf-2016-final-508c-may-2018.pdf>, (Accessed: 2019-05-20).

- [9] The Federal Highway Administration (FHWA). Traffic recorder instruction manual, classifying vehicles. http://onlinemanuals.txdot.gov/txdotmanuals/tri/classifying_vehicles.htm, (Accessed: 2019-05-20).
- [10] Erik Eckermann. *World History of the Automobile*. Society of Automotive Engineers, 2001.
- [11] Amir Khajepour, M Saber Fallah, and Avest aGoodarzi. *Electric and hybrid vehicles: technologies, modeling and control-A mechatronic approach*. John Wiley & Sons, 2014.
- [12] David Crolla and Behrooz Mashadi. *Vehicle powertrain systems*. John Wiley & Sons, 2011.
- [13] Annika Stensson Trigell, Malte Rothmel, Joop Pauwelussen, and Karel Kural. Advanced vehicle dynamics of heavy trucks with the perspective of road safety. *Vehicle System Dynamics*, 55(10):1572–1617., 2017.
- [14] Gianpiero Mastinu and Manfred Ploechl. *Road and off-road vehicle system dynamics handbook*. CRC Press, 2014.
- [15] Tankut Acarman and Ümit Özgüner. Rollover prevention for heavy trucks using frequency shaped sliding mode control. *Vehicle System Dynamics*, 44(10):737–762, 2006.
- [16] NL Azad, A Khajepour, and J McPhee. A survey of stability enhancement strategies for articulated steer vehicles. *International Journal of Heavy Vehicle Systems*, 16(1-2):26–48, 2009.
- [17] AG Nalecz and J Genin. Dynamic stability of heavy articulated vehicles. *International Journal of Vehicle Design*, 5(4):417–426, 1984.
- [18] F Vlk. Handling performance of truck–trailer vehicles: A state–of–the–art survey. *International Journal of Vehicle Design*, 6(3):323–361, 1985.

- [19] M.F.J. Luijten. Lateral dynamic behaviour of articulated commercial vehicles. *Masters' Thesis, Eindhoven University of Technology*, 2010.
- [20] M. F.J. van de Molengraft-Luijten, I. J.M. Besselink, R. M.A.F. Verschuren, and H. Nijmeijerk. Analysis of the lateral dynamic behaviour of articulated commercial vehicles. *Vehicle System Dynamics*, 50(1):169–189, 2012.
- [21] Eungkil Lee, Saurabh Kapoor, Tushita Sikder, and Yuping He. An optimal robust controller for active trailer differential braking systems of car-trailer combinations. *International Journal of Vehicle Systems Modelling and Testing*, 12(1-2):72–93, 2017.
- [22] American Association of Motor Vehicle Administrators (AAMVA). *Florida commercial driver license (CDL) handbook 2015-2016*. Florida DHSMV Information, 2016.
- [23] N. T. Koussoulas S. A. Manesis and G. N. Davrazos. Off-tracking elimination in multi-articulated vehicles. *Mobile Robots: New Research, John X. Liu (Editor)*, pages 319–344, 2005.
- [24] A. James McKnight George T. Bahouth. Analysis of large truck rollover crashes. *Traffic injury prevention*, 10(5):421–426, 2009.
- [25] R.D. Ervin C.B. Winkler, D. Blower and R.M. Chalasani. Rollover of heavy commercial vehicles. *SAE Research Report*, 2000.
- [26] Zhilin Jin, Lei Zhang, Jiale Zhang, and Amir Khajepour. Stability and optimised h-infinity control of tripped and untripped vehicle rollover. *Vehicle System Dynamics*, 54(10):1405–1427, 2016.
- [27] Jeffrey P Chrstos and Dennis A Guenther. The measurement of static rollover metrics. *SAE Technical Paper*, 1992.
- [28] J Preston-Thomas and John H.F. Woodrooffe. Feasibility study of a rollover warning device for heavy trucks. 1990.
- [29] Hai Yu, Levent Güvenc, and Ü Özgüner. Heavy duty vehicle rollover detection and active roll control. *Vehicle system dynamics*, 46(6):451–470, 2008.

- [30] Dongyoon Hyun and Reza Langari. Modeling to predict rollover threat of tractor-semitrailers. *Vehicle System Dynamics*, 39(6):401–414, 2003.
- [31] Caizhen Cheng and David Cebon. Improving roll stability of articulated heavy vehicles using active semi-trailer steering. *Vehicle System Dynamics*, 46(S1):373–388, 2008.
- [32] Hongliang Zhou and Zhiyuan Liu. Vehicle yaw stability-control system design based on sliding mode and backstepping control approach. *IEEE Transactions on Vehicular Technology*, 59(7):3674–3678, 2010.
- [33] B.L. Boada, M.J.L. Boada, and V Diaz. Fuzzy-logic applied to yaw moment control for vehicle stability. *Vehicle System Dynamics*, 43(10):753–770, 2005.
- [34] Vito Cerone, Mario Milanese, and Diego Regruto. Yaw stability control design through a mixed-sensitivity approach. *IEEE Transactions on Control Systems Technology*, 17(5):1096–1104, 2009.
- [35] M. K. Aripin, Yahaya Md Sam, Kumeresan A. Danapalasingam, Kemao Peng, N. Hamzah, and M. F. Ismail. A review of active yaw control system for vehicle handling and stability enhancement. *International journal of vehicular technology*, 2014, 2014.
- [36] Shenjin Zhu, Yuping He, and Jing Ren. On robust controllers for active steering systems of articulated heavy vehicles. *International Journal of Heavy Vehicle Systems*, 26(1):1–30, 2019.
- [37] Paolo Falcone, Francesco Borrelli, Jahan Asgari, Hongtei Eric Tseng, and Davor Hrovat. Predictive active steering control for autonomous vehicle systems. *IEEE Transactions on control systems technology*, 15(3):566–580, 2007.
- [38] Rongrong Wang, Hui Zhang, and Junmin Wang. Linear parameter-varying controller design for four-wheel independently actuated electric ground vehicles with active steering systems. *IEEE Transactions on Control Systems Technology*, 22(4):1281–1296, 2013.

- [39] Yubiao Zhang, Amir Khajepour, and Xiaoping Xie. Rollover prevention for sport utility vehicles using a pulsed active rear-steering strategy. *Proceedings of the Institution of Mechanical Engineers, Part D: Journal of Automobile Engineering*, 230(9):1239–1253, 2016.
- [40] Johannes Tjonnas and Tor A Johansen. Stabilization of automotive vehicles using active steering and adaptive brake control allocation. *IEEE Transactions on Control Systems Technology*, 18(3):545–558, 2009.
- [41] Jun Wang and Shuiwen Shen. Integrated vehicle ride and roll control via active suspensions. *Vehicle System Dynamics*, 46(S1):495–508, 2008.
- [42] Michael K Binder and Amir Khajepour. Optimal control allocation for coordinated suspension control. In *2014 American Control Conference*, pages 2126–2131. IEEE, 2014.
- [43] David JM Sampson and David Cebon. Active roll control of single unit heavy road vehicles. *Vehicle System Dynamics*, 40(4):229–270, 2003.
- [44] Daofei Li, Shangqian Du, and Fan Yu. Integrated vehicle chassis control based on direct yaw moment, active steering and active stabilizer. *Vehicle System Dynamics*, 46(S1):341–351, 2008.
- [45] Hui Zhang and Junmin Wang. Vehicle lateral dynamics control through afs/dyc and robust gain-scheduling approach. *IEEE Transactions on Vehicular Technology*, 65(1):489–494, 2015.
- [46] Shao-Bo Lu, Yi-Nong Li, Seung-Bok Choi, Ling Zheng, and Min-Sang Seong. Integrated control on mr vehicle suspension system associated with braking and steering control. *Vehicle System Dynamics*, 49(1-2):361–380, 2011.
- [47] Q. Miao and D. Cebon. Path-following control based on ground-watching navigation. *IEEE Transactions on Intelligent Transportation Systems*, 19(8):2592–2602, 2018.

- [48] Hong Wang, Yanjun Huang, Amir Khajepour, Yadollah Rasekhipour, Yubiao Zhang, and Dongpu Cao. Crash mitigation in motion planning for autonomous vehicles. *IEEE Transactions on Intelligent Transportation Systems*, 2019.
- [49] Yanjun Huang, Haitao Ding, Yubiao Zhang, Hong Wang, Dongpu Cao, Nan Xu, and Chuan Hu. A motion planning and tracking framework for autonomous vehicles based on artificial potential field-elaborated resistance network (apfe-rn) approach. *IEEE Transactions on Industrial Electronics*, 2019.
- [50] Kang Yuan, Hong Shu, Yanjun Huang, Yubiao Zhang, Amir Khajepour, and Lin Zhang. Mixed local motion planning and tracking control framework for autonomous vehicles based on model predictive control. *IET Intelligent Transport Systems*, 2018.
- [51] Wanki Cho, Jaewoong Choi, Chongkap Kim, Seibum Choi, and Kyongsu Yi. Unified chassis control for the improvement of agility, maneuverability, and lateral stability. *IEEE Transactions on vehicular Technology*, 61(3):1008–1020, 2012.
- [52] A. Wong, D. Kasinathan, A. Khajepour, S. Chen, and B. Litkouhi. Integrated torque vectoring and power management framework for electric vehicles. *Control Engineering Practice*, 48:22–36, 2016.
- [53] Milad Jalali, Amir Khajepour, Shih ken Chen, and Bakhtiar Litkouhi. Integrated stability and traction control for electric vehicles using model predictive control. *Control Engineering Practice*, 54:256–266, 2016.
- [54] Junmin Wang and Raul G Longoria. Coordinated and reconfigurable vehicle dynamics control. *IEEE Transactions on Control Systems Technology*, 17(3):723–732, 2009.
- [55] S.-K. Chen, W. Deng, Y. A. Ghoneim, N. K. Moshohum, J. Ryu F. Nardi, and K. A. Odea. Architecture and methodology for holistic vehicle control. *US Patents*, (8417417B2), 2013.
- [56] A. Nahidi, A. Kasaiezadeh, S. Khosravani, A. Khajepour, S.-K. Chen, and B. Litkouhi. Modular integrated longitudinal and lateral vehicle stability control for electric vehicles. *Mechatronics*, 44(Supplement C):60–70, 2017.

- [57] Milad Jalali, Saeid Khosravani, Amir Khajepour, Shih ken Chen, and Bakhtiar Litkouhi. Model predictive control of vehicle stability using coordinated active steering and differential brakes. *Mechatronics*, 48:30–41, 2017.
- [58] Moad Kissai, Bruno Monsuez, and Adriana Tapus. Review of integrated vehicle dynamics control architectures. In *2017 European Conference on Mobile Robots (ECMR)*, pages 1–8. IEEE, 2017.
- [59] Mansour Ataei. *Reconfigurable integrated control for urban vehicles with different types of control actuation, Chapter 3*. PhD thesis, University of Waterloo, 2017.
- [60] Mansour Ataei, Amir Khajepour, and Soo Jeon. A novel reconfigurable integrated vehicle stability control with omni actuation systems. *IEEE Transactions on Vehicular Technology*, 67(4):2945–2957, 2017.
- [61] Riccardo Marino, Stefano Scalzi, and Fabio Cinili. Nonlinear pi front and rear steering control in four wheel steering vehicles. *Vehicle System Dynamics*, 45(12):1149–1168, 2007.
- [62] Benoit Lacroix, Zhao Heng Liu, and Patrice Seers. A comparison of two control methods for vehicle stability control by direct yaw moment. In *Applied Mechanics and Materials*, volume 120, pages 203–217. Trans Tech Publ, 2012.
- [63] RS Sharp and Huei Peng. Vehicle dynamics applications of optimal control theory. *Vehicle System Dynamics*, 49(7):1073–1111, 2011.
- [64] Shuibo Zheng, Houjun Tang, Zhengzhi Han, and Yong Zhang. Controller design for vehicle stability enhancement. *Control Engineering Practice*, 14(12):1413–1421, 2006.
- [65] Zhituo Ni and Yuping He. Design and validation of a robust active trailer steering system for multi-trailer articulated heavy vehicles. *Vehicle System Dynamics*, pages 1–27, 2018.

- [66] Massimo Canale, Lorenzo Fagiano, Antonella Ferrara, and Claudio Vecchio. Vehicle yaw control via second-order sliding-mode technique. *IEEE Transactions on Industrial Electronics*, 55(11):3908–3916, 2008.
- [67] Nasser Lashgarian Azad, Amir Khajepour, and John Mcphee. Robust state feedback stabilization of articulated steer vehicles. *Vehicle System Dynamics*, 45(3):249–275, 2007.
- [68] Nenggen Ding and Saied Taheri. An adaptive integrated algorithm for active front steering and direct yaw moment control based on direct lyapunov method. *Vehicle System Dynamics*, 48(10):1193–1213, 2010.
- [69] Stefano Di Cairano and Ilya V Kolmanovsky. Real-time optimization and model predictive control for aerospace and automotive applications. In *2018 Annual American Control Conference (ACC)*, pages 2392–2409. IEEE, 2018.
- [70] Francesco Borrelli, Alberto Bemporad, and Manfred Morari. *Predictive control for linear and hybrid systems*. Cambridge University Press, 2017.
- [71] Saa V. Rakovi and William S. Levine. *Handbook of Model Predictive Control*. Springer, 2019.
- [72] Craig Earl Beal. *Applications of model predictive control to vehicle dynamics for active safety and stability*. PhD Thesis, Stanford University, 2011.
- [73] Tor A Johansen and Thor I Fossen. Control allocation: a survey. *Automatica*, 49(5):1087–1103, 2013.
- [74] Dhanaraja Kasinathan, Alireza Kasaiezadeh, Andy Wong, Amir Khajepour, Shih-Ken Chen, and Bakhtiar Litkouhi. An optimal torque vectoring control for vehicle applications via real-time constraints. *IEEE Transactions on Vehicular Technology*, 65(6):4368–4378, 2015.
- [75] Yubiao Zhang, Amir Khajepour, and Yanjun Huang. Multi-axle/articulated bus dynamics modeling: a reconfigurable approach. *Vehicle System Dynamics*, 56(9):1315–1343, 2018.

- [76] S. S. Institute. SS-ISO 8855:2011. *Road vehicles - Vehicle dynamics and road-holding ability - Vocabulary*. 2012.
- [77] Reza N Jazar. *Vehicle dynamics: theory and application*. Springer, 2017.
- [78] Hans B. Pacejka. *Tire and vehicle dynamics*. Elsevier, 2005.
- [79] Howard Dugoff, P.S. Fancher, and Leonard Segel. An analysis of tire traction properties and their influence on vehicle dynamic performance. *SAE transactions*, pages 1219–1243, 1970.
- [80] E. Fiala. Lateral forces on rolling pneumatic tires. *Zeitschrift V.D.I.*, 96(29):973–979, 1954.
- [81] Hans B. Pacejka and Egbert Bakker. The magic formula tyre model. *Vehicle system dynamics*, 21(S1):1–18, 1992.
- [82] Tielking JT. A finite element tire model. *Tire Science and Technology*, 11(1):50–63, 1983.
- [83] Peter Helnwein, Chang Hong Liu, Günther Meschke, and Herbert A Mang. A new 3-d finite element model for cord-reinforced rubber composites application to analysis of automobile tires. *Finite elements in analysis and design*, 14(1):1–16, 1993.
- [84] Craig E. Beal and J. Christian Gerdes. Model predictive control for vehicle stabilization at the limits of handling. *IEEE Transactions on Control Systems Technology*, 21(4):1258–1269, Jul. 2013.
- [85] Joseph Funke, Matthew Brown, Stephen M Erlien, and J Christian Gerdes. Collision avoidance and stabilization for autonomous vehicles in emergency scenarios. *IEEE Transactions on Control Systems Technology*, 25(4):1204–1216, 2016.
- [86] Wei Liu, Hongwen He, Fengchun Sun, and Jiangyi Lv. Integrated chassis control for a three-axle electric bus with distributed driving motors and active rear steering system. *Vehicle System Dynamics*, 55(5):601–625, 2017.

- [87] CarSim User Manual. Mechanical simulation corp. *Ann Arbor, MI*, 2009.
- [88] Yubiao Zhang, Amir Khajepour, and Mansour Ataei. Universal model-based stability control for ground vehicles with any axle and actuation configuration. *IEEE Transactions on Industrial Electronics*, 2019, Under Review-R2.
- [89] Yubiao Zhang, Amir Khajepour, and Mansour Ataei. A universal and reconfigurable methodology to articulated vehicles stability control. *IEEE Transactions on Vehicular Technology*, 2019, Under Review.
- [90] R Tchamna and I Youn. Yaw rate and side-slip control considering vehicle longitudinal dynamics. *International Journal of Automotive Technology*, 14(1):53–60, 2013.
- [91] R Thomas Bundorf. The influence of vehicle design parameters on characteristic speed and understeer. *SAE Transactions*, pages 548–560, 1968.
- [92] Aleksander Hac, Daniel Fulk, and Hsien Chen. Stability and control considerations of vehicle-trailer combination. *SAE International Journal of Passenger Cars-Mechanical Systems*, 1(2008-01-1228):925–937, 2008.
- [93] Rajesh Rajamani. *Vehicle dynamics and control*. Springer Science & Business Media, 2011.
- [94] Yubiao Zhang, Yanjun Huang, Hong Wang, and Amir Khajepour. A comparative study of equivalent modelling for multi-axle vehicle. *Vehicle System Dynamics*, 56(3):443–460, 2018.
- [95] Jo Yung Wong. *Theory of ground vehicles*. John Wiley & Sons, 2008.
- [96] Mansour Ataei, Amir Khajepour, and Soo Jeon. A general rollover index for tripped and un-tripped rollovers on flat and sloped roads. *Proceedings of the Institution of Mechanical Engineers, Part D: Journal of Automobile Engineering*, 233(2):304–316, 2019.

- [97] Juyong Kang, Jinho Yoo, and Kyongsu Yi. Driving control algorithm for maneuverability, lateral stability, and rollover prevention of 4wd electric vehicles with independently driven front and rear wheels. *IEEE Transactions on vehicular technology*, 60(7):2987–3001, 2011.
- [98] Sehyun Chang and Timothy J. Gordon. Model-based predictive control of vehicle dynamics. *International Journal of Vehicle Autonomous Systems*, 5(1-2):3–27, 2007.
- [99] Paolo Falcone, Francesco Borrelli, H Eric Tseng, Jahan Asgari, and Davor Hrovat. Linear time-varying model predictive control and its application to active steering systems: Stability analysis and experimental validation. *International Journal of Robust and Nonlinear Control: IFAC-Affiliated Journal*, 18(8):862–875, 2008.
- [100] H.J. Ferreau, C. Kirches, A. Potschka, H.G. Bock, and M. Diehl. qpOASES: A parametric active-set algorithm for quadratic programming. *Mathematical Programming Computation*, 6(4):327–363, 2014.
- [101] David Q Mayne, James B Rawlings, Christopher V. Rao, and Pierre OM Sokaert. Constrained model predictive control: Stability and optimality. *Automatica*, 36(6):789–814, 2000.
- [102] Manfred Morari and Jay H Lee. Model predictive control: past, present and future. *Computers & Chemical Engineering*, 23(4-5):667–682, 1999.
- [103] Graham Goodwin, María M Seron, and José A De Doná. *Constrained control and estimation: an optimisation approach, Chapter 5*. Springer Science & Business Media, 2006.
- [104] Ehsan Hashemi, Mohammad Pirani, Amir Khajepour, Alireza Kasaiezadeh, Shih-Ken Chen, and Bakhtiar Litkouhi. Corner-based estimation of tire forces and vehicle velocities robust to road conditions. *Control Engineering Practice*, 61:28–40, 2017.
- [105] Ayyoub Rezaeian, Reza Zarringhalam, Saber Fallah, W. Melek, Amir Khajepour, S-Ken Chen, N Moshchuck, and Bakhtiar Litkouhi. Novel tire force estimation strategy for real-time implementation on vehicle applications. *IEEE Transactions on Vehicular Technology*, 64(6):2231–2241, 2014.

- [106] Jorge L Garriga and Masoud Soroush. Model predictive control tuning methods: A review. *Industrial & Engineering Chemistry Research*, 49(8):3505–3515, 2010.
- [107] S. Joe Qin and Thomas A Badgwell. A survey of industrial model predictive control technology. *Control engineering practice*, 11(7):733–764, 2003.
- [108] Alberto Bemporad, Manfred Morari, and N Lawrence Ricker. Model predictive control toolbox users guide. *The mathworks*, 2010.
- [109] Paul R Maurath, Alan J Laub, Dale E Seborg, and Duncan A Mellichamp. Predictive controller design by principal components analysis. *Industrial & engineering chemistry research*, 27(7):1204–1212, 1988.
- [110] K Yamuna Rani and Heinz Unbehauen. Study of predictive controller tuning methods. *Automatica*, 33(12):2243–2248, 1997.
- [111] Willy Wojsznis, John Gudaz, Terry Blevins, and Ashish Mehta. Practical approach to tuning mpc. *ISA transactions*, 42(1):149–162, 2003.
- [112] Apostolos Georgiou, Christos Georgakis, and William L Luyben. Nonlinear dynamic matrix control for high-purity distillation columns. *AIChE Journal*, 34(8):1287–1298, 1988.
- [113] Richard M Murray. Optimization-based control. *California Institute of Technology, CA*, pages 111–128, 2009.
- [114] Rafay Shamim, Md Manjurul Islam, and Yuping He. A comparative study of active control strategies for improving lateral stability of car-trailer systems. Technical report, SAE Technical Paper, 2011.
- [115] Connor Fry Sykora. *Trailer sway control using an active hitch*. Masters’ Thesis, University of Waterloo, 2018.

APPENDICES

Appendix A

State-space Matrices

A.1 State-space Formulation (3.31) (Single Unit)

$$\dot{x} = Ax + BF_{CG}$$

where

$$x = [v_x \ v_y \ r \ \phi \ \dot{\phi}]^T, F_{CG} = [F_x \ F_y \ M_z]^T,$$

$$A = M_1^{-1}A_1, B = M_1^{-1}B_1,$$

wherein,

$$M_1 = \begin{bmatrix} m & 0 & 0 & 0 & 0 \\ 0 & m & 0 & 0 & -m_s h_s \\ 0 & 0 & I_{zz} & 0 & 0 \\ 0 & 0 & 0 & 1 & 0 \\ 0 & -m_s h_s & 0 & 0 & I_{xx} \end{bmatrix}; A_1 = \begin{bmatrix} 0 & 0 & 0 & 0 & 0 \\ 0 & 0 & -mv_x & 0 & 0 \\ 0 & 0 & 0 & 0 & 0 \\ 0 & 0 & 0 & 0 & 1 \\ 0 & 0 & -m_s h_s v_x & -K_\varphi + m_s g h_s & -C_\varphi \end{bmatrix};$$

$$B_1 = \begin{bmatrix} 1 & 0 & 0 \\ 0 & 1 & 0 \\ 0 & 0 & 1 \\ 0 & 0 & 0 \\ 0 & 0 & 0 \end{bmatrix}.$$

A.2 State-space Formulation (3.34) (Tractor Unit)

$$\dot{x}^t = A^t x^t + B^t F_{CG}^t + C^t F_H^t$$

where

$$x^t = \begin{bmatrix} v_x^t & v_y^t & r^t & \phi^t & \dot{\phi}^t \end{bmatrix}^T, F_{CG}^t = \begin{bmatrix} F_x^t & F_y^t & M_z^t \end{bmatrix}^T, F_H^t = \begin{bmatrix} F_{x,h}^t & F_{y,h}^t & M_{z,h}^t & M_{x,h}^t \end{bmatrix}^T,$$

$$A^t = M_{1t}^{-1} A_{1t}, B^t = M_{1t}^{-1} B_{1t}, C^t = M_{1t}^{-1} C_{1t},$$

wherein,

$$M_{1t} = \begin{bmatrix} m^t & 0 & 0 & 0 & 0 \\ 0 & m^t & 0 & 0 & -m_s^t h_s^t \\ 0 & 0 & I_{zz}^t & 0 & 0 \\ 0 & 0 & 0 & 1 & 0 \\ 0 & -m_s^t h_s^t & 0 & 0 & I_{xx}^t \end{bmatrix}; A_{1t} = \begin{bmatrix} 0 & 0 & 0 & 0 & 0 \\ 0 & 0 & -m^t v_x^t & 0 & 0 \\ 0 & 0 & 0 & 0 & 0 \\ 0 & 0 & 0 & 0 & 1 \\ 0 & 0 & -m_s^t h_s^t v_x^t & -K_\varphi^t + m_s^t g h_s^t & -C_\varphi^t \end{bmatrix};$$

$$B_{1t} = \begin{bmatrix} 1 & 0 & 0 \\ 0 & 1 & 0 \\ 0 & 0 & 1 \\ 0 & 0 & 0 \\ 0 & 0 & 0 \end{bmatrix}; C_{1t} = \begin{bmatrix} 1 & 0 & 0 & 0 \\ 0 & 1 & 0 & 0 \\ 0 & l_h^t & 1 & 0 \\ 0 & 0 & 0 & 0 \\ 0 & h_h^t & 0 & 1 \end{bmatrix}$$

A.3 State-space Formulation (3.36) (Trailer Unit)

$$\dot{x}^i = A^i x^i + B^i F_{CG}^i + C^i F_H^i$$

where

$$x^i = \begin{bmatrix} v_x^i & v_y^i & r^i & \phi^i & \dot{\phi}^i \end{bmatrix}^T, F_{CG}^i = \begin{bmatrix} F_x^i & F_y^i & M_z^i \end{bmatrix}^T, F_H^i = \begin{bmatrix} F_{x,h}^i & F_{y,h}^i & M_{z,h}^i & M_{x,h}^i \end{bmatrix}^T,$$

$$A^i = M_{1i}^{-1} A_{1i}, B^i = M_{1i}^{-1} B_{1i}, C^i = M_{1i}^{-1} C_{1i},$$

wherein,

$$M_{1i} = \begin{bmatrix} m^i & 0 & 0 & 0 & 0 \\ 0 & m^i & 0 & 0 & -m_s^i h_s^i \\ 0 & 0 & I_{zz}^i & 0 & 0 \\ 0 & 0 & 0 & 1 & 0 \\ 0 & -m_s^i h_s^i & 0 & 0 & I_{xx}^i \end{bmatrix}; A_{1i} = \begin{bmatrix} 0 & 0 & 0 & 0 & 0 \\ 0 & 0 & -m^i v_x^i & 0 & 0 \\ 0 & 0 & 0 & 0 & 0 \\ 0 & 0 & 0 & 0 & 1 \\ 0 & 0 & -m_s^i h_s^i v_x^i & -K_\varphi^i + m_s^i g h_s^i & -C_\varphi^i \end{bmatrix};$$

$$B_{1i} = \begin{bmatrix} 1 & 0 & 0 \\ 0 & 1 & 0 \\ 0 & 0 & 1 \\ 0 & 0 & 0 \\ 0 & 0 & 0 \end{bmatrix}; C_{1i} = \begin{bmatrix} 1 & 0 & 0 & 0 \\ 0 & 1 & 0 & 0 \\ 0 & l_h^i & 1 & 0 \\ 0 & 0 & 0 & 0 \\ 0 & h_h^i & 0 & 1 \end{bmatrix}$$

Appendix B

Footage of Vehicle Tests

The figures in this appendix are video footage and snapshots captured from the video filmed by the drone. The drone floated at certain height and position to record the performing maneuvers with control off and control on of the tractor-trailer. Figure [B.1](#) compares the trajectory and trailer sway in sine steer maneuver while Figure [B.2](#) compares these in a double lane change maneuver. Both are performed at a initial speed of 48km/h. The ‘sad’ face marks the moments when the trailer is experiencing a large art. angle. The cross lines (red and blue) demonstrate and compare the art. angles in selected moments of Control OFF and ON.

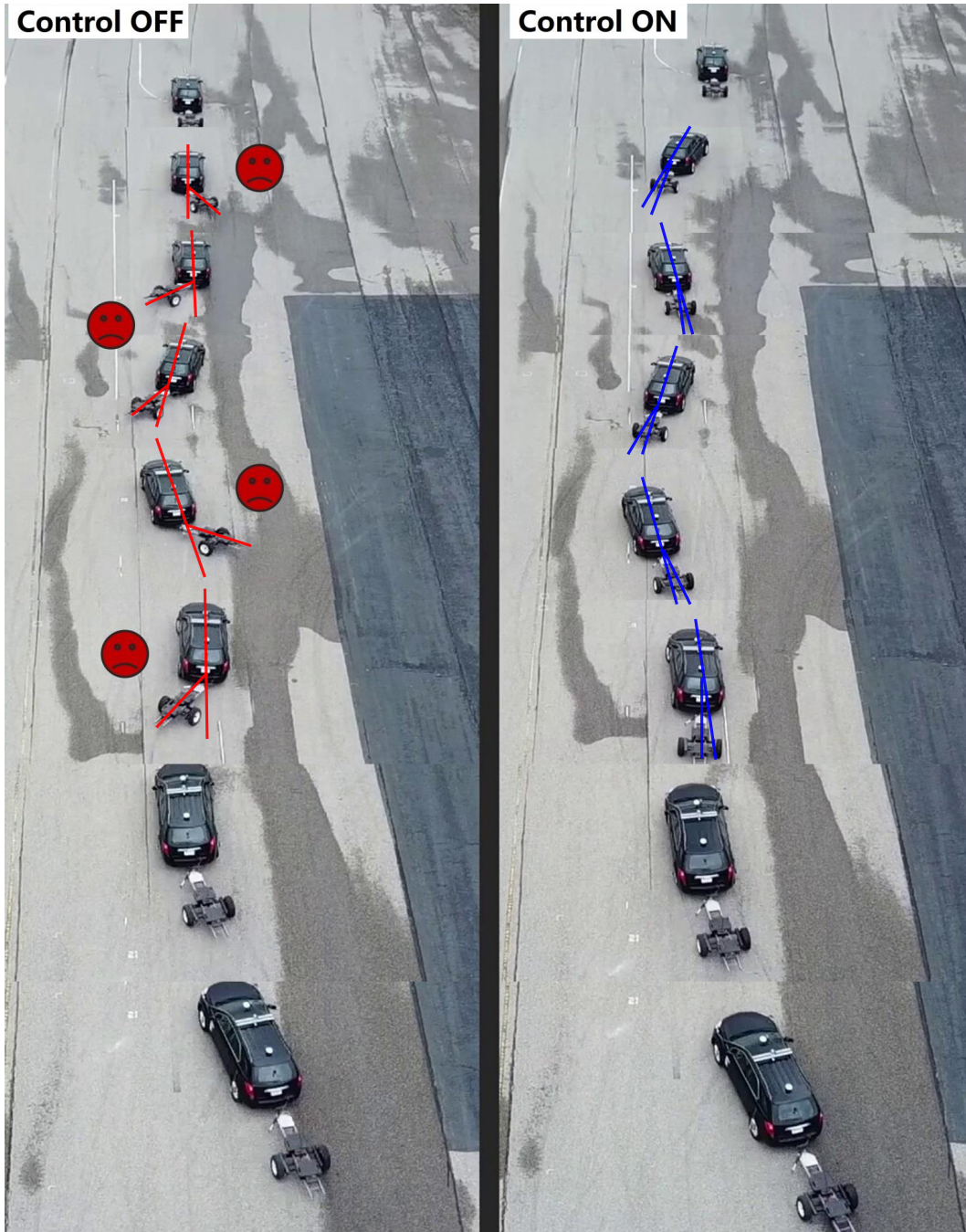


Figure B.1: Footage for Control OFF and Controller A in sine steer

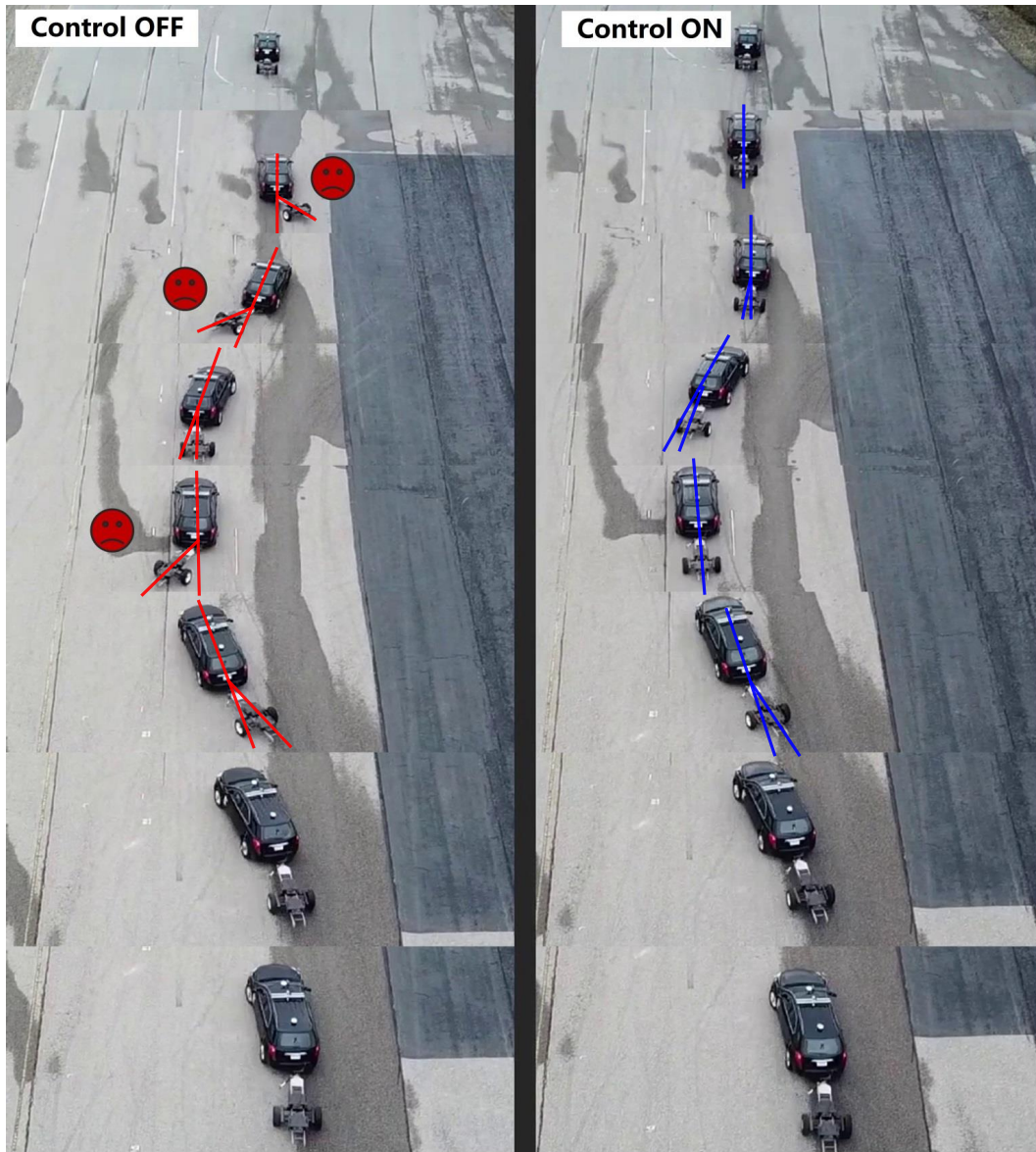


Figure B.2: Footage for Control OFF and Controller A in DLC